T.C.
SÜLEYMAN DEMİREL UNIVERSITY
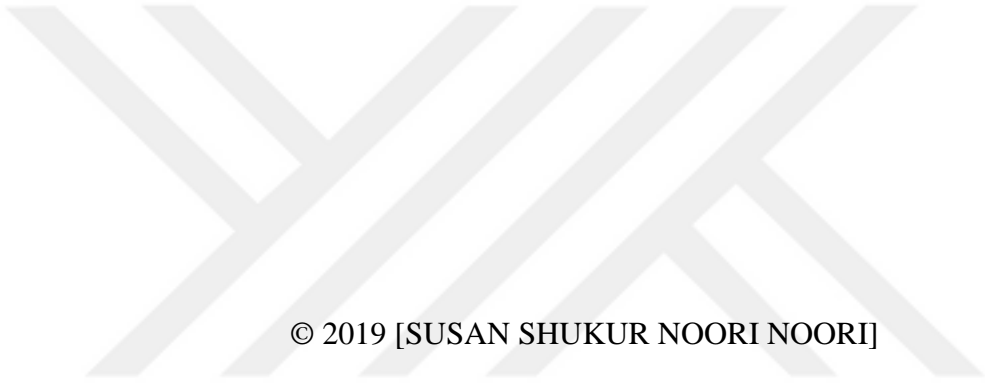# GRADUATE SCHOOL OF NATURAL AND APPLIED SCIENCES

THEORETICAL INVESTIGATION OF THE CROSS-SECTIONS FOR SOME RADIOISOTOPES USED IN MEDICINE

SUSAN SHUKUR NOORI NOORI

Supervisor
Prof. Dr. İskender AKKURT

II. Supervisor

Asst. Prof. Dr. Nurdan KARPUZ DEMİR

Ph.D. THESIS
DEPARTMENT OF PHYSICS
ISPARTA – 2019

APPROVAL OF THE THESIS

"Theoretical investigation of the cross-sections for some radioisotopes used in medicine" submitted by **SUSAN SHUKUR NOORI NOORI** in partial fulfillment of the requirements for the **Ph.D.** degree in **Department of Physics**, Graduate School of Natural and Applied Sciences, Süleyman Demirel University by,

Supervisor   **Prof. Dr. İskender AKKURT**
Süleyman Demirel University

Committee Member   **Assoc. Prof. Dr. Yusuf CEYLAN**
Selçuk University

Committee Member   **Assoc. Prof. Dr. Nurten Ayten UYANIK**
Isparta University of Applied sciences TBMYO

Committee Member   **Asst. Prof. Dr. Kadir GÜNOĞLU**
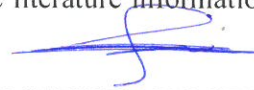Isparta University of Applied sciences TBMYO

Committee Member   **Asst. Prof. Dr. Gaber FAİSEL**
Süleyman Demirel University

Director   **Assoc. Prof. Dr. Şule Sultan UĞUR**

COMMITMENT

I hereby declare that all information in this document has been obtained and presented in accordance with academic rules and ethical conduct. I also declare that, as required by these rules and conduct, and that all the literature information used is taken as a reference in the thesis.

SUSAN SHUKUR NOORI NOORI

TABLE OF CONTENTS

ABSTRACT

Ph.D. Thesis

THEORETICAL INVESTIGATION OF THE CROSS-SECTIONS FOR SOME RADIOISOTOPES USED IN MEDICINE

SUSAN SHUKUR NOORI NOORI

Süleyman Demirel University
Graduate School of Natural and Applied Sciences
Department of Physics

Supervisor: Prof. Dr. İskender AKKURT

II. Supervisor: Asst. Prof. Dr. Nurdan KARPUZ DEMİR

Advances in medical knowledge and better understanding of disease processes are driving the search for early diagnosis and screening methods, and for new therapy options. Diagnostic and therapeutic applications using radioisotopes and radiopharmaceuticals continue to be the key elements in this context. Different radioactive isotopes play significant roles in technological applications of importance to our daily life as well for scientific research. Thus demand for such nuclear based services is expected to be expanded.

Production of the radioisotopes used in medical diagnosis and treatment are based on nuclear reactions. The data of the cross section is important to understand nuclear reaction models and to improve radioisotopes and neutron usage well that generated by this reaction. Energy dependence of nuclear reactions is not known. Therefore, the cross sections need to be examined for multi number of energies.

In this study, the investigation of neutrons, photons, protons, deuterons, ^{3}He and alpha particles induced to production cross sections of some medical radioisotopes by using Monte Carlo nuclear reaction simulation program TALYS version 1.6 code has been done.

In addition, double differential cross sections and energy dependent differential cross sections of neutron, proton, and alpha particles occured consequently in the bombardment of ^{56}Fe, ^{50}Cr and ^{19}F nuclei with deuteron, proton and neutrons respectively, were also investigated in this study. Optimum energy ranges for radioisotopes production efficiency and average cross sections in these energies have been determined. The obtained results have been discussed and compared with the experimental data taken from the Experimental Nuclear Reaction Data Library.

Keywords: Cross-section, radioisotopes used in medicine, TALYS 1.6.

2019, 112 pages

ÖZET

DoktoraTezi

TIPTA KULLANILAN BAZI RADYOİZOTOPLAR İÇİN TESİR KESİTLERİNİN TEORİK İNCELENMESİ

SUSAN SHUKUR NOORI NOORI

Süleyman Demirel Üniversitesi
Fen Bilimleri Enstitüsü
Fizik Anabilim Dalı

Danışman: Prof. Dr. İskender AKKURT

II. Danışman: Dr. Öğr. Üyesi. Nurdan KARPUZ DEMİR

Tıbbi bilgilerdeki ilerlemeler ve hastalık süreçlerinin daha iyi anlaşılması, erken tanı ve tarama yöntemleri arayışını ve yeni tedavi seçeneklerini teşvik etmektedir. Radyoizotoplar ve radyofarmasötiklerin kullanıldığı diagnostik ve terapötik uygulamalar bu bağlamda kilit elementler olmaya devam etmektedir. Farklı radyoaktif izotoplar, bilimsel araştırmalarda olduğu gibi, günlük hayatımıza da önem veren teknolojik uygulamalarda önemli roller oynamaktadır. Bu tür nükleer bazlı hizmetlere olan talebin artması bekleniyor.

Tıbbi tanı ve tedavide kullanılan radyoizotopların üretimi nükleer reaksiyonlara dayanmaktadır. Tesir kesitin verileri nükleer reaksiyon modellerini anlamak ve bu reaksiyon tarafından üretilen radyoizotopların ve nötron kullanımının iyileştirilmesi için önemlidir. Nükleer reaksiyonların enerji bağımlılığı detaylı olarak bilinmemektedir. Bu nedenle, çok sayıda enerjinin kesitleri incelenmelidir.

Bu çalışmada, bazı medikal radyoizotopların üretim tesir kesitler nötron, foton, proton, döteron, ^{3}He ve alfa reaksiyonları, Monte Carlo nükleer reaksiyon simülasyon programı TALYS sürüm 1.6 kodu kullanılarak araştırılmıştır.

Bu ilave olarak, sırasıyla nötron, proton ve alfa parçacıklarının çift diferansiyel kesitleri ve enerjiye bağlı tesir kesitleri, sırasıyla ^{56}Fe, ^{50}Cr ve ^{19}F çekirdeklerinin döteron, proton ve nötronlarla bombardımanında incelenmiştir. Bu enerjilerdeki radyoizotopların üretim verimliliği ve ortalama kesitleri için optimum enerji aralıkları belirlenmiştir. Elde edilen sonuçlar tartışılmış ve Deneysel Nükleer Reaksiyon Veri Kütüphanesi'nden alınan deneysel veriler ile karşılaştırılmıştır.

Anahtar Kelimeler: Tesir kesiti, tıpta kullanılan radyoizotoplar, TALYS 1.6.

2019, 112 sayfa

ACKNOWLEDGEMENTS

LIST OF FIGURES

LIST OF TABLES

LIST OF SYMBOLS AND ABBREVIATION

^{3}He	Helium-3
a	alpha
b	Barn
c	Speed of Light
CT	Computed tomography
d	Deuotron
DDX	Double differential cross section
DTC	Differentiated thyroid carcinoma
$d\Omega$	Solid angle in nuclear reaction geometry
FDG	Fluorodeoxyglucose
g	gamma
Gen IV	Generation fourth reactor
GeV	Giga electron volts
HSA	High specific activity
$h\nu$	Photon energy
I	Intensity
IAEA	International atomic energy agency
keV	Kilo electron volt
mb	Milli barn
MeV	Mega electron volt
n	Neutron
p	Proton
PET	Positron emission tomography
Q	Reaction energy
SPECT	Single photon emission computed tomography
$T_{1/2}$	Half life
TAT	Targeted alpha therapy
Z	Atom number
μ	Absorption coefficient
σ	Cross section
σ_t	Total cross section

1. INTRODUCTION

Nuclear physics as a subject of distinct from atomic physics since 1896, the year that Henri Becquerel observed that photographic plates were being fogged by an unknown radiation emitted from uranium ores. He had accidentally discovered radioactivity: the fact that some nuclei are unstable and spontaneously decay. In the following years, the phenomenon was extensively investigated, notably by the husband and wife team of Pierre and Marie Curie and by Ernest Rutherford and his collaborators. It was established that there were three distinct types of radiation involved: these were named (by Rutherford) α-, β- and γ -rays. We know now that α -rays are bound states of two protons and two neutrons , β -rays are electrons and γ-rays are photons, the quanta of electromagnetic radiation, but the historical names are still commonly used.

Nowadays nuclear medicine has become widely used in medical diagnostics of some diseases and the treatment of others, such as medical imaging Positron Emission Tomography (PET), tumors, nuclear imaging of primary bone tumors, cancers, etc. The most important problem is to obtain clean and safe energy. And the nuclear reaction data are mainly needed in the radioisotope production procedure. In general, the significance of nuclear reaction cross section data in radionuclide production programmes is well established. However, the radioactive tracers that emit gamma radiation can offer a large amount of information about the anatomy and the well functioning of different organs in the human body.

Calculations based on nuclear reaction models play an important role in the development of reaction cross sections. The concept of cross section is based upon a consideration of the physical situation encountered in determining reaction probability in the laboratory. In nuclear reaction an incident collimated beam of particles impinges upon target nuclei in a suitable specimen of material and interacts with these through the processes of scattering, absorption and/or reaction, thereby becoming attenuated may be in intensity or energy, or both by an amount which can be determined by measurements of the emergent beam. Production of medical isotope is an important and constantly evolving issue. Cyclotrons and reactors are used for radionuclide production purposes (Qaim, 2004). The cross–section data for

nuclear reactor production are generally well-known and can be satisfactorily reproduced by nuclear model calculations.

Theoretical and experimental studies play an important role in the development of the nuclear physics. The data obtained from the experimental results are important to understand the basic of nuclear physics. However, if the experimental data are unobtainable or are not possible to be produced because of the experimental difficulties, the theoretical calculations are needed to obtain double differential cross sections of the differential cross sections, stimulation response of the cross-sections. Besides the recent experimental studies, the theoretical studies contributes to rapid progress in science. The compatible results of calculated theoretical studies with experimental studies provide significant progress of the studies. On the basis of theoretical studies, the nuclear reactions cross sections for many energy values should be examined. Monte Carlo techniques and another programs based on these techniques are used in the investigation of the cross sections.

Monte Carlo is a numerical method for simulating the behavior of various physical and mathematical systems. It provides a solution of a problem that model objects interacting with other objects or with their environment based on simple relationships (Bielajew, 2001). It was developed in 1940 by Stanislaw Ulam while working on nuclear weapons projects at the Los Alamos National Laboratory. ''Monte Carlo'' named for a dedicated to the gambling in Monte Carlo township. The origin of the name Monte Carlo comes from its gambling aspect. Every Monte Carlo simulation is based on randomly happening events so that the outcome is not always absolute. The general idea of Monte Carlo analysis is simulation.

The idea is to build a model which, in all means, is able to represent the real system of interest. Deterministic methods, the most common of which is the discrete ordinates method, solve the transport equation for the average particle behavior. By contrast, Monte Carlo does not solve an explicit equation, but rather obtains answers by simulating individual particles and recording some aspects (tallies) of their average behavior. The average behavior of particles in the physical system is then inferred (using the central limit theorem) from the average behavior of the simulated particles. Monte Carlo techniques has also applications in nuclear and particle

2

physics, medical physics, detector designs, designing and resolving costly experiments. Monte Carlo techniques have great significance in determining the probability of reaction at certain energies. TALYS is a Monte Carlo code and a computer code system programming with Fortran language working in Linux operating system and developed for the prediction and analysis of nuclear reactions for target nuclides of mass 12 and heavier.

In this work, the total cross section, differential cross sections and double differential cross sections were calculated to obtain some medical radioisotopes used in diagnosis and treatment of different diseases by using TALYS 1.6 program where the total cross section were calculated to produce Fluorine-18, Iodine-124, Bromine-75,76, Technetium-94,99, the differential cross sections to produce Cobalt-57, Manganese-50 radioisotopes induced by different charged particles at different energies has been calculated. Also the double differential cross sections to produce Carbon-11, Nitrogen-13 and Copper-64 radioisotopes at different energies and different angles were calculated. The proton emission spectrum, neutron emission spectrum and alpha emission spectrum were investigated too.

1.1. Nuclear Reactions

The study of nuclear reactions is important for a number of reasons. Progress in the understanding of nuclear reactions has occurred at a faster pace and generally, a higher level of sophistication has been achieve compared to similar studies of chemical reactions. A large fraction of our knowledge on the properties of nuclei is derived from nuclear reactions. When an incoming particle is scattered of a target nucleus, the outcome depends on a combination of three factors: the reaction mechanism, interaction between the projectile and the target, and the internal structure of the nuclei involved. Different probes complete each other in what we can learn from an investigation. Furthermore, it is often possible to select the bombarding energy and the reaction in such a way that we can focus on particular aspects of the problem (Wong, 1998).

Nuclear reactions and nuclear scattering were used to measure the properties of nuclei. Reactions that exchange energy or nucleons can be used to measure the

3

energies of binding and excitation, quantum numbers of energy levels, and transition rates between levels. A particle accelerator, which produces a beam of high-velocity charged particles (electrons, protons, alphas, or "heavy ions"), creates these reactions when they strike a target nucleus. Nuclear reactions can also be produced in nature by high-velocity particles from cosmic rays, for instance in the upper atmosphere or in space. Beams of neutrons can be obtained from nuclear reactors or as secondary products when a charged-particle beam knocks out weakly bound neutrons from a target nucleus. Beams of photons, mesons, muons, and neutrinos can also produce nuclear reactions.

In order for a nuclear reaction to occur, the nucleons in the incident particle, or projectile, must interact with the nucleons in the target. Thus, the energy must be high enough to overcome the natural electromagnetic repulsion between the protons. This energy "barrier" is called the Coulomb barrier. If the energy is below the barrier, the nuclei will bounce of each other. Early, experiments by Rutherford used low-energy alpha particles from naturally radioactive material to bounce of target atoms and measure the size of the target nuclei (Serber, 1992). When a collision occurs between the incident particle and a target nucleus, either the beam particle scatters elastically leaving the target nucleus in its ground state or the target nucleus is internally excited and subsequently decays by emitting radiation or nucleons. A nuclear reaction can be described by identifying the incident particle, target nucleus, and reaction products.

1.2. Photonuclear Physics

The objective of photonuclear experiments is to determine the gross features of the photon absorption cross section, such as its magnitude and energy, and then to explore the detailed shape of the cross section with better energy resolution or by examining the spectra of outgoing nucleons (Hayward, 1970). The photonuclear definition as relating to or caused by the incidence of radiant energy (as gamma rays) on atomic nuclei. A photonuclear interaction begins with the absorption of a photon by a nucleus, leaving the nucleus in an excited state. The excited nucleus behaves like any compound nucleus with an excitation energy. The nucleus then

undergoes multiple de-excitation processes emitting secondary particles and possibly undergoing fission (Brown et al., 2010).

The first photonuclear reaction studies were carried out by Chadwick and Goldhaber's (Chadwick et al., 1935) and experiments with photo-dissociation of deuteron by using γ-rays emitted from the thorium source (Akkurt, 1998).

Since the electromagnetic properties of photonuclear reactions are well known, it is advantageous compared to other reactions that basis of nuclear studies. The interaction of photons with nuclei is energy dependent because of the changing wavelength of the photons, and the photon energy range below 1 GeV may be conveniently divided into three regions, on the basis of the physical process believed to dominate in a region. Figure1.1 shows the total photoabsorption crosssection per nucleon for various nuclei.
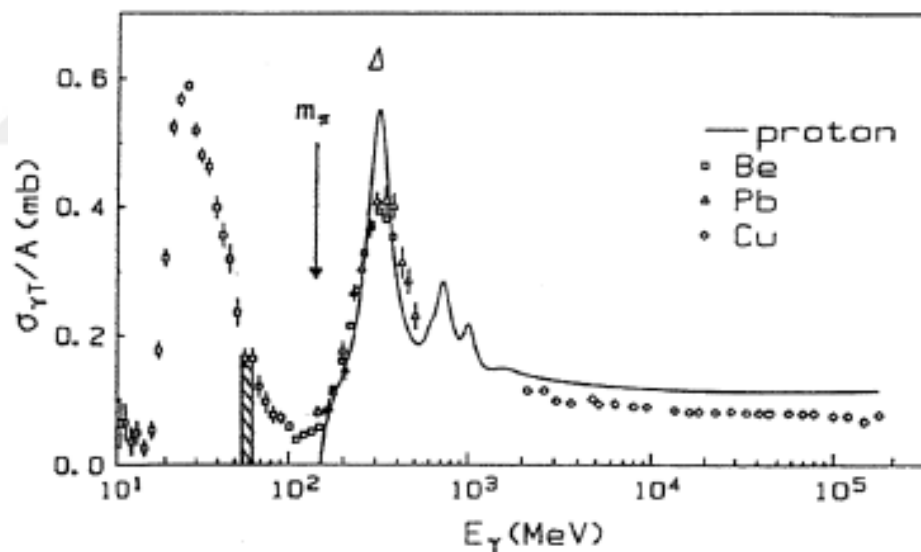
Figure 1.1. Total photon absorption cross section per nucleon (Ahrens, 1985;Akkurt, 1998)

There are three main mechanisms for photon absorption by a nucleus: the giant dipole resonance (relevant for photon energies in the range 10-40 MeV) , quasi-deuteron absorption (relevant for energies < 140 MeV) and the (Nucleon Resonance Region >140 MeV).

The giant dipole resonance can be viewed as an electromagnetic wave (photon) inducing an electric dipole-like vibrational resonance of the nucleus as a whole, which results in a collective excitation of the nucleus (Brown et al., 2010). The giant dipole resonance occurs with highest probability when the wavelength of the photon is comparable to the size of the nucleus. This typically occurs for photon energies in the range of 10 to 40 MeV and has a resonance width of a few MeV. Photonucleon emission is well described by a collective excitation of the nucleus to 1-particle, 1-hole states and subsequent nucleon emission by an evaporation process, Since the momentum transfer from the photon to the target nucleus is relatively small in this photon energy range, the photoexcitation is an electric dipole (E1) character.

Photons are mostly absorbed through the quasi-deuteron absorption process. Here the incident photon interacts with the dipole moment of a correlated neutron-proton pair inside the target nucleus, where a large part of the total absorption cross section is due to the (γ, np) reaction. The photon may interact with a single nucleon or with a virtual meson exchanged between nucleons (correlated pair) and the relative importance of these two mechanismsis still not well understood. Single nucleon processes could give some information on high momentum components of the nucleon in the nucleus and the absorption on pairs may give information on meson exchange currents.

The region where the photon energy range is greater than 140 MeV is called the nucleon resonance region (Akkurt, 1998). Photonuclear reactions have been used in basic and applied sciences in nuclear and radiation physics related fields (Akkoyun et al., 2015)

1.3. Interaction of Photon With Matter

Nuclear radiation normally consists of energetic particles or photons. The interaction of radiation with matter is useful in applications of nuclear physics: detectors, material modification, analysis, radiation therapy. The interaction can damage the materials, especially living tissues and therefore is considered as dangerous. The effects of interaction depend greatly on the intensity, energy and type of the radiation as well as on the nature of absorbing material.

Although a large number of possible interaction mechanisms are known for photon in matter, only three major types play an important role in radiation measurements: photoelectric absorption, Compton scattering, and pair production. All these processes lead to the partial or complete transfer of the gamma-ray photon energy to electron energy. In the photoelectric (photon-electron) interaction, a photon transfers all its energy to an electron located in one of the atomic shells. The electron is ejected from the atom by this energy and begins to pass through the surrounding matter. The electron rapidly loses its energy and moves only a relatively short distance from its original location.

Photoelectric interactions usually occur with electrons that are firmly bound to the atom, that is, those with a relatively high binding energy. Photoelectric interactions are most probable when the electron binding energy is only slightly less than the energy of the photon. If the binding energy is more than the energy of the photon, a photoelectric interaction cannot occur. This interaction is possible only when the photon has sufficient energy to overcome the binding energy and remove the electron from the atom.

Following a photoelectric interaction, an ionized absorber atom is created with a vacancy in one of its bound shells. This vacancy is will be quickly filled by an electron from a shell with a lower binding energy (other shells) or through capture of a free electron from the material. The rearrangement of electrons from other shells creates another vacancy, which, in turn, is filled by an electron from an even lower binding energy shell. Therefore a cascade of more characteristic x-rays can be also generated. The probability of characteristic x-ray emission decreases as the atomic number of the absorber decreases. Sometimes , the emission of an Auger electron occurs.

The photoelectric is very phenomenon. No scattering radiation because all the photon energy is absorbed by the atom of the material. Since all of the photon energy is absorbed, none of them can go on, so that a regular white shadow appears under the part of the material that is exposed to photoelectric absorption in the x-ray film. Photoelectric absorption is the reason of the appearnce of bones white in an x-ray film (Ulu, 2008).

As for Compton effect, it is characterized by that, only part of its total amount of energy is transferred from the entering photon to an electron. The freed electron which is called Compton electron (recoil electron), reaches a certain velocity that is dependent on the energy transferred to the electron. The rest of the energy continues as a photon of lower energy in another direction and is therefore called a scattered photon. Because of the lower energy the scattered photon has a longer wavelength than the original.

The Compton process occurs only then when the photon energy passes the limiting value of the photoelectric process. Since the impulse and the energy are divided among the Compton electron and the scattered photon, the law of preservation of impulse is complied with, and the process occurs with the electrons from the outer shells as well. For this reason, the atomic number (Z) of the material is less influential. The freed Compton electrons can, depending on the energy content, ionize other atoms along their routes. The scattered photon continues its way and continues to enter into Compton processes up until the energy is reduced to such an extent that a photoelectric process takes place. Only then the photon has disappeared. Thus, the gamma ray photon scattere because it cannot transfer the entire energy to electron. The scattered gamma ray photon will have less energy and longer wavelength than the incoming. The energy difference between incoming and scattered gamma ray photons is transferred to the electron as kinetic energy.

In general, pair production is a phenomenon of nature where energy is direct converted to matter. The phenomenon of pair production can be viewed two different ways. One way is as a particle and antiparticle and the other is as a particle and a hole. The first way can be represented by formation of electron and positron, from a packet of electromagnetic energy (high energy photon − gamma ray) traveling through matter. It is one of the possible ways in which gamma rays interact with matter. At high energies this interaction dominates.

In order for electron-positron pair production to occur, the electromagnetic energy of the photon must be above a threshold energy, which is equivalent to the rest mass of two electrons. The threshold energy (the total rest mass of produced particles) for electron-positron pair production is equal to 1.02 MeV (2×0.511 MeV) because the

rest mass of a single electron is equivalent to 0.511 MeV of energy. If the original photon's energy is greater than 1.02 MeV, any energy above 1.02 MeV is according to the conservation law split between the kinetic energy of motion of the two particles.

The presence of an electric field of a heavy atom such as lead or uranium is essential in order to satisfy conservation of momentum and energy. In order to satisfy both conservation of momentum and energy, the atomic nucleus must receive some momentum. Therefore a photon pair production in free space cannot occur. Moreover, the positron is the anti-particle of the electron, so when a positron comes to rest, it interacts with another electron, resulting in the annihilation of the both particles and the complete conversion of their rest mass back to pure energy (according to the $E=mc^2$ Einstein formula) in the form of two oppositely directed 0.511 MeV gamma rays (photons). The pair production phenomenon is therefore connected with creation and destruction of matter in one reaction.

They result in sudden and abrupt changes in the gamma-ray photon history, in that the photon either disappears entirely or is scattered through a significant angle. This behavior is in marked contrast to the charged particles, which slow down gradually through continuous, simultaneous interactions with many absorber atoms. (Knoll,2000). The relative importance of σ, T , and K is shown graphically in Figure 1.2, Photoelectric collisions are important only for small hv and large Z and are responsible for the practical saying "lead is opaque to photons below ~ 0.3 MeV". Pair production is of major importance only for large hv and large Z. Compton collisions predominate in the entire domain of intermediate hv, for all Z.
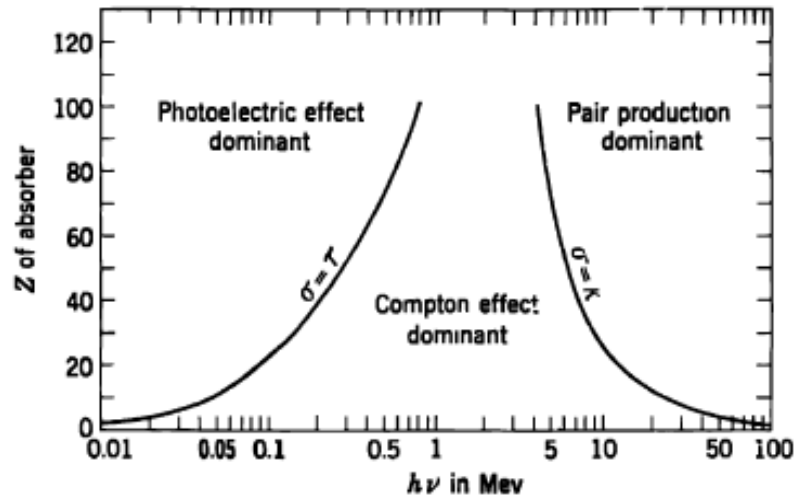
Figure 1.2. Relative importance of the three major types of photon interaction. The lines show the values of Z and photon energy hv for which the two neighboring effects are just equal (Evans, 1955)

Interaction of nuclear radiation with matter includes: charged particles, photons and neutrons. In the case of uncharged radiations (Photons or neutrons) there is first transfer of all part of the energy to charged particles before there is any measurable effect on the absorbing medium (Lilley, 2001). When a beam of gamma ray photon is incident on any material it removed individually in a single event. The event may be an actual absorption process in which case photon disappears or the photon may be scattered out of the beam. When a gamma rays passes through matter, probability for absorption is proportional to thickness of the layer, the density of the material, and absorption, cross section of the material. The total absorption shows an exponential decrease of intensity with distance from the decrease of intensity with distance from the incident surface.

$$I(x) = I_0 e^{-\mu x} \tag{1.1}$$

Where, x is the distance from the incident surface, $\mu = n\sigma$ is the absorption coefficient, measured in cm^{-1}, n is the number of atoms per cm^3 of the material (atomic density), σ is the absorption cross section in cm^2.

10

1.4. Cross Section

The concept of cross section is the crucial key that opens the communication between the real world of experiment and the abstract, idealized world of theoretical models. In a high- energy physics experiment, we specify interactions of elementary particles quantitatively in terms of cross sections. The cross section is the probability that an interaction will occur between a projectile particle and a target particle.

We can measure the probability that two particles will interact in experiments. In the famous experiment in which Rutherford studied the scattering of alpha particles off a foil target, the cross section gives the probability that the alpha particle is deflected from its path straight through the target. The cross section for large-angle scattering is the fraction of alpha particles that bounce back from the target, divided by the density of nuclei in the target and the target thickness. In a reaction symbolized as A(a,b) B, N number of nuclei, A the flow of particles on the target nucleus per unit time, I_a the bombardment particles are sent out, the resulting reaction occurs the number of particles in unit time will be proportional to R_b, I_a and N. then this ratio defined as nuclear reaction cross section and written as proportional:

$$\sigma = \frac{R_b}{I_a N_A} \qquad (1.2)$$

Where R_b the number of resulting particles, I_a the number of particles in a unit time, and N_A represents the number of target nuclei per unit area. The product of the number of particles in the unit volume n and sigma is also called the macroscopic effect section denoted by $\sum$

$$\sum = n\sigma \qquad (1.3)$$

If we are only interested in absorption in this case we can use the absorption coefficient term (μ) instead of $\sum$

$$\mu = n\sigma \qquad (1.4)$$
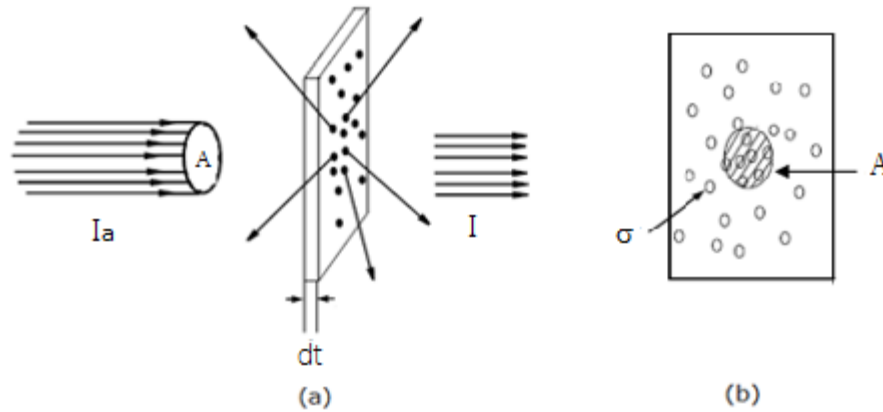
Figure 1.3. (a) Incident particle beam with intensity of I_a on thin plate (b) Appearance in front of thin plate

We can picture the cross section as the effective area that a target presents to the projected particle. If an interaction is highly probable, it's as if the target particle is large compared to the whole target area, while if the interaction is very rare, it's as if the target is small. The cross section for an interaction to occur does not necessarily depend on the geometric area of a particle. It's possible for two particles to have the same geometric area (sometimes known as geometric cross section) and yet have very different interaction cross section or probability for interacting with a projectile particle. When an accelerated charged particle interacts with a target nucleus a nuclear reaction takes place, ultimately leading to a stable or radioactive product nucleus. A nuclear reaction is characterized by a cross-section, describing the probability that a particle, with a beam intensity of 1 particle per 1 cm^2, incident on 1 target nucleus will lead to a specific physical process, where the incident particle, target nucleus, reaction channel and the final nucleus are exactly specified (IAEA, 2001). Cross section is one of the most important physical quantity describing nuclear reactions. It can be experimentally measured or calculated using different mechanism (models) of nuclear reactions.

1.4.1. Differential cross section

When a cross section is specified as a function of some final-state variable, such as particle angle or energy, it is called a differential cross section. A differential cross

section calculation is made, when information about the angular distributions of the products of the nuclear reactions is needed.

When incoming particles interact with the target nuclei, there is always only one kind nuclear reaction has occured. If more than one type of reaction occurs, the cross section for each species will usually be different. These special cross sections are called partial cross sections and the total cross section is equal to the sum of them. After the nuclear reaction or scattering occurs, the outgoing particles often exhibit anisotropic distribution and at the same time have different energies at different angles. It is important to know the number of particles in the $d\Omega$ solid angle at the moment by making θ angle at the incoming direction. The calculated cross section in this case is angle-dependent and it is another cross-section, and the unit is defined as the cross-sectional area per solid angle, this show by (θ, Φ):

$$\sigma(\theta, \phi) = \frac{d\sigma}{d\Omega} \tag{1.5}$$

Thus, the total cross-section will be

$$\sigma_T = \int_\Omega \frac{d\sigma}{d\Omega} d\Omega \tag{1.6}$$

The value of $d\Omega$ solid angle is given by

$$d\Omega = \frac{area}{(distance)^2} = \frac{dA}{r^2} = \frac{(rd\theta)(r\sin\theta d\phi)}{r^2} = \sin\theta d\theta d\phi \tag{1.7}$$

Total solid angle is

$$\Omega = \int_\Omega d\Omega = \int_0^{2\pi} \int_0^\pi \sin\theta d\theta d\phi = 4\pi \tag{1.8}$$
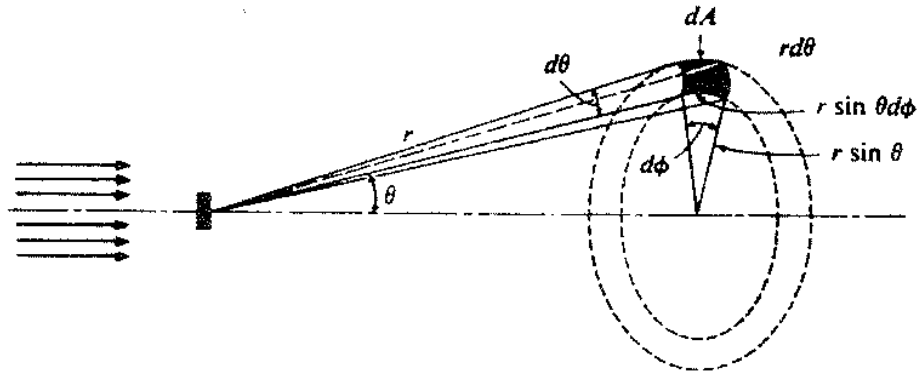
Figure 1.4. The reaction geometry showing the beam emitted in the dΩ solid angle (Krane, 2006)

While the solid angle is the fraction

$$\frac{d\Omega}{\Omega} = \frac{A}{r^2}\frac{1}{4\pi} = \frac{A}{4\pi r^2} \tag{1.9}$$

σ_T, the total cross section can be found by incorporating the two equations (1.6), (1.7)

$$\sigma_T = \int \frac{d\sigma}{d\Omega}d\Omega = \int \frac{d\sigma}{d\Omega}\sin\theta d\theta d\phi \tag{1.10}$$

If the differential cross section is independent of Φ, the cross section (after integration over Φ) will be

$$\sigma_T = 2\pi \int \frac{d\sigma}{d\Omega}\sin\theta d\theta \tag{1.11}$$

Here $d\sigma / d\Omega = \sigma(\theta)$ is the differential-cross-section.

Differential cross section measurement is useful in finding the energy dependent partial cross section. However, it is also useful to find the directional dependence of the cross section on the nature of the nuclear reaction. By accepting a nuclear force type, it is possible to express the angular distribution of different nuclear reactions.

Conformity between theory and experiment will give the degree of the accuracy of the accepted model of nuclear model is proven.

1.4.2. Double differential cross section

In many nuclear physics applications, for X(a,b)Y reaction we are concerned not only with the possibility of particle b being spread at a certain angle, but also with the possibility that certain nuclei Y will emit certain energy in versus the specific energy of the nucleus. The detector located in Figure 1.4 counts all the particles in the $d\Omega$ solid angle around $\Omega(\theta, \phi)$.

The influence cross-section measurements associated with the solid angle in the concept of differential cross section leave the results of the double differential cross section (DDX) with the addition of the energy analysis as well as the counting rate per unit solid angle and unit energy interval and the normalization of the initial flow. Therefore, we must change the definition of the cross section to give the probability of observing the particle b at $d\Omega$ solid angle and dE_b energy range. This gives us the quantity $d^2\sigma / dE_b\, d\Omega$ called the double differential cross section. In the literature, this additional energy dependence is not usually expressed explicitly; generally the cross sections are plotted as $d\sigma / d\Omega$ according to θ which leads to the specific final energy state. In this case, although it does not look like this, $d^2\sigma / dE_b\, d\Omega$. For intermittent conditions, there can be only one level in the dE_b energy range, and the difference becomes insignificant.

On the other hand, if we do not consider the direction of the particle b (by enclosing the cross-sectional area of the target with the 4π solid angle of the detectors or without observing b at all), then we measure the other $d\sigma / dE$ differential cross section, where E can represent an excited energy of Y. Another cross section that we can consider is the total cross section of σ_t. Here, for a particular incoming particle, we sum up the reaction cross sections σ of the directions and the energies for all possible different outgoing particles. Such a calculation may indicate probability that the incoming particle will enter any reaction with the target and thus be removed from the incoming beam of particles. It can be obtained directly by measuring the loss in the intensity of the beam passing through the target at a particular thickness.

1.5. Radioisotopes Used in Nuclear Medicine

Nuclear medicine uses radiation to provide information about the functioning of a person's specific organs, or to treat disease. There is widespread awareness of the use of radiation and radioisotopes, particularly for diagnosis (identification) and therapy (treatment) of various medical conditions. And in most cases, the information is used by physicians to make a quick diagnosis of the patient's illness. The thyroid, bones, heart, liver, and many other organs can be easily imaged, and disorders in their function revealed. In some cases radiation can be used to treat diseased organs, or tumors. Nuclear reactors, cyclotrons and accelerators are used for the production of radionuclides for both diagnostic and therapeutic purposes in nuclear medicine

- Nuclear medicine uses radiation to provide diagnostic information about the functioning of a person's specific organs, or to treat them. Diagnostic procedures using radioisotopes are now routine.
- Radiotherapy can be used to treat some medical conditions, especially cancer, using radiation to weaken or destroy particular targeted cells.
- Sterilization of medical equipment is also an important use of radioisotopes.
- Over 40 million nuclear medicine procedures are performed each year, and demand for radioisotopes is increasing at up to 5% annually (Int. Ref. 1).

Many of the chemical elements have a number of isotopes. The isotopes of an element have the same number of protons in their atoms (atomic number) but different masses due to different numbers of neutrons. In an atom in the neutral state, the number of external electrons also equals the atomic number. These electrons determine the chemistry of the atom. The atomic mass is the sum of the protons and neutrons. There are 82 stable elements and about 275 stable isotopes of these elements. When a combination of neutrons and protons, which does not already exist in nature, is produced artificially, the atom will be unstable and is called a radioactive isotope or radioisotope. There are also a number of unstable natural isotopes arising from the decay of primordial Uranium and Thorium. Overall there are 3800 radioisotopes. At present there are up to 200 radioisotopes used on a regular basis, and must be produced artificially (Int. Ref. 2).

The use of radioisotopes in biological sciences began by Von G. Hevesy in 1923 (Hevesy, 1923). Hevesy has shown that the amount of radiation required for such studies is very small. At this time, the radioisotopes needed for such studies were not available yet. This problem was solved by Curie and Joliot in 1934 who discovered that radioisotopes could be produced artificially. Many scientists have devoted themselves to the work of new radionuclide production and in a short time have prepared a large number of radionuclides for use by biological scientists (Curie, et al. 1934). Herz and his friends showed that the thyroid gland was holding the ^{131}I radioisotope in the rabbit in 1938. In 1939, Hamilton and Soley measured the involvement of ^{131}I in thyroid with a simple Geiger-Müller counter. These studies, gathered under the name of nuclear medical science, have found numerous methods to be applied in diagnosis and treatment.

Radioisotopes are mostly produced in cyclotrons and reactors. The energy of the incoming particles and the target nucleus, determines the method by which radioisotopes are produced. The production of radioisotopes are carried out in three different ways: nuclear reactors, cyclotrons and radioisotope generators. The most important criterion in production of radioisotopes is time. Short half-life isotopes may not be deliver to the places in time, therefore, radioisotope generators are used to meet the demands of facilities that are remote from the production site, particularly those requiring short half-life radioisotopes.

Radionuclides used in nuclear medicine production can be classified as follows:

a) Nuclear reactor products: ^{133}Xe, ^{99}Mo, ^{131}I
b) Cyclotron products:
      i. Positron emitting isotopes: ^{11}C, ^{13}N, ^{15}O, ^{18}F
      ii. Gamma emitting isotopes: ^{57}Co, ^{67}Ga, ^{111}In, ^{123}I, ^{201}Tl
c) Generator products: ^{68}Ga, ^{81m}Kr, ^{82}Ru, ^{99m}Tc and ^{113m}In.

1.5.1. Reactor radioisotopes (half-life indicated)

Molybdenum-99 (66 h): Used as the 'parent' in a generator to produce technetium-99m.

Phosphorus-32 (14 d): Used in the treatment of polycythemia Vera (excess red blood cells). Beta emitter.

Iodine-125 (60 d): Used in cancer brachytherapy (prostate and brain), also diagnostically to evaluate the filtration rate of kidneys and to diagnose deep vein thrombosis in the leg. It is also widely used in radioimmune-assays to show the presence of hormones in tiny quantities.

Iodine-131 (8 d): Widely used in treating thyroid cancer and in imaging the thyroid; also in diagnosis of abnormal liver function, renal (kidney) blood flow and urinary tract obstruction. A strong gamma emitter, but used for beta therapy.

Bismuth-213 (46 min): Used for targeted alpha therapy (TAT), especially cancers, as it has a high energy (8.4 MeV).

Cobalt-60 (5.27 year): Formerly used for external beam radiotherapy, now almost universally used for sterilizing. High-specific-activity (HSA) Co-60 is used for brain cancer treatment.

Chromium-51 (28 d): Used to label red blood cells and quantify gastro-intestinal protein loss or bleeding.

Dysprosium-165 (2 h): Used as an aggregated hydroxide for synovectomy treatment of arthritis.

Erbium-169 (9.4 d): Use for relieving arthritis pain in synovial joints.

Palladium-103 (17 d): Used to make brachytherapy permanent implant seeds for early stage prostate cancer. Emits soft x-rays.

Holmium-166 (26 h): Being developed for diagnosis and treatment of liver tumors.

Iridium-192 (74 d): Supplied in wire form for use as an internal radiotherapy source for cancer treatment (used then removed), e.g. for prostate cancer. Strong beta emitter for high dose-rate brachytherapy.

Palladium-103 (17 d): Used to make brachytherapy permanent implant seeds for early stage prostate cancer. Emits soft x-rays.

Potassium-42 (12 h): Used for the determination of exchangeable potassium in coronary blood flow.

Iron-59 (46 d): Used in studies of iron metabolism in the spleen.

Rhenium-186 (3.8 d): Used for pain relief in bone cancer. Beta emitter with weak gamma for imaging.

Rhenium-188 (17 h): Used to beta irradiate coronary arteries from an angioplasty balloon.

Caesium-137 (30 year): Used for low-intensity sterilization of blood.

Yttrium-90 (64 h): Used for cancer brachytherapy and as silicate colloid for the relieving the pain of arthritis in larger synovial joints. Pure beta emitter and of growing significance in therapy, especially liver cancer.

Samarium-153 (47 h): Sm-153 is very effective in relieving the pain of secondary cancers lodged in the bone, sold as quadramet. Also very effective for prostate and breast cancer. Beta emitter.

Technetium-99m (6 h): Used in to image the skeleton and heart muscle in particular, but also for brain, thyroid, lungs (perfusion and ventilation), liver, spleen, kidney (structure and filtration rate), gall bladder, bone marrow, salivary and lacrimal glands, heart blood pool, infection and numerous specialized medical studies. Produced from Mo-99 in a generator.

Strontium-89 (50 d): Very effective in reducing the pain of prostate and bone cancer. Beta emitter.

Ytterbium-169 (32 d): Used for cerebrospinal fluid studies in the brain.

Xenon-133 (5 d): Used for pulmonary (lung) ventilation studies.

1.5.2. Cyclotron radioisotopes (half-life indicated)

Carbon-11, Nitrogen-13, Oxygen-15, Fluorine-18: These are positron emitters used in PET for studying brain physiology and pathology, in particular for localising epileptic focus, and in dementia, psychiatry and neuropharmacology studies. They also have a significant role in cardiology. ^{18}F in FDG (fluorodeoxyglucose) has become very important in detection of cancers and the monitoring of progress in their treatment, using PET.

Copper-64 (13 h): Used to study genetic diseases affecting copper metabolism, such as Wilson's and Menke's diseases, and for PET imaging of tumors, and therapy.

Copper-67 (2.6 d): Beta emitter, used in therapy.

Bromine-75 (96.7 min): Positron emitter used in PET for fast metabolic processes.

Cobalt-57 (272 d): Used as a marker to estimate organ size and for in-vitro diagnostic kits.

Gallium-67 (78 h): Used for tumour imaging and localisation of inflammatory lesions (infections).

Gallium-68 (68 min): Positron emitter used in PET and PET-CT units. Derived from germanium-68 in a generator.

Iodine-123 (13 h): Increasingly used for diagnosis of thyroid function, it is a gamma emitter without the beta radiation of I-131.

Iodine-124 (4.2 d): Used in a variety of PET applications, such as protein and antibody iodinations, as well as in the design and synthesis of new PET tracers.

Indium-111 (2.8 d): Used for specialist diagnostic studies, eg brain studies, infection and colon transit studies.

Rubidium-82 (1.26 min): Convenient PET agent in myocardial perfusion imaging.

Thallium-201 (73 h): Used for diagnosis of coronary artery disease other heart conditions such as heart muscle death and for location of low-grade lymphomas. It is the most commonly used substitute for technetium-99 in cardiac-stress tests.

Strontium-82 (25 d): Used as the 'parent' in a generator to produce Rb-82

Krypton-81m(13sec) from rubidium-81 (4.6h): Kr-81m gas can yield functional images of pulmonary ventilation, e.g. in asthmatic patients, and for the early diagnosis of lung diseases and function (Int. Ref. 1).

1.6. Positron Emission Tomography (PET)

Positron emission tomography (PET), shown in Figure 1.6, is a nuclear medicine imaging technology that provides moderate-resolution, sensitive images of the biodistribution of a radiotracer in vivo (Jacobson, et al., 2015). Radioisotopes are an essential part of medical diagnostic procedures. In combination with imaging devices which register the gamma rays emitted from within, they can study the dynamic processes taking place in various parts of the body.

PET is based on the detection of very small (picomolar) quantities of biological substances which are labelled with a positron emitter (Ziegler, 2005). The use of positron emitting radioisotopes such as ^{11}C, ^{13}N, ^{15}O, and ^{18}F together with PET offers a highly selective and quantitative means for investigating regional tissue

biochemistry, physiology and pharmacology the ^{11}C, ^{13}N, ^{15}O and ^{18}F, with relatively short half-life of 20.334, 9.967, 2.037 and 110 min, respectively. Note that among of the nuclides mentioned above, ^{18}F has the most ideal half-life for labeling of radiopharmaceuticals and has a unique and diverse chemistry for introduction into various molecules.

The positron emitting nuclei which are neutron deficient isotopes are important for PET studies. Positrons annihilate with electrons emitting two photons (Eγ = 511 keV) in opposite direction. Most of the positron emitters are still being studied in terms of their applicability for diagnostic purposes. PET has been developing with the increasing number of clinical facilities raising interest in the use of PET in routine practice (Tel, et al. 2011). A PET scanner measures important body functions, such as blood flow, oxygen use, and sugar (glucose) metabolism, to help doctors evaluate how well organs and tissues are functioning. The scanner works by detecting radioactive emissions from the radiotracer and producing pictures that provide molecular information.
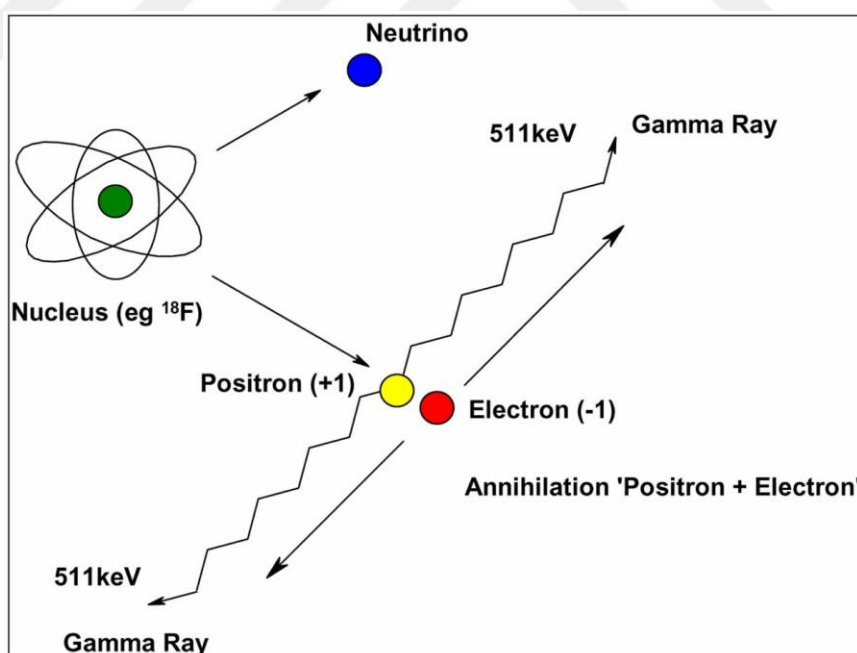
Figure 1.5. A schematic diagram showing positron emission during the decay process of a radionuclide (Kitson, et al. 2009)

For example, (Figure 1.5) the radioactive ^{18}F, produced from the cyclotron, is a positron emitter. The positron from the unstable ^{18}F nucleus collides with an electron

and both are annihilated. This results in two gamma rays of equal energy but going in opposite directions.

The gamma rays leave the patient's body and interact with the scintillation crystals and the photomultiplier tubes in the detectors. These crystals act like transducers by converting the gamma rays into 'light' photons. The photons are then converted into electrical signals that are registered by the tomography electronics. The information is then processed by a computer to form a complex 3- D real time image of a particular part of the body such as the brain or a whole body scan.

Figure 1.6. Positron emission tomography (PET)

PET/CT this advanced nuclear imaging technique combines positron emission tomography (PET) and computed tomography (CT) into one machine. A PET/CT scan reveals information about both the structure and function of cells and tissues in the body during a single imaging session.

During a PET/CT scan, the patient is first injected with a glucose (sugar) solution that contains a very small amount of radioactive material. The substance is absorbed by the particular organs or tissues being examined. The patient rests on a table and slides into a large tunnel-shaped scanner. The PET/CT scanner is then able to "see"

damaged or cancerous cells where the glucose is being taken up (cancer cells often use more glucose than normal cells) and the rate at which the tumor is using the glucose (which may help determine the tumor grade). The procedure is painless and varies in length, depending on the part of the body that is being evaluated

By combining information about the body's anatomy and metabolic function, a PET/CT scan provides a more detailed picture of cancerous tissues than either test does alone. The images are captured in a single scan, which provides a high level of accuracy as in Figure 1.7.
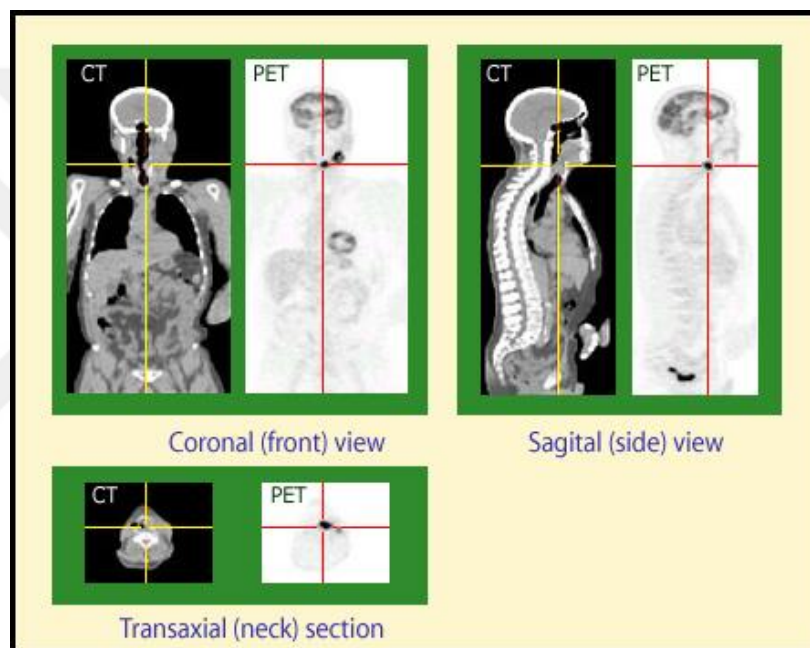
Figure 1.7. PET procedures allow for the early discovery of cancers and are useful in following the evolution of any specific cancerous growth. These three images of the same patient taken with a CT (Computed Tomography) scanner and a PET camera show the advantages of these nuclear imaging techniques

1.7. Single Photon Emission Computed Tomography (SPECT)

A Single Photon Emission Computed Tomography (SPECT), shown in Figure 1.8, is a similar tomographic technique. However, the substances used in SPECT are radioactive labeled with isotopes having longer decay times than those used in PET. This makes SPECT centers more common and SPECT scan much cheaper.

However, the radio labeled substances used in SPECT emit single instead of double gamma rays.

SPECT scan is a type of nuclear imaging test that shows how blood flows to tissues and organs. A SPECT scan integrates two technologies to view the body: computed tomography (CT) and a radioactive material (tracer). The tracer is what allows doctors to see how blood flows to tissues and organs.

Before the SPECT scan, the patient is injected with a chemical that is radiolabled, meaning it emits gamma rays that can be detected by the scanner. In this technique, the camera rotates around the patient and takes images from many angles of gamma rays. The computer uses this information to develop a much more detailed and precise image. The computer collects the information emitted by the gamma rays and translates them into two-dimensional cross-sections. These cross-sections can be added back together to form a 3D image of brain. The radioisotopes typically used in SPECT to label tracers are ^{123}I, ^{99m}Te, ^{133}Xe, ^{201}Th, and ^{18}F. These radioactive forms of natural elements will pass safely through the body and be detected by the scanner.

The type of tracer used depends on what the doctor wants to measure. For example, if the doctor is looking at a tumor, he might use radiolabled glucose (FDG) and watch how it is metabolized by the tumor. The test differs from a PET scan in that the tracer stays in blood stream rather than being absorbed by surrounding tissues, thereby limiting the images to areas where blood flows. SPECT scans are cheaper and more readily available than higher resolution PET scans. Since low-energy radioisotopes are used in SPECT, radiation protection is easier and the process possibilities are higher in images. SPECT has become an increasingly common imaging technique as it provides these and similar advantages (Holly et al., 2010). Furthermore, combining SPECT with CT in a SPECT/CT system can assist in defining the anatomic context of biochemical processes and improve the quantitative accuracy of the SPECT data.

Figure 1.8. Single Photon Emission Computed Tomography (SPECT)

2. LITERATURE BACKGROUND

The importance of studying nuclear reactions and reaction cross sections comes from the fact that many information are obtained such as nuclear size, charge distribution, nuclear forces etc.

Sarpün, et al. (2018) focused on the effects of the deformation parameter on the cross sections. By determined the deformation parameters of target nucleus ^{110}Pd using interacting boson model (IBM). Then the parameters was used in the TALYS-1.8 code to calculate the cross sections of the ^{110}Pd (d,n)^{111}Ag and ^{110}Pd(d, 2n)^{110m}Ag reactions.

Sahan, et al. (2018) calculated the double-differential neutron emission cross sections for n+209Bi reactions at an incident energy of 14.2 MeV at angles from 15 to 150 degrees using the HMS-ALICE-2011, TALYS 1.6 simulation model codes based on the unified Hauser-Feshbach and exciton model.

Artun and Aytekin (2017) studied the production of medical radioisotopes $^{94m, 94g, 96m, 96g, 96, 99m}$Tc which some of which are used in SPECT and PET and investigated the excitation functions of proton-induced reactions on even-even $^{94-100}$Mo isotopes via proton-induced reactions. To obtain the excitation functions they carried out cross-section calculations in the frameworks of the generalized superfluid model, microscopic level density model, and three options of the preequilibrium process in the TALYS 1.6 code.

Guertin et al. (2017) presented experimental nuclear data collected in the framework of the production radionuclides for therapy and diagnosis applications in collaboration with the GIP ARRONAX, which possesses a multi-particle high-energy cyclotron. In order to assess the cross section of a given production route, experiments have been carried out for a set of radionuclides of medical interest: photon (Tc-99m) and positon (Sc-44g) emitters for diagnosis, electron (Re-186g, Tb-155, Sn-117m) and alpha particle (Th-226, Ra-233, Bi-213) emitters for therapeutic applications.

A systematic comparison has been performed between the results from the TALYS1.6 code at energy range up to 70MeV. A good agreement with experimental data has been obtained and the TALYS code.

Yalım et al., (2017), by using TALYS 1.6 nuclear reaction code with incident particle energy up to 50 MeV for copper radioisotopes ^{60,61,62,64,67}Cu that are used for various biomedical applications in diagnostic or therapeutic nuclear medicine, the excitation functions of copper radioisotopes have been investigated through the theoretical calculation of cross sections.

Kılınç et al. (2016), studied the cross section calculation of the (p, 2n) reaction, which is necessary for production of the nuclei of ^{57}Co, ^{111}In, ^{99m}Tc using TALYS 1.6 nuclear reaction code. This radioisotope are widely used in nuclear medicine and are successfully implemented in renal imaging.

Karpuz and Mavi (2016), this study was performed using Monte Carlo nuclear reaction simulation code TALYS 1.6 to obtain radiopharmaceuticals Tl-201 and Tc-99m which are used in myocardial perfusion scintigraphy imaging technique, which are used for diagnostics of coronary artery disease in people by evaluating the amount of blood reaching the heart muscle.

Kılınç et al (2016), calculated the theoretical cross section of some radioisotopes used in medicine. The calculation was done using Monte Carlo code of TALYS 1.6 in the energy range between 0.5 and 100 MeV for ^{13}N ^{18}F radioisotopes, via the ^{12}C(d,n)^{13}N, ^{20}Ne(d,α)^{18}F and ^{16}O(3He,p)^{18}F reactions.

Kılınç (2016), using TALYS 1.6 nuclear simulation code, (p,n) reaction cross sections of some radionuclides used in the PET imaging ^{61}Cu, ^{66}Ga, ^{76}Br, were calculated for reactions in the energy range between 1 and 100 MeV. By ^{61}Ni (p,n) ^{61}Cu, ^{66}Zn (p,n) ^{66}Ga and ^{76}Se (p,n) ^{76}Br reactions.

Nasrabadi et al. (2015), studied simulation of excitation functions and nuclear reaction mechanisms in the TALYS, EMPIRE & LISE++ reaction codes, for production of most widely used ^{64}Cu and ^{67}Ga radioisotopes that have been used as a

very interesting and powerful tracer for imaging by positron emitting tomography (PET) at last years.

Duchemin et al. (2015), have measured reaction cross section using a thorium target irradiated by light charged particles (protons and deuterons) leads to the production of several isotopes ^{225}Ac, ^{227}Th, ^{230}Pa, ^{99}Mo, ^{115g}Cd, ^{131}I of medical interest. The experimental cross section data compared with the calculated data were carried out by TALYS 1.6 code.

Salman et al. (2015), by using TALYS 1.6 and in energy range of 5–40 MeV, the reaction cross-sections of charged particle-induced reactions that leading to ^{75}Br radioisotope were calculated. ^{75}Br is a positron emitter and is useful in positron emission tomography (PET) for fast metabolic processes.

Kara et al. (2015), they calculated production cross sections Indium-111 that is one of the most useful radioisotopes used in nuclear medicine via ^{111}Cd(p,n), ^{112}Cd(p,2n), ^{113}Cd(p,3n), ^{114}Cd(p,4n) nuclear reactions up to 60 MeV energy. By using ALICE/ASH, TALYS 1.6 and EMPIRE 3.2 nuclear reaction code.

Azzam et al. (2014), obtained Lead radioisotope ^{203}Pb used in medicine experimentally by using medium size cyclotrons and theoretically by used the models TALYS 1.4, and EMPIRE 3.1 to construct the excitation functions for protons, deuterons, helium-3 and helium-4 induced reactions on Tl and Hg targets.

Eslami and Kakavand (2014), studied the direct production of ^{99m}Tc radioisotope by charged particle irradiation using Monte Carlo method. After scouting of the reactions that produce ^{99m}Tc, excitation functions of these reactions were predicted by optical model components in the TALYS-1.6 code. This study demonstrated that Monte Carlo provides a method for the design and optimization of targets for the radionuclide production purposes.

Braghirolli et al. (2014), reviewed and summarized the recent advances in ^{124}I radionuclide production and medical use in PET technology application. Its applications range from simple imaging of the thyroid and parathyroid to functional

studies of neurotransmitter receptors, through monoclonal antibodies for the study of cancer. ^{124}I has furthermore been used to label molecules such as fatty acids, and fibrinogen, allowing the study of diseases of different organs such as brain and heart. Moreover, the labeling chemistry for ^{124}I is well established, and wide varieties of compounds have been labeled for molecular imaging purposes with PET.

Webster et al. (2014), theoretical cross-sections were generated using TALYS to produced three medically important radionuclides ^{89}Zr, ^{64}Cu, and ^{103}Pd with activity yields suitable for medical diagnostics and therapy via the ^{89}Y(p,n), ^{64}Ni(p,n) and ^{103}Rh(p,n) reactions, respectively at a proton energy of 10 MeV.

Sadeghi et al. (2012), presented a experimental method for the production of Iodine-124 using a cyclotron. In an amounts of 124I with high chemical and radionuclides purity for both diagnostic and therapeutic applications. and they calculated excitation functions via ^{124}Te(p,n)^{124}I, ^{125}Te(p,2n)^{124}I, ^{126}Te(p,3n)^{124}I, ^{124}Te(d,2n)^{124}I, ^{121}Sb(a,n)^{124}I and ^{nat}Te(p,xn)^{124}I reactions by ALICE/ASH and TALYS codes and compared it to existing data. Theoretical calculation of production yield and calculation of target thickness requirement were obtained by TALYS and SRIM codes for each reaction.

Tel et al. (2011), studied the newly calculations of proton induced production cross sections in some PET, SPECT and others used in medical applications for some radioisotopes used in medical applications like ^{18}F, ^{57}Co, ^{54}Mn, ^{67}Ga, ^{68}Ga, ^{90}Mo, ^{111}In, ^{125}Xe, ^{128}Ba and ^{201}Pb were investigated in a range of 5–100 MeV incident proton energy range. In addition, Excitation functions for pre-equilibrium calculations were newly calculated by using hybrid model, geometry dependent hybrid (GDH) model.

Al-Abyad (2011), He studied excitation function related to the production for some medical radioisotopes such as ^{123,124}I, ^{67,68}Ga and ^{111}In and calculated for statistical and preequilibrium models. Excitation functions of these routes were calculated by using EMPIRE-03 and TALYS codes. The reactions were investigated in the energy range from threshold up to 30 MeV.

3. MATERIALS AND METHOD

In nuclear physics and medical science, the cross sections formed by neutrons, photons, protons, deuterons, ^{3}He and alpha particles are particularly important. Changes may occur during the formation of such reactions which may affect the structure of the materials. In order to understand the importance of these problems and to solve the problems, it is necessary to measure the cross sections experimentally but theoretical calculations should be done in advance. For example, the importance of the theoretical calculations is to see which energy range of sending particle can be the maximum cross-section, or in which range the particle must be sent. In particular, data are needed to optimize a production process, i.e. to maximize the yield of the desired product and to minimize the level of radionuclides impurities.

Among Monte Carlo computer nuclear model codes applications (TALYS, ALICE, GNASH, EMPIRE etc.) solving complex problems, simulating experimental designs and are useful in predicting experimental results before the experiment carried out. In this work nuclear simulation code program TALYS 1.6 are used for calculations of total cross section, differential cross section and double differential cross section.

3.1. TALYS Code

In this thesis, the cross sections calculations were done using nuclear reaction simulation code program. For this purpose, TALYS 1.6 Monte Carlo simulation code program is used.

TALYS is a computer code system programming with Fortran language working in Linux operating system and developed for the prediction and analysis of nuclear reactions. The basic objective behind its construction is the simulation of nuclear reactions that involve neutrons, photons, protons, deuterons, tritons, helium-3 and alpha-particles, in the 1 keV - 200 MeV energy range and for target nuclides of mass 12 and heavier. To achieve this, we have implemented a suite of nuclear reaction models into a single code system. This enables us to evaluate nuclear reactions from the unresolved resonance range up to intermediate energies.

In TALYS output files, elastic and inelastic and total cross section, elastic scattering angular distributions, angular distributions at cut-off levels, Isomeric and ground state effect cross section, double differential cross sections, single or multiple emission cross sections, results of formation cross section can be obtained for product nucleus. Important applications that rely directly or indirectly on data generated by nuclear reaction simulation codes like TALYS are: conventional and innovative nuclear power reactors (GEN-IV), transmutation of radioactive waste, fusion reactors, accelerator applications, homeland security, medical isotope production, radiotherapy, single-event upsets in microprocessors, oil-well logging, geophysics and astrophysics.There are twomain purposes of TALYS, which are strongly connected. First, it is a nuclear physics tool that can be used for the analysis of nuclear reaction experiments. The second namely as a nuclear data tool (Koning et al, 2013).

3.1.1. Optical model

During the last forty years the nuclear optical model has been extensively applied to analyse the elastic scattering of pions, nucleons and heavier particles by nuclei over a wide range of energies. It has been extended to include inelastic scattering by the coupled-channels formalism and consideration of dispersion effects enables both bound and scattering states to be described by the same mean field (Hodgson, 1963) (Boffi and Passatore, 1976).

The central assumption underlying the optical model is that the complicated interaction between an incident particle and a nucleus can be represented by a complex mean-field potential, which divides the reaction flux into a part covering shape elastic scattering and a part describing all competing non-elastic channels. Solving the Schrödinger equation numerically with this complex potential yields a wealth of valuable information. First, it returns a prediction for the basic observables, namely the elastic angular distribution and polarization, the reaction and total cross section and for low energies, the s, p-wave strength functions and the potential scattering radius R'. The essential value of a good optical model is that it can reliably predict these quantities for energies and nuclides for which no measurements exist. Also, the quality of the not directly observable quantities that are provided by the

optical model has an equally important impact on the evaluation of the various reaction channels. Well-known examples are transmission coefficients, for compound nucleus and multi-step compound decay, and the distorted wave functions that are used for direct inelastic reactions and for transitions to the continuum that describe statistical multi-step direct reactions. Also, the cross sections that are calculated with the optical model are crucial for the semi-classical pre-equilibrium models (Koning et al, 2013).

3.1.2. Pre-equilibrium model

The pre-equilibrium mechanism depends on the mass of the target nuclei and on the excitation energy of the compound system. The pre-equilibrium process occurs after the first phase of reactions. This pre-equilibrium state continues until the statistical equilibrium of the compound nuclei. In pre-equilibrium processes a part of the reaction flux is emitted in the pre-equilibrium stage, i.e. it takes place after the first stage of the reaction but long before statistical equilibrium of the compound nucleus is attained. It is imagined that the incident particle step-by-step creates more complex states in the compound system and gradually loses its memory of the initial energy and direction (Koning, and Rochman, 2012). Pre-equilibrium processes cover a sizable part of the cross section for incident energies between 10 and (at least) 200 MeV. Pre-equilibrium reactions have been modeled both classically and quantum-mechanically and both are included in TALYS.

Pre-equilibrium plays an important role in nuclear reactions induced by light projectiles with incident energies above 8–10 MeV. Starting with the introduction of pre-equilibrium reactions, a series of semiclassical models of varying complexities have been developed for calculating and evaluating particle emissions in the continuum (Aydin et al, 2010). Several models have been proposed to explain the emission of energetic light particles by the equilibration process (pre-equilibrium emission) from the nuclear system excited at medium energies (Ismail, 1989).

The default pre-equilibrium model of TALYS is the two-component exciton model, which has been tested against basically all available experimental nucleon spectra for A > 24 (Koning and Duijvestijn, 2004).

3.2. Radioisotope Production and Applications

There are many uses of radiation or radioactive material in medicine. These are for treatment of disease or cancer and are commonly called therapy. A subspecialty in nuclear medicine is nuclear medicine therapy. In areas cardiology, neurology, and oncology.

In the last decade, a big success has been provided on production and usage of the radioisotopes. Medical and industrial radioisotopes are produced using nuclear reactors and cyclotrons. Commercially, cyclotrons are widely used as accelerators for production radioisotopes that uses in Single Photon Emission Computed Tomography (SPECT) and Positron Emission Tomography (PET). Both PET and SPECT radioisotopes are obtained as a result of bombardment of targets in solid, liquid or gaseous form with accelerated charged particles or ions (proton, deuteron, alpha ^3H, ^3He, etc.) from the cyclotron. which play an important role in medical applications.

A medical radioisotope can be classified as a diagnostic or a therapeutic radionuclide, depending on its decay properties. Radioisotope are used in diagnostic studies via emission tomography, i.e. Positron Emission Tomography (PET), Single Photon Emission Computed Tomography (SPECT), and Endoradiotheraphy (internal therapy with radio nuclides).

3.2.1. Radioisotopes used in (PET) and (SPECT)

Radiohalogens play a very important role in radiopharmaceuticals used for medical imaging (now referred to as molecular imaging) and therapy applications. The positron-emitting radiohalogens ^{18}F, ^{124}I, ^{75}Br and ^{76}Br are reviewed regarding their relevance for positron emission tomography (PET) and in Single Photon Emission Computed Tomography (SPECT) in oncology (Glaser et al., 2003).

Fluorine-18 with (110 min) half life produced in cyclotron is a positron emitters used in PET. It used in the care of patients with soft tissue sarcomas to predict malignant potential of tumors, F-18 in FDG (fluorodeoxyglucose) has become very

important in detection of cancers and the monitoring of progress in their treatment, using (PET). Once injected into the body, it will go to places where glucose is used for energy. For instance, the brain uses glucose as its primary source of energy, and so FDG will go to the brain, and in particular, to those parts of the brain that are actively burning glucose for energy which is preferentially taken up by brain and cancer cells making an ideal tool for detecting tumors and also to map brain function and the diagnosis of conditions such as Alzheimer's disease (Cole et al. 2014; Pahk et al. 2015).

Radionuclides of **Iodine** are widely used in nuclear medicine to label monoclonal antibodies, and measurement of biologic processes at the molecular and cellular levels in human beings and other living systems. In patients with advanced differentiated thyroid carcinoma (DTC), this includes imaging iodine transport, and because success or failure of therapy depends on the degree of iodine uptake by the tumor cells which is active in about 80% of well-differentiated thyroid malignancies.

In diagnostic and therapeutic applications, quantitative imaging over a period of several days is necessary. ^{124}I is the only long-life positron emitter isotope of iodine, which can be used both for diagnosis and a therapy, remain the most frequently used radionuclides for thyroid imaging. ^{124}I used in (PET) applications and it attracting increasing interest for long-term clinical studies. With availability high quality of (PET) technology, warrant an actual role in thyroid cancer imaging, as well as promising applications in neurology and oncology. Because of ^{124}I long half life (4.2 d), could permit quantitative imaging over several days using PET. Which makes ^{124}I is ideal for this purpose because (PET) provides tomographic images with spatial and contrast resolution. in addition stability, and radiation emissions, this permitted to use in several applications in oncological and non oncological fields.

The positron-emitting radiohalogens **Bromine-**75 ($T_{1/2}$ = 96.7 min) and ^{76}Br ($T_{1/2}$ = 16.2 h) are reviewed regarding their relevance for positron emission tomography (PET) and (SPECT). in oncology. these cyclotron-generated isotopes ^{76}Br was used in studies of monoclonal antibody kinetics, which requires a radionuclide with a longer half-life than the standard PET nuclides, and in brain tumors. the cyclotron

production of ^{75}Br requiring a relatively high beam energy which is available only in a few centres (Ribeiro et al., 1999; Glaser et al., 2003).

Technetium-94m (T$_{1/2}$= 4.88 h) is used in (PET) to study brain tumors, cerebral perfusion, detect blood brain barrier defect, as well as imaging, bone, pulmonary, myocardial and also hepatobiliary and renal function. **Technetium**-99m (T$_{1/2}$= 6 h) is a widely used radioisotope in nuclear medicine. That is used in tens of millions of medical diagnostic procedures annually, making it the most commonly used medical radioisotope. its half-life make it an ideal isotope for single photon emission computed tomography (SPECT) It can be used for imaging a variety of ailments such as impeded blood flow to the heart, the spread of cancer to bones, liver disease (gastroenterology), lungs, kidney imaging and early diagnosis of Alzheimer's disease.

As for the **Cobalt**-57 (T$_{1/2}$ = 272 d) is applied in various studies as a radioactive tracer. ^{57}Co with Vitamin B 12 (albumin) labeled is used in diagnostic kits to study anemia. In addition, ^{57}Co is a useful Mossbauer radioisotope, its use as a calibration standard for gamma-spectrometers and single photon emission tomography (SPECT) is the most general use. Moreover, is used too in medicine to help detect cancerous tumors. It is also used as a component in the medical equipment's studying the chemical properties of various materials or testing the response of gamma cameras (Spellerberg et al., 1998; Mastren et al., 2015)

Manganese-50 (T$_{1/2}$ = 283.29 ms) human body use manganese it aids in the formation of connective tissue, bones, blood-clotting factors, and sex hormones and plays a role in fat and carbohydrate metabolism, calcium absorption, and blood sugar regulation. Manganese is also necessary for normal brain and nerve function.

Carbon-11 radioisotope (T$_{1/2}$ = 20.34 min) it's primarily use is for the early diagnosis of cancer, monitoring therapeutic response to cancer treatment, and pharmacokinetic investigations of anticancer drugs. (PET) imaging permits monitoring of metabolic processes and molecular targets, Identifies possible risk of prostate cancer, help locate tumors, a tracer used in the study of myocardial

metabolism, used to study metabolism, also used to scan: brain, head, neck, lung, breast cancer, and lymphomas (Grassi et al., 2012).

Nitrogen-13 ($T_{1/2}$ =10 min) labelled amines are of interest for improving positron emission tomography (PET). These are positron emitters used in PET for studying brain physiology and pathology, in particular for localising epileptic focus, and in dementia, psychiatry and neuropharmacology studies. Also used for assessing myocardial blood perfusion in the evaluation of coronary artery diseasecardial perfusion imaging and representing metabolism (Phillips, 1994).

Copper-64 radioisotope ($T_{1/2}$ = 12.7 h) is an important positron-emitting radionuclide for (PET) and used in nuclear medicine for diagnosing tumors. It has several advantages, including the fact that it can be readily produced with an in-hospital small cyclotron and can be used not only for imaging but also has a large applications in internal radiation therapy. ^{64}Cu is important in the treatment planning, diagnosis, and evaluation of the treatment response in patients with cancer. And also diagnosis of human copper-associated diseases such as atherosclerosis, Alzheimer's. It is also used in diagnose the blood supply to the kidney, in studies radiation doses measuring in diagnostic imaging, and in colorectal cancer treatment. As this isotope is a positron emission radioisotope, it is known as a particularly effective radioisotope in (PET) imaging study (Obata et al., 2003; Noori et al., 2017).

The use of positron emission tomography (PET) for radionuclide imaging provides better sensitivity, better spatial and temporal resolution and better quantification accuracy in comparison with single photon emission computed tomography (SPECT). One limitation of (PET) is the predominant use of short-lived (with half-life up to 2 h) radionuclides. Extension of (PET) utility might be achieved by the use of more long-lived, "non-conventional" positron emitters.

4. RESULTS AND DISCUSSION

In order to investigate the possibility of producing radioisotopes used in diagnosis and treatment, total cross sections, differential cross sections and double differential cross sections were calculated by using TALYS 1.6 program and compared with experimental data taken from the Experimental Nuclear Reaction Data EXFOR library. EXFOR libraries are a very powerful database.

4.1. Total Cross Sections

4.1.1. Fluorine-18 production reactions

In this study of the nuclear reactions $^{16}O(^{3}He,p)^{18}F$, $^{18}O(p,n)^{18}F$, $^{19}F(g,n)^{18}F$, $^{19}F(n,2n)^{18}F$, $^{20}Ne(^{3}He,x)^{18}F$, $^{21}Ne(p,a)^{18}F$, $^{20}Ne(d,x)^{18}F$, $^{19}F(p,n+p)^{18}F$, the cross sections were calculated using TALYS 1.6, and the results were compared with the experimental data available in EXFOR library and displayed in Figures 4.1-4.8.
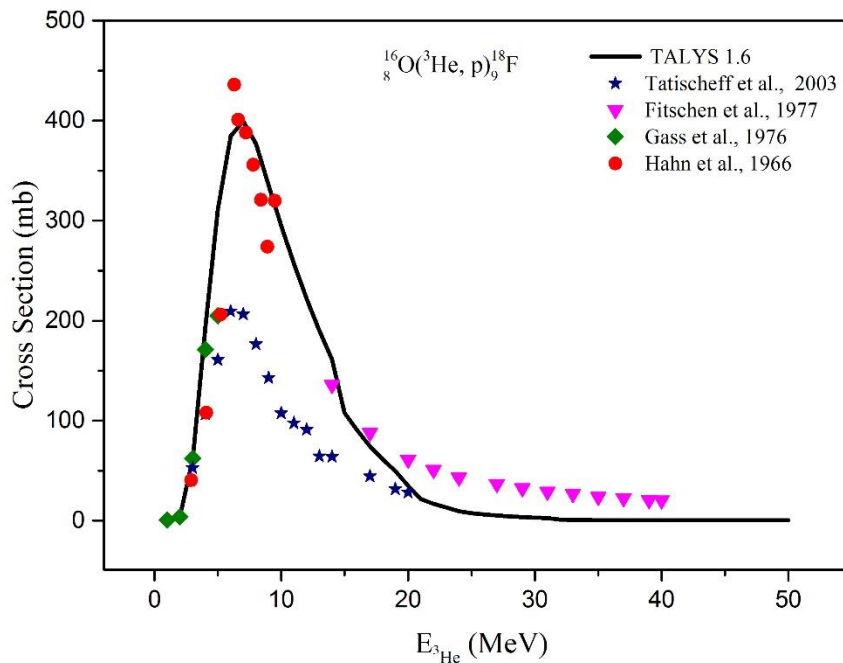
Figure 4.1. Total cross section for $^{16}O(^{3}He, p)^{18}F$ reaction and comparsion with experimental data
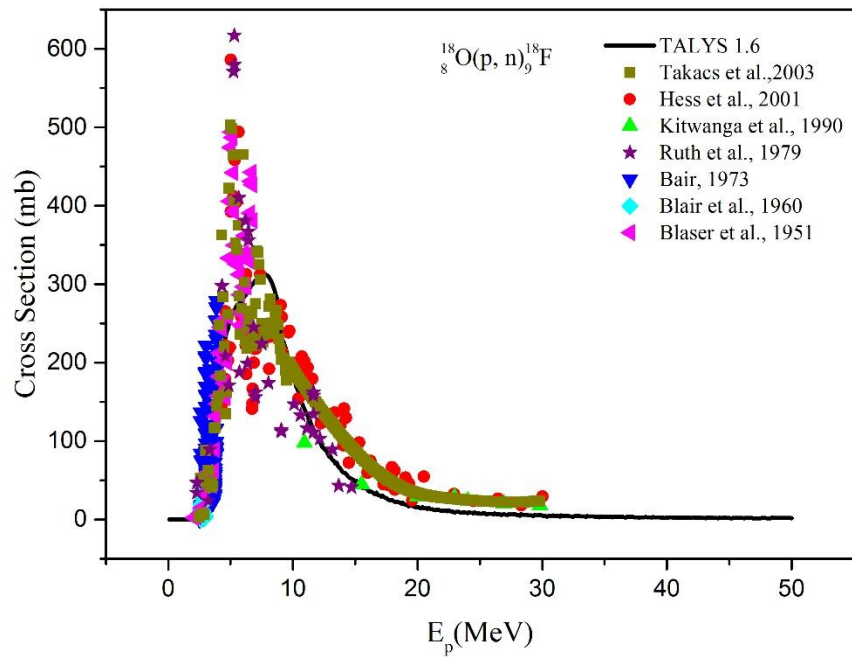
Figure 4.2. Total cross section for $^{18}O(p, n)^{18}F$ reaction and comparsion with the experimental data
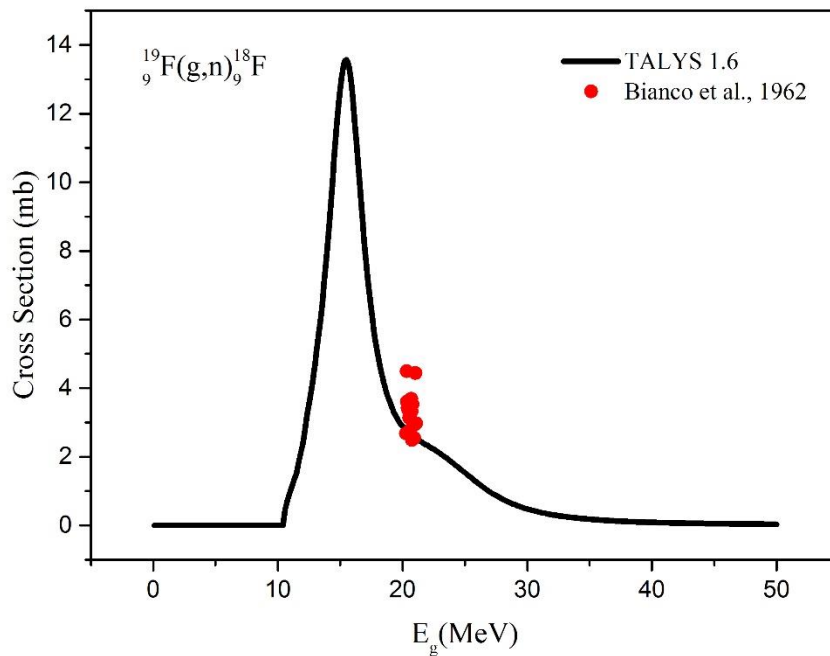
Figure 4.3. Total cross section for $^{19}F(g, n)^{18}F$ reaction and comparison with the experimental data
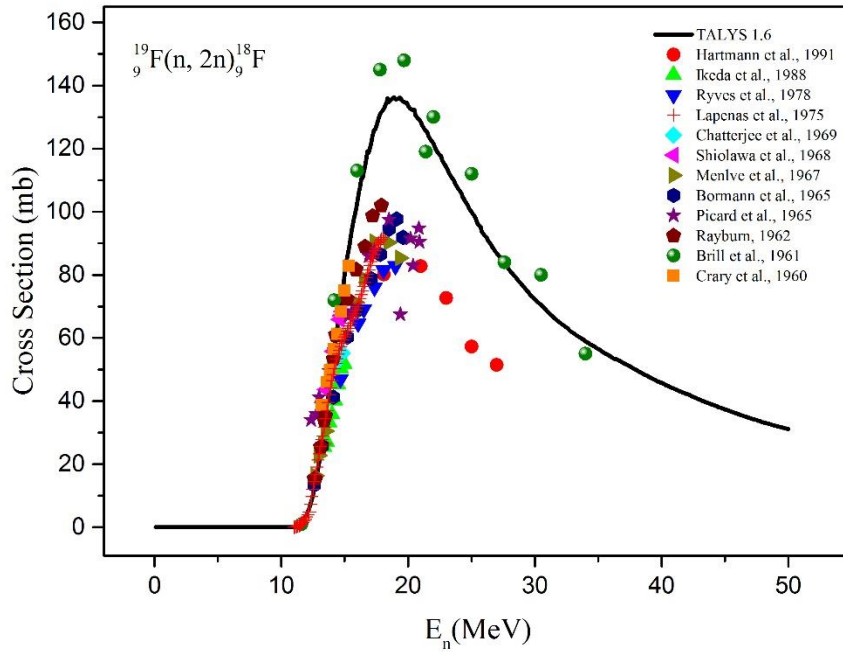
Figure 4.4. Total cross section for $^{19}F(n, 2n)^{18}F$ reaction and comparison with the experimental data
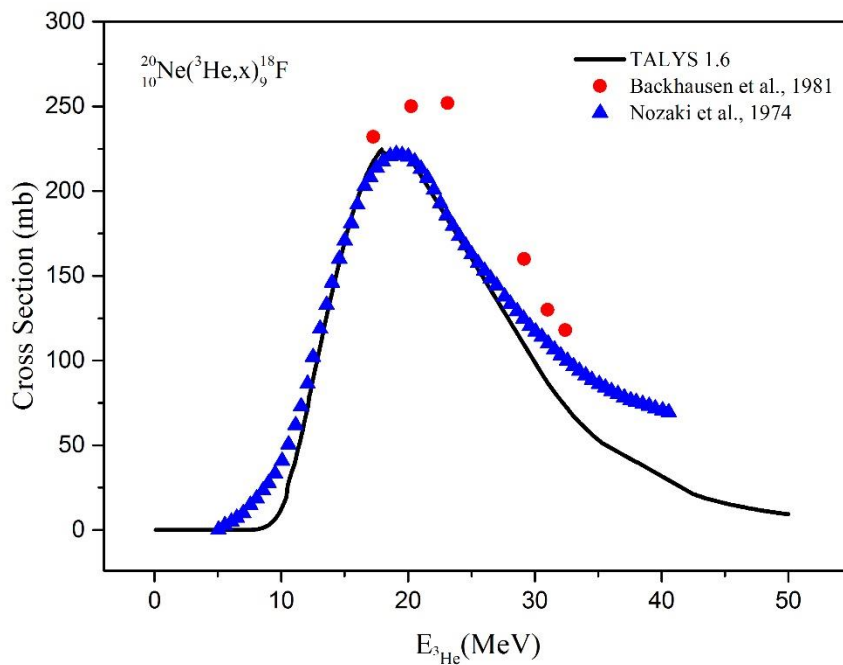
Figure 4.5. Total cross section for $^{20}Ne(^{3}He, x)^{18}F$ reaction and comparsion with the experimental data
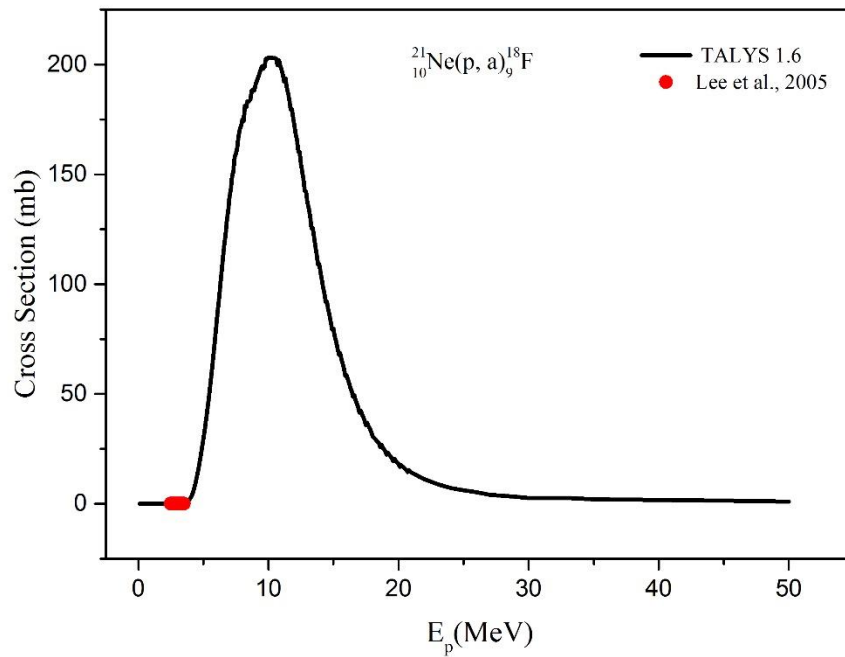
Figure 4.6. Total cross section for ^{21}Ne(p, a)^{18}F reaction and comparison with the experimental data
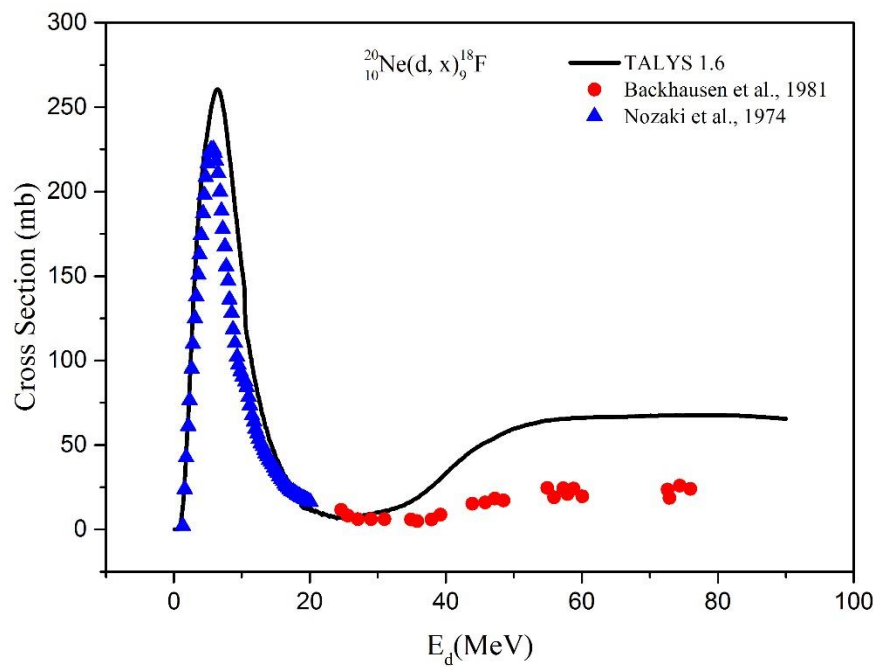
Figure 4.7. Total cross section for ^{20}Ne(d, x)^{18}F reaction and comparison with the experimental data
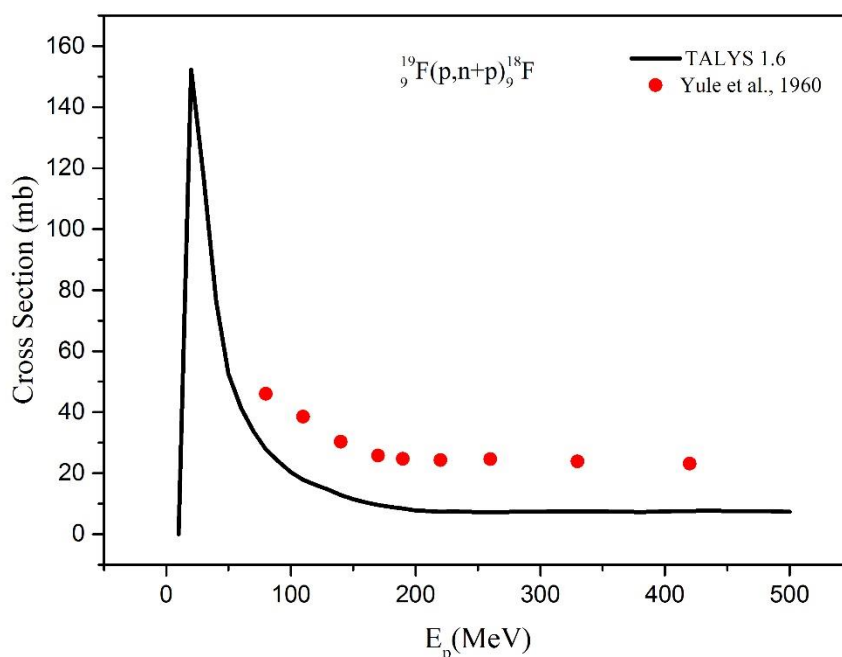
Figure 4.8. Total cross section for $^{19}F(p, n+p)^{18}F$ reaction and comparison with the experimental data

In this study, the use of cyclotron-mediated medical radioisotopes known as PET radioisotope was investigated. The theoretical calculated total cross sections of ^{18}F radioisotope used in the nuclear medicine of $^{16}O(^{3}He,p)^{18}F$, $^{18}O(p,n)^{18}F$, $^{19}F(g,n)^{18}F$, $^{19}F(n,2n)^{18}F$, $^{20}Ne(^{3}He,x)^{18}F$, $^{21}Ne(p,a)^{18}F$, $^{20}Ne(d,x)^{18}F$ and $^{19}F(p, n+p)^{18}F$ reactions were displayed and compared with available experimental data in EXFOR library in Figures 4.1-4.8.

In Figure 4.1 theoretical cross section compared with experimental data available in literature performed by Hahn et al. (1966), Filschen et al. (1977), Gass et al. (1976) and Tatischeff et al. (2003). From the comparison, it is noted the experimental value performed by Hahn et al. (1966) is in a good agreement with present calculated results from 3 MeV to 9.5 MeV. Regarding Filschen et al. (1977) data available in this study between 14 MeV to 40 MeV, it is consistent with current results. Gass et al. (1976) they presented in their studies experimental data between 1-5 MeV and they are exactly identical to calculated results. As for Tatischeff et al. (2003) the data show a similar pattern, and the size of the cross section is approximately 50% different.

41

For $^{18}O(p, n)^{18}F$ reaction as shown in Figure 4.2 a good agreement is observed between present calculations cross sections results and experimental data made by Hess et al. (2001), Kitwanga et al (1990), Bair (1973), Blair et al. (1960), Blaser et al. (1951), Takas et al (2003) and Ruth et al (1979).

As for nuclear reactions $^{19}F(g,n)^{18}F$ in Figure 4.3, $^{21}Ne(p,a)^{18}F$ in Figure 4.6 and $^{19}F(p, n+p)^{18}F$ in Figure 4.8 when comparing the calculated cross section and experimental data to obtaine ^{18}F, there are only one previous experimental study per reaction which made by Bianco et al. (1962), Lee et al. (2005) and Yule et al. (1960) respectively. Therefore, the theoretical calculations of ^{18}F production in this study helps to do other experiments for these reaction.

As can be seen in Figure 4.4, for $^{19}F(n, 2n)^{18}F$ reaction it can be said that the cross section results calculated with the TALYS 1.6 code shows a similar pattern with experimental data from literatures. In addition to that the literatures data are in complete agreement with the cross sections that they have achieved in their experimental work and it is lower than current calculation about 30%. Except Brill et al. (1961) their data are consistent with the current calculations.

$^{20}Ne(^{3}He, x)^{18}F$ reaction in Figure 4.5 and $^{20}Ne(d, x)^{18}F$ reaction in Figures 4.7 show a good agreement between the theoretical calculation and experimental data reported by Bakhausen et al. (1981) and Nozaki et al. (1974) except the experimental data made by Bakhausen et al. (1981) which are lower than the calculated results. From the calculation of cross sections of ^{18}F radioisotope production the optimum energy range, threshold energy (E-threshold) and Q-values of each reaction are shown in table 4.1.

Table 4.1. Optimum energy range, the average cross section of these energies, E-threshold and Q-values for ^{18}F production

Reactions	Optimum energy range (MeV)	Average cross section (mb)	E-threshold (MeV)	Q-values (MeV)
^{16}O(^{3}He,p)^{18}F	$E_h = 5 \to 10$	$311 \to 350$	0.00000	2.03198
^{18}O(p,n)^{18}F	$E_p = 4 \to 10$	$183 \to 205$	3.64964	-2.51902
^{19}F(g,n)^{18}F	$E_g = 14 \to 17$	$9 \to 11$	11.4131	-10.4759
^{19}F(n,2n)^{18}F	$E_n = 15 \to 22$	$90 \to 120$	11.0321	-10.4759
^{20}Ne(^{3}He,x)^{18}F	$E_h = 13 \to 22$	$106 \to 170$	3.21072	-2.78985
^{21}Ne(p,a)^{18}F	$E_p = 8 \to 14$	$150 \to 170$	1.82436	-1.74083
^{20}Ne(d,x)^{18}F	$E_d = 3 \to 9$	$165 \to 190$	0.00000	2.70364
^{19}F(p,n+p)^{18}F	$E_p = 20 \to 30$	$110 \to 130$	-10.4759	11.0313

4.1.2. Iodine-124 production reactions

In this study, the use of cyclotron-mediated medical radioisotope, known as PET radioisotope was investigated. The total cross section were calculated using nuclear reaction simulation TALYS 1.6 codes for ^{127}I(g,3n)^{124}I, ^{121}Sb(a,n)^{124}I, ^{123}Sb(a,3n)^{124}I, ^{123}Te(d,n)^{124}I, ^{124}Te(p,n)^{124}I, ^{125}Te(p,2n)^{124}I, ^{126}Te(p,3n)^{124}I reactions. The results were compared with the experimental data available in EXFOR library and displayed in Figures 4.9-4.15.
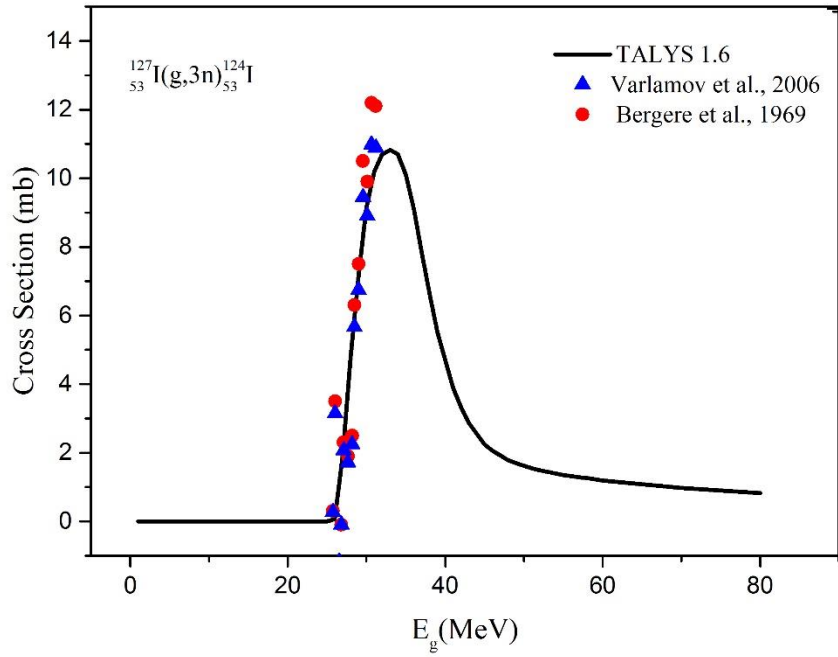
Figure 4.9. Total cross section for ^{127}I(g, 3n)^{124}I reaction and comparison with the experimental data
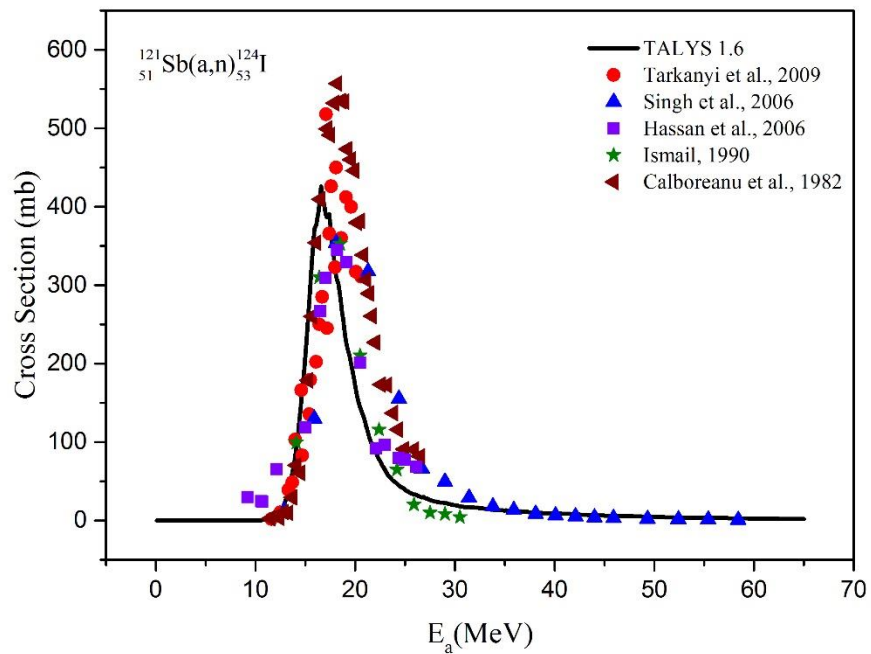
Figure 4.10. Total cross section for ^{121}Sb(a, n)^{124}I reaction and comparison with the experimental data
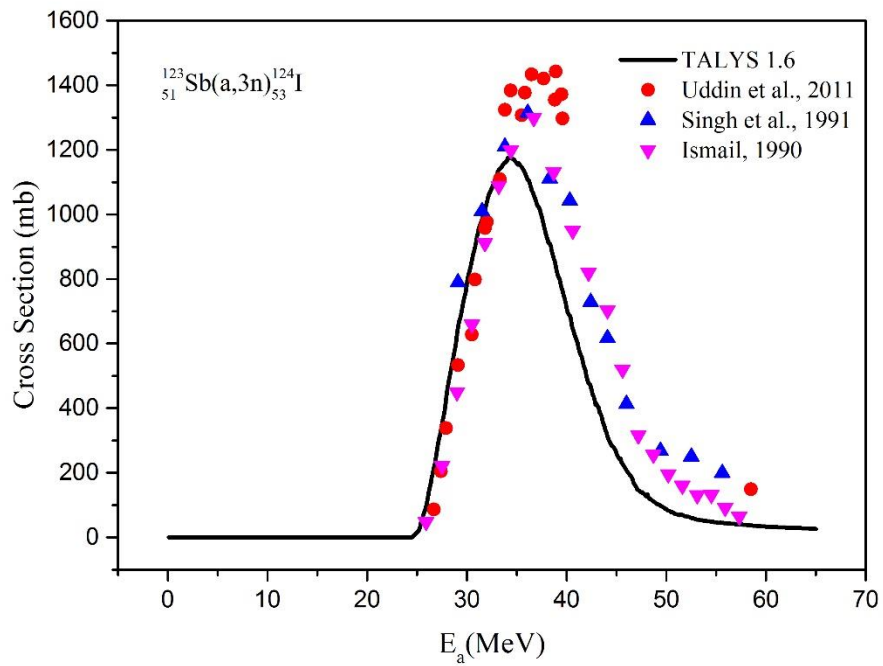
Figure 4.11. Total cross section for ^{123}Sb(a, 3n)^{124}I reaction and comparison with the experimental data
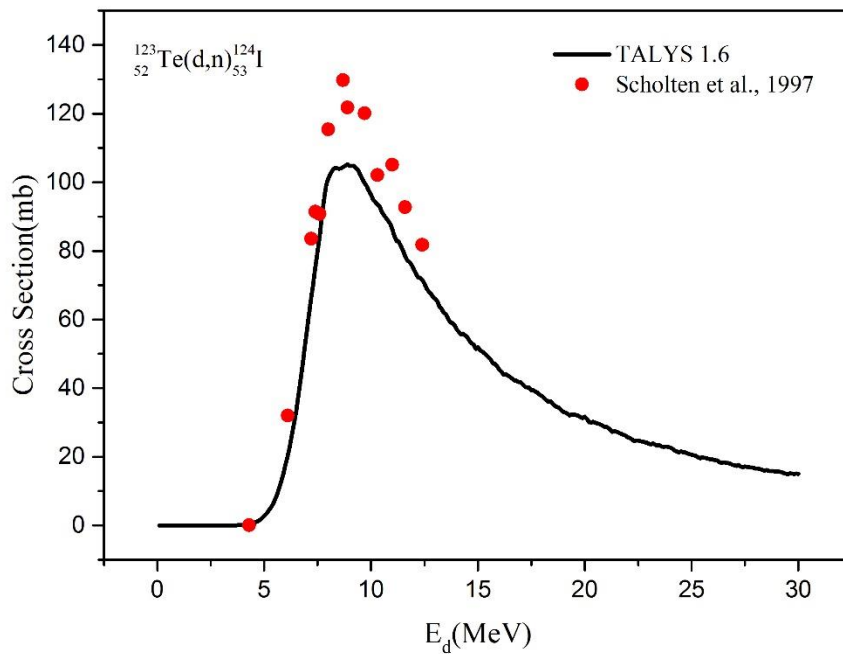
Figure 4.12. Total cross section for ^{123}Te(d, n)^{124}I reaction and comparsion with the experimental data
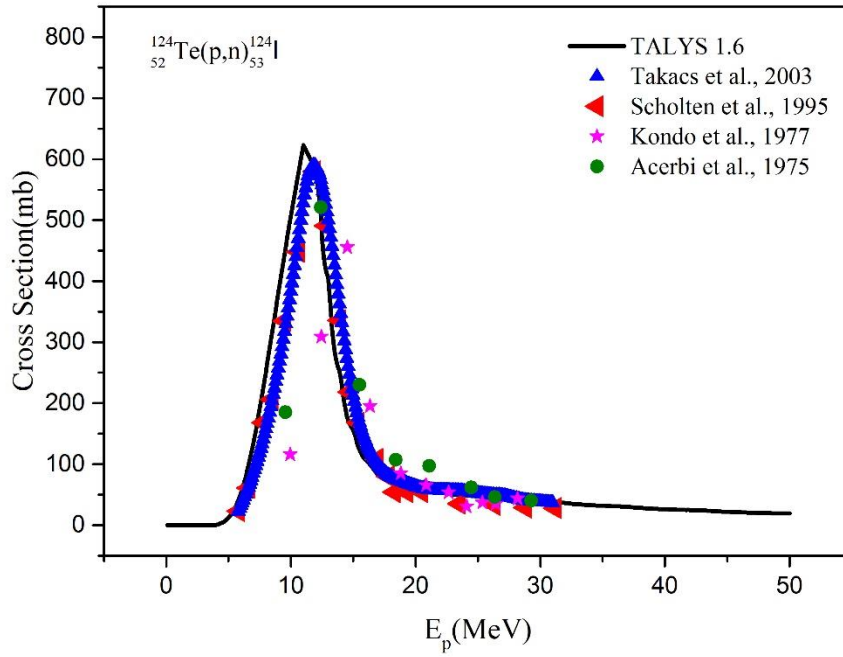
Figure 4.13. Total cross section for ^{124}Te(p, n)^{124}I reaction and comparsion with the experimental data
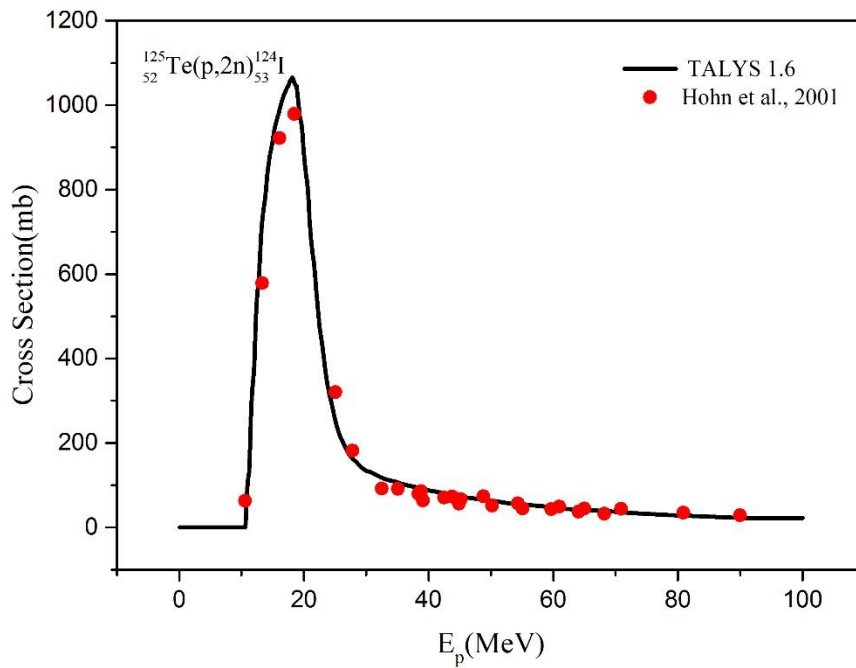
Figure 4.14. Total cross section for ^{125}Te(p, 2n)^{124}I reaction and comparsion with the experimental data
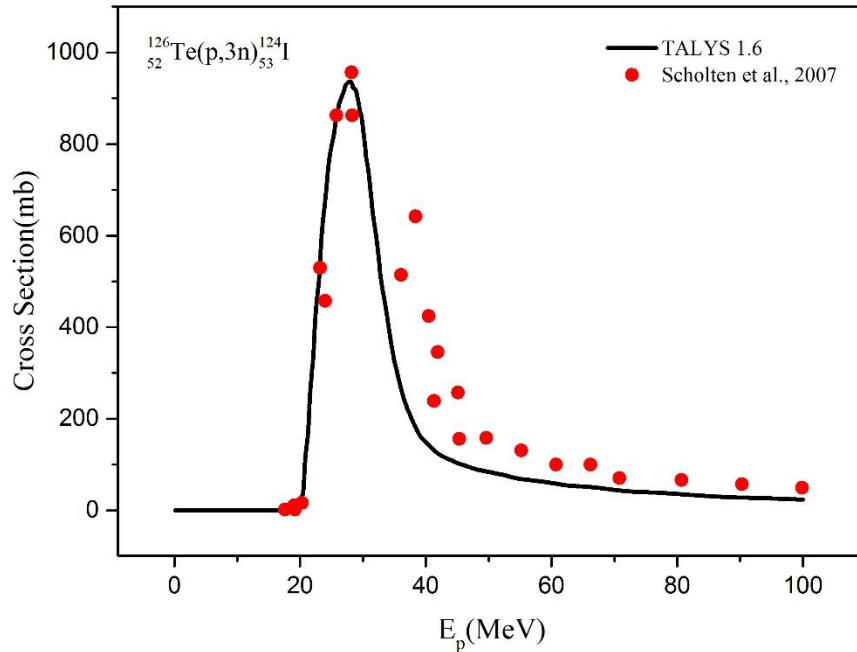
Figure 4.15. Total cross section for ^{126}Te(p, 3n)^{124}I reaction and comparison with the experimental data

When the calculated cross-sections to produce ^{124}I radioisotope are examined, for ^{127}I(g,3n)^{124}I reaction in Figure 4.9 and compared with experimtal data reported by Bergere et al. (1969) and Varlamov et al. (2006) we noted that there are no practical data in their studies after 31.2 MeV and the calculated results is in agreement with availible experimental data before this energy.

The theoretical calculated cross section and experimental data which made by Tarkanyi et al. (2009), Singh et al. (2006), Ismail (1990), Calboreanu et al. (1982), Hassan et al. (2006) for ^{121}Sb(a,n)^{124}I reaction are displayed in Figure 4.10. By the comparison we observe that the experimental data and the theoretical cross section calculations were harmonious. With very well matched at energies between 12-18 and 34-58.4 MeV and with a small shift to the right in the peak region about 2 MeV.

In Figure 4.11 the experimental and theoretical cross section calculations are compared for ^{123}Sb(a,3n)^{124}I reaction. It is seen to be compatible up to 35 MeV between theoretical calculation and literature's data made by Uddin et al. (2011), Singh et al. (1991) and Ismail (1990). After this energy value, they have higher

experimental data than the calculated results. Also a good match between theoretical and experimental value reported by Scholten et al. (1997) up to 7.5 MeV for ^{123}Te(d,n)^{124}I reaction shown in Figure 4.12. After this energy, the experimental data of the cross sections are higher than the calculated results.

In Figure 4.13 the experimental and theoretical cross section calculations are compared for ^{124}Te(p,n)^{124}I reaction. As seen calculated cross section and experiment data reported by Scholten et al. (1995), Takacs et al. (2003) and Aeerbi et al. (1975) are in a good agreement. While Knodo et al. (1977) data are lower than the theoretical results. For ^{125}Te(p,2n)^{124}I and ^{126}Te(p,3n)^{124}I reactions that shown in Figure 4.14 and 4.15 respectively.

When the theoretical cross section calculations and experimental that made by Hohn et al. (2001) are compared in Figure 4.14 we observe a very good agreement between them. As for ^{126}Te(p,3n)^{124}I reactions in Figure 4.15 the experimental data reported by Scholten et al. (2007) and the theoretical cross section calculations were in agreement in an acceptable manner. From the calculation of cross sections of ^{124}I radioisotope production the optimum energy range, threshold energy (E-threshold) and Q-values of each reaction are shown in table 4.2.

Table 4.2. Optimum energy range, the average cross section of these energies, E-threshold and Q-values for ^{124}I production

Reactions	Optimum energy range (MeV)	Average cross section (mb)	E-threshold (MeV)	Q-values (MeV)
^{127}I(g,3n)^{124}I	$E_g = 29 \rightarrow 38$	$8 \rightarrow 9$	25.8321	-25.8321
^{121}Sb(a,n)^{124}I	$E_a = 16 \rightarrow 18$	$325 \rightarrow 375$	8.19744	-7.87927
^{123}Sb(a,3n)^{124}I	$E_a = 31 \rightarrow 38$	$850 \rightarrow 950$	24.4183	-23.6482
^{123}Te(d,n)^{124}I	$E_d = 7 \rightarrow 12$	$80 \rightarrow 90$	0.0000	3.25798
^{124}Te(p,n)^{124}I	$E_p = 9 \rightarrow 13$	$400 \rightarrow 500$	4.02992	-3.94194
^{125}Te(p,2n)^{124}I	$E_p = 15 \rightarrow 21$	$800 \rightarrow 900$	10.5957	-10.5109
^{126}Te(p,3n)^{124}I	$E_p = 25 \rightarrow 32$	$700 \rightarrow 800$	19.97816	-19.6246

4.1.3. Bromine-75,76 production reactions

The total cross section was obtained in order to produce ^{75}Br and ^{76}Br radioisotopes using TALYS 1.6 via reactions of ^{74}Se(a,x)^{75}Br, ^{75}As(a,4n)^{75}Br, ^{75}As(^{3}He,3n)^{75}Br, ^{76}Se(d,3n)^{75}Br, ^{76}Se(p,2n)^{75}Br, ^{77}Se(p,3n)^{75}Br, ^{78}Se(p,4n)^{75}Br, ^{78}Kr(d,n+a)^{75}Br, and ^{74}Se(a,x)^{76}Br, ^{75}As(a,3n)^{76}Br, ^{75}As(^{3}He,2n)^{76}Br, ^{76}Se(p,n)^{76}Br, ^{77}Se(p,2n)^{76}Br, ^{78}Se(p,3n)^{76}Br and ^{78}Kr(d,a)^{76}Br respectively. The results were displaye in Figures 4.16-4.23 with the experimental data available in EXFOR library.
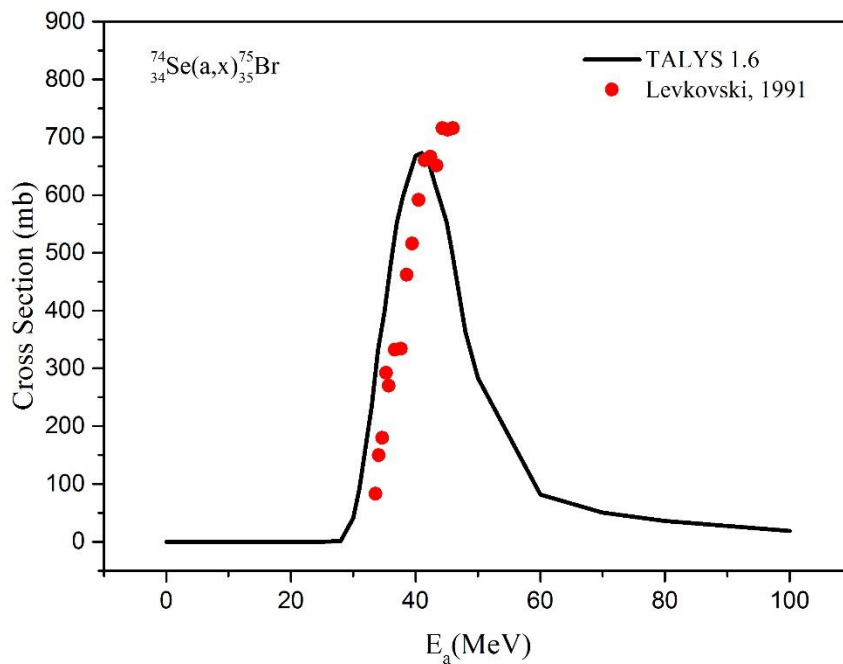
Figure 4.16. Total cross section for ^{74}Se(a,x)^{75}Br reaction and comparsion with the experimental data
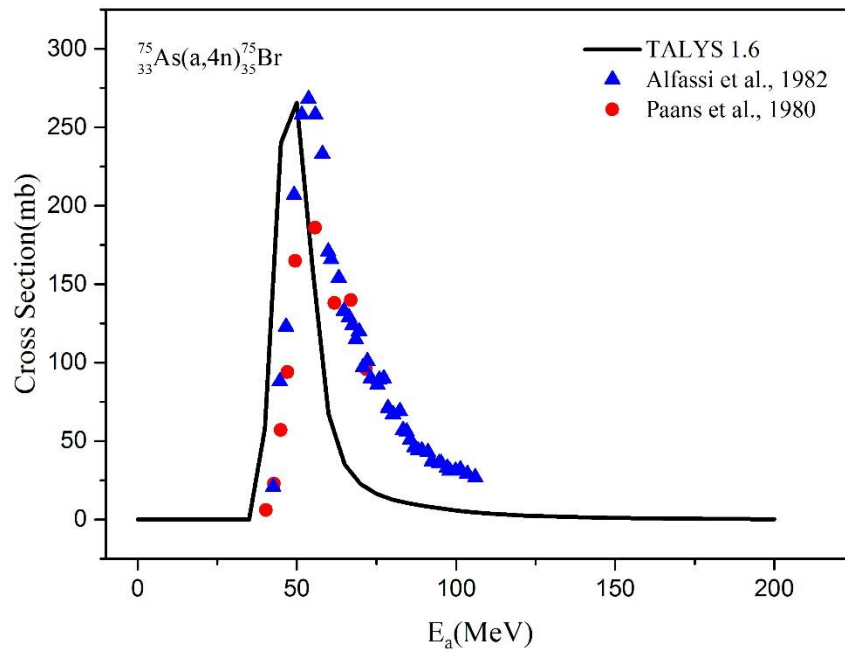
Figure 4.17. Total cross section for ^{75}As(a,4n)^{75}Br reaction and comparison with the experimental data
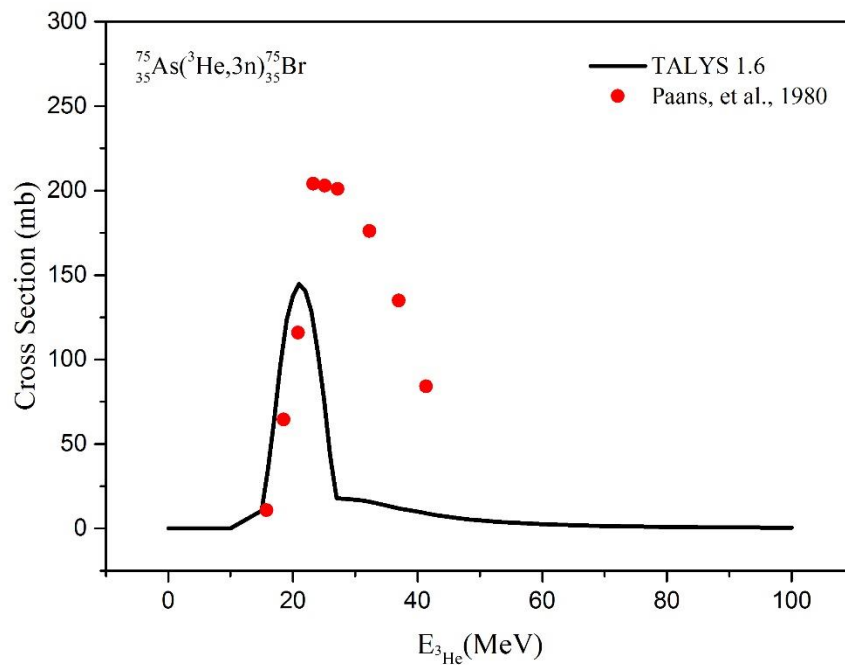
Figure 4.18. Total cross section for ^{75}As(^{3}He,3n)^{75}Br reaction and comparison with the experimental data
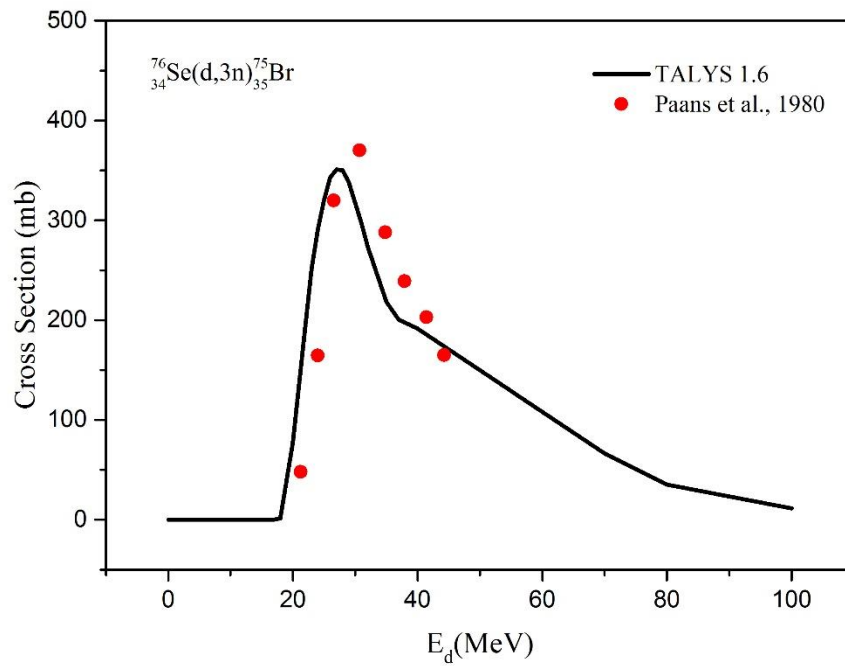
Figure 4.19. Total cross section for ^{76}Se(d,3n)^{75}Br reaction and comparison with the experimental data
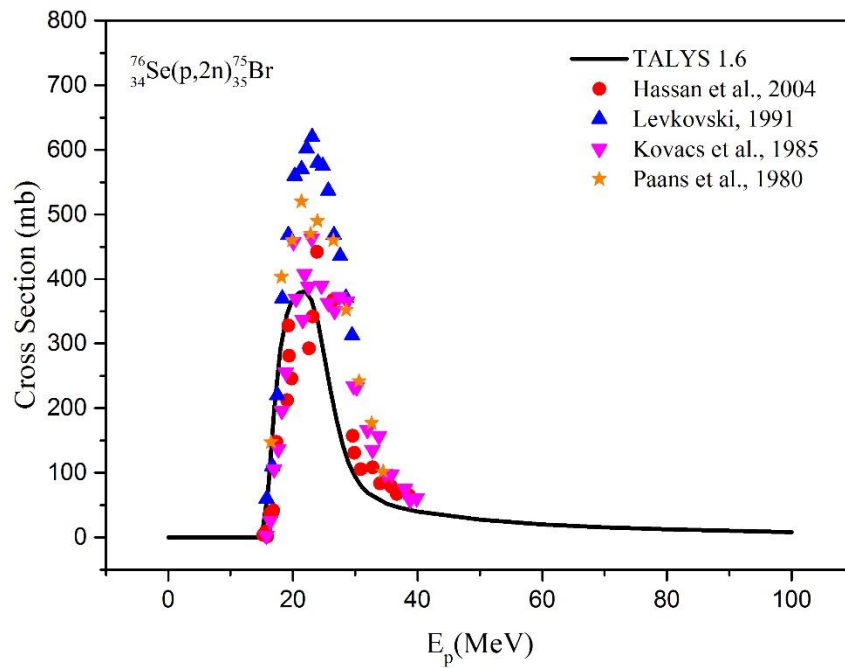
Figure 4.20. Total cross section for ^{76}Se(p,2n)^{75}Br reaction and comparison with the experimental data
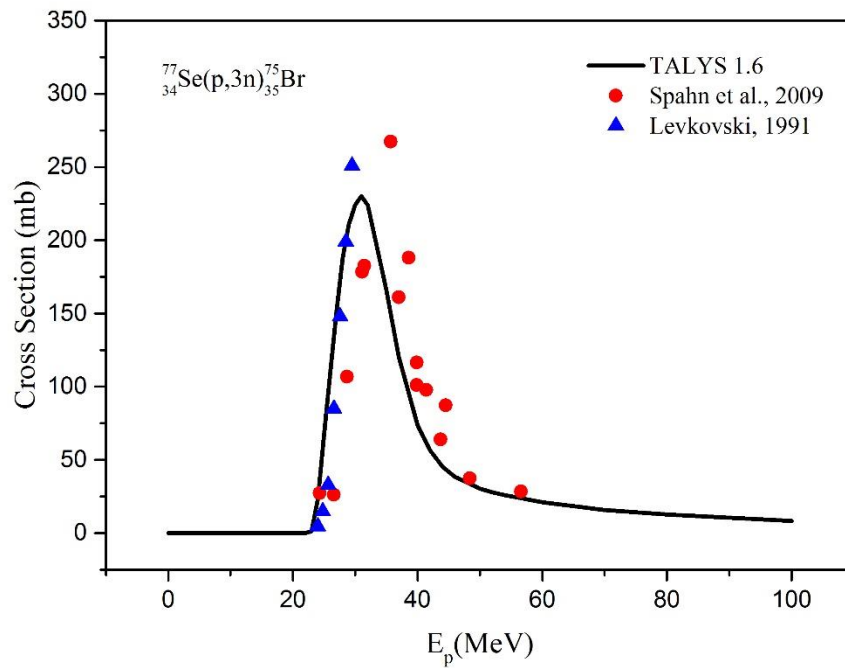
Figure 4.21. Total cross section for ^{77}Se(p,3n)^{75}Br reaction and comparison with the experimental data
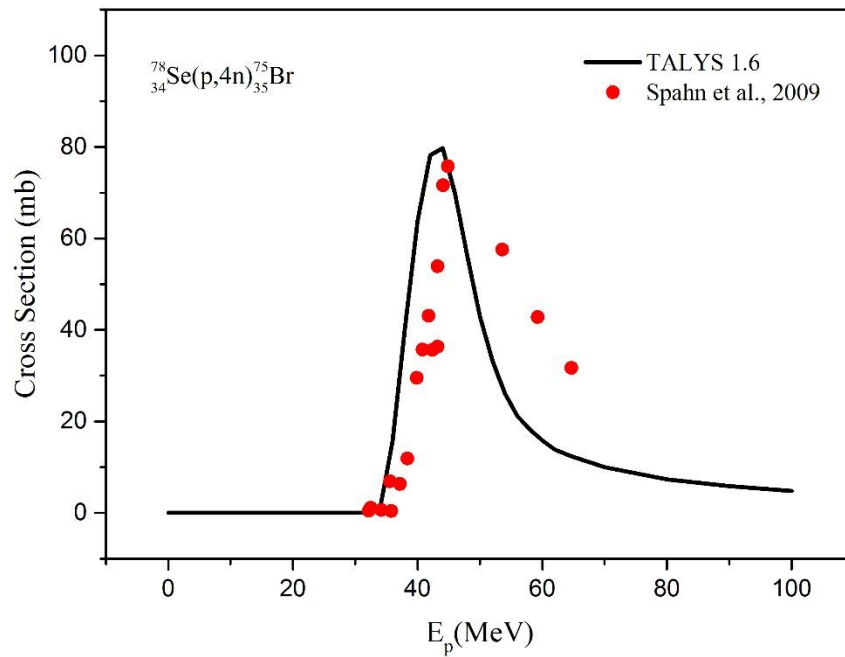
Figure 4.22. Total cross section for ^{78}Se(p,4n)^{75}Br reaction and comparison with the experimental data

Figure 4.23. Total cross section for ^{78}Kr(d,n+a)^{75}Br reaction and comparison with the experimental data

The incoming energies of the proton, helium-3, deuteron and alpha particles in the ^{75}Br produced reactions (a,x), (a,4n), (^{3}He,n), (d,3n), (p,2n), (p,3n), (p,4n) and (d,n+a) were determined to be in the range of 100 MeV.

For ^{74}Se(a,x)^{75}Br reaction, shown in Figure 4.16, a good agreement has been formed between present calculation results and experimental data made by Levkovski (1991). The calculated cross section for the ^{75}As(a,4n)^{75}Br reaction given in Figure 4.17 is in agreement with the experimental measurements made by Panns et al. (1980) and Alfassi et al. (1982) up to 50 MeV. However, after this value, a phase shift observed but it goes in parallel.

The calculated cross section results and experimental data for the ^{75}As(^{3}He,3n)^{75}Br, ^{76}Se(d,3n)^{75}Br and ^{78}Se(p,4n)^{75}Br reactions are shown in Figure 4.18, 4.19 and 4.22 respectively. It can be said that the results calculated by the TALYS 1.6 program and experimental data provided by Paans et al. (1980) for ^{75}As(^{3}He,3n)^{75}Br and ^{76}Se(d,3n)^{75}Br reactions, Spahn et al. (2009) for ^{78}Se(p,4n)^{75}Br reaction are in a good agreement but not in perfect agreement after the peak region. As can be seen in

53

Figure 4.20, for ^{76}Se(p,2n)^{75}Br reaction it can be said that the cross section results calculated with the TALYS 1.6 code are show a similarity with experimental data from literatures and the size of the cross section is approximately 40% different with the experimental data reported by Levkovski (1991). On the other hand, they are consistent with those presented by Kovacs et al. (1985).

For the case of reaction ^{77}Se(p,3n)^{75}Br shown in Figure 4.2, it is seen that there is a harmony between the experimental data and the calculated results in this study. In particular those presented by Levkoski (1991) where they correspond exactly to the calculated data up to 29 MeV. It is seen that this adaptation become less after 27 MeV for Saphn et al. (2009) but it is in harmony again afterwards.

In Figure 4.23 of ^{78}Kr(d,n+a)^{75}Br reaction, the calculated cross section for incident deuteron have been completely identical with the only one experimental work made by Scholten et al. (2004) in the 11-13.2 MeV energy range. Therefore, the theoretical calculations of ^{75}Br production in this study helps to do other experiments for this reaction. From the calculation of cross sections of ^{75}Br radioisotope production the optimum energy range, threshold energy (E-threshold) and Q-values of each reaction are shown in table 4.3.

Table 4.3. Optimum energy range, the average cross section of these energies, E-threshold and Q-values for ^{75}Br production

Reactions	Optimum energy range (MeV)	Average cross section (mb)	E-threshold (MeV)	Q-values (MeV)
^{74}Se(a,x)^{75}Br	$E_a = 38 \rightarrow 45$	$525 \rightarrow 600$	16.4773	-15.631
^{75}As(a,4n)^{75}Br	$E_a = 45 \rightarrow 55$	$200 \rightarrow 225$	35.5925	-33.7874
^{75}As(^{3}He,3n)^{75}Br	$E_h = 18 \rightarrow 24$	$80 \rightarrow 100$	13.7416	-13.2098
^{76}Se(d,3n)^{75}Br	$E_d = 22 \rightarrow 32$	$210 \rightarrow 280$	17.6799	-17.2231
^{76}Se(p,2n)^{75}Br	$E_p = 18 \rightarrow 25$	$250 \rightarrow 300$	15.1975	-14.9985
^{77}Se(p,3n)^{75}Br	$E_p = 27 \rightarrow 35$	$150 \rightarrow 200$	22.7109	-22.4174
^{78}Se(p,4n)^{75}Br	$E_p = 40 \rightarrow 48$	$55 \rightarrow 65$	33.3406	-32.9151
^{78}Kr(d,n+a)^{75}Br	$E_d = 18 \rightarrow 24$	$25 \rightarrow 30$	2.49584	-2.43297

From $^{74}Se(a,x)^{76}Br$, $^{75}As(a,3n)^{76}Br$, $^{75}As(^3He,2n)^{76}Br$, $^{76}Se(p,n)^{76}Br$, $^{77}Se(p,2n)^{76}Br$, $^{78}Se(p,3n)^{76}Br$, $^{78}Kr(d,a)^{76}Br$ reactions where Bromine-76 produced, the results of the cross section obtained from calculations made with TALYS 1.6 code in the energy range between 0-200 MeV are compared with experimental data presented in (EXFOR) library to obtained Bromine-76 radioisotope are shown in Figures 4.24-4.30.

Figure 4.24. Total cross section for $^{74}Se(a, x)^{76}Br$ reaction and comparison with the experimental data

Figure 4.25. Total cross section for ^{75}As(a, 3n)^{76}Br reaction and comparison with the experimental data

Figure 4.26. Total cross section for ^{75}As(^{3}He, 2n)^{76}Br reaction and comparison with the experimental data

Figure 4.27. Total cross section for ^{76}Se(p, n)^{76}Br reaction and comparison with the experimental data

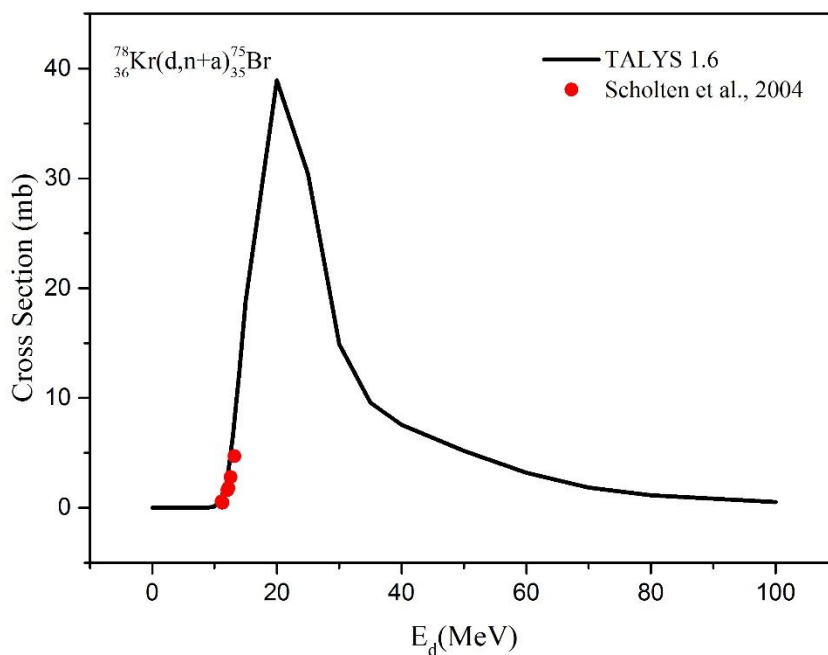Figure 4.28. Total cross section for ^{77}Se(p, 2n)^{76}Br reaction and comparison with the experimental data

Figure 4.29. Total cross section for ^{78}Se(p, 3n)^{76}Br reaction and comparison with the experimental data

Figure 4.30. Total cross section for ^{78}Kr(d, a)^{76}Br reaction and comparison with the experimental data

In ^{74}Se(a, x)^{76}Br reaction shown in Figure 4.24 the calculations made with the TALYS 1.6 program code are in a good agreement with available experimental data Levovski (1991), although they have higher results than experimental data. Figure 4.25 which represents ^{75}As(a, 3n)^{76}Br reaction current calculation results of cross section shows similarity with experimental data provided by Alfassi et al (1982).

The calculated cross section results and experimental data obtained for the ^{75}As(^{3}He, 2n)^{76}Br reaction are shown in Figure 4.26. By comparison, of present calculated results with literature data of Alfassi et al. (1982) a general good agreement were noted, especially for the work made by Misaelides et al. (1987) although the available practical data are in the range of energy between 7.75 to 11.7 MeV.

The calculated theoretical results by using TALYS 1.6 code in a very good agreement with the experimental data for ^{76}Se(p, n)^{76}Br reaction shown in Figure 4.27. At 5 - 40 MeV energy range, Hassan et al. (2004), Levkovski (1991) and Kovacs et al. (1985) are clearly in agreement with the reaction cross-sections they have achieved in the experimental work they have conducted.

For the ^{77}Se(p, 2n)^{76}B reaction, the cross section calculated by TALYS 1.6 code and experimental data reported by Spahn et al. (2009), Hasan et al. (2004) and Levkovski (1991) are shown in Figure 4.28, Spahn et al. (2009) reported similar experimental data which start from 21.3 MeV. Either Hasan et al. (2004) show a similar pattern, and the size of the cross section is approximately 50% different. It can also be said that the experimental data reported by Levkovski (1991) are more in agreement with the calculated results.

The results of calculation of the cross section for ^{78}Se(p, 3n)^{76}Br reaction, have been carried out using TALYS 1.6, are plotted in Figure 4.29, with the experimental data made by Spahn et al. (2009) and Levkovski (1991). Experimental data reported by Spahn et al. (2009) show a similar pattern, but the size of the cross section is about 10% lower. However, it is noted from the Figure 4.29 that current calculations have been exactly identical with experimental data provided by Levkovski (1991) in the 24.8-29.5 energy range where there is no experimental data after 29.5 MeV energy value.

In Figure 4.30 experimental data and theoretical cross section calculations are compared for ^{78}Kr(d, a)^{76}Br reaction. Scholten et al. (2004) reported experimental data exactly matching with calculated results up to 13.2 MeV, in case before equilibrium but since there is no experimental data after this energy value. It is not possible to say anything about post equilibrium. From the calculation of cross sections of ^{76}Br radioisotope production the optimum energy range, threshold energy (E-threshold) and Q-values of each reaction are shown in table 4.4.

Table 4.4. Optimum energy range, the average cross section of these energies, E-threshold and Q-values for ^{76}Br production

Reactions	Optimum energy range (MeV)	Average cross section (mb)	E-threshold (MeV)	Q-values (MeV)
^{74}Se(a,x)^{76}Br	$E_a = 25 \rightarrow 35$	$500 \rightarrow 600$	13.3191	-12.6349
^{75}As(a,3n)^{76}Br	$E_a = 30 \rightarrow 40$	$300 \rightarrow 360$	25.8449	-24.5342
^{75}As(^{3}He,2n)^{76}Br	$E_h = 15 \rightarrow 20$	$175 \rightarrow 200$	4.11584	-3.95656
^{76}Se(p,n)^{76}Br	$E_p = 10 \rightarrow 15$	$600 \rightarrow 700$	5.86753	-5.74523
^{77}Se(p,2n)^{76}Br	$E_p = 20 \rightarrow 25$	$550 \rightarrow 600$	13.3365	-13.1641
^{78}Se(p,3n)^{76}Br	$E_p = 30 \rightarrow 40$	$250 \rightarrow 300$	23.9677	-23.6618
^{78}Kr(d,a)^{76}Br	$E_d = 10 \rightarrow 18$	$15 \rightarrow 18$	0.0000	6.8203

4.1.4. Technetium 94,99 production reactions

The results of calculation cross section for ^{nat}Mo(p, x)^{94}Tc, ^{94}Mo(p, n)^{94}Tc, ^{96}Mo(p, 3n)^{94}Tc, ^{nat}Mo(d, x)^{94}Tc, ^{93}Nb(^{3}He, 2n)^{94}Tc, ^{nat}Mo(a, x)^{94}Tc and ^{nat}Mo(p, x)^{99}Tc reactions to produce Technetium radioisotopes were carried out using TALYS 1.6. The calculated results plotted in Figures 4.31- 4.37 where comparison with the experimental data from (EXFOR) library.
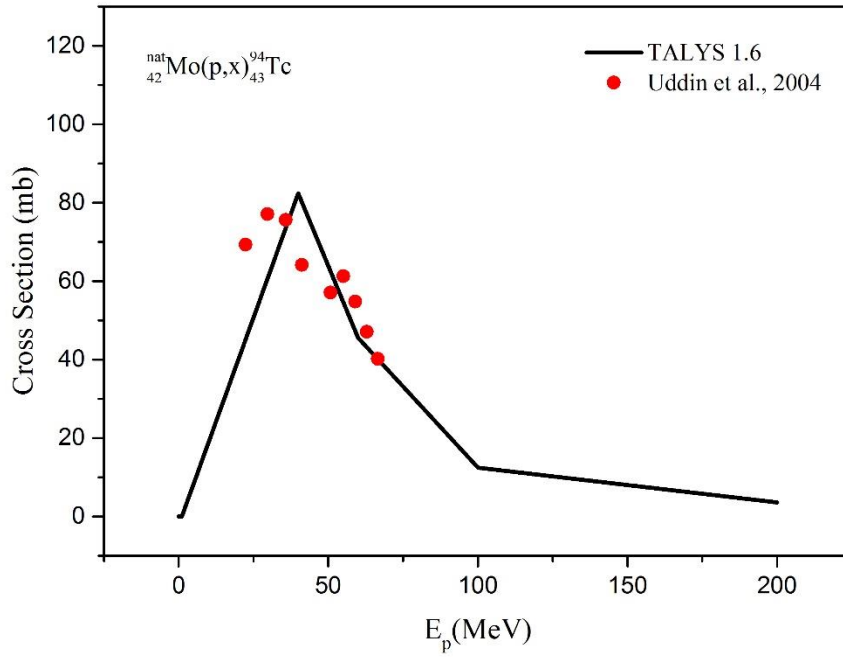
Figure 4.31. Total cross section for ^{nat}Mo(p, x)^{94}Tc reaction and comparison with the experimental data
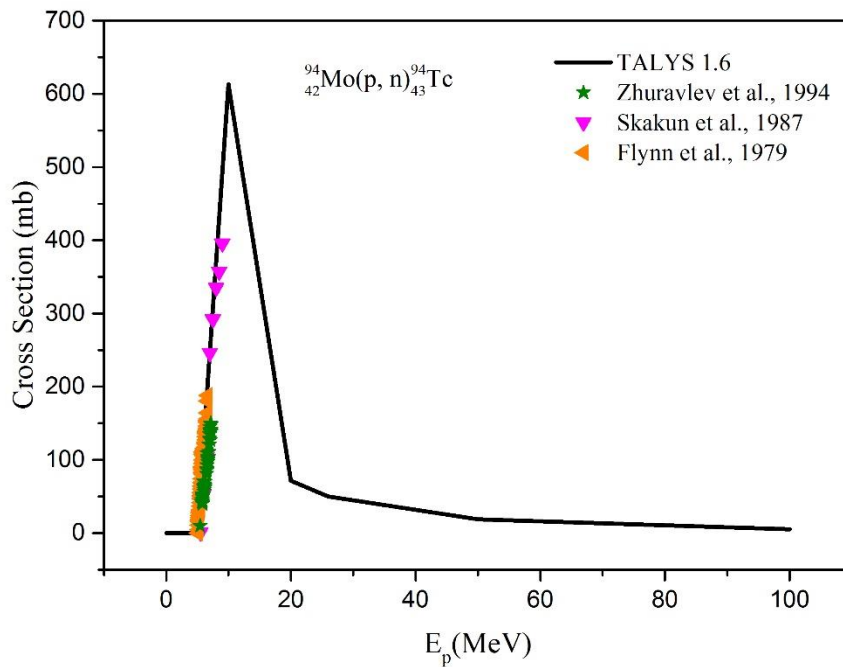
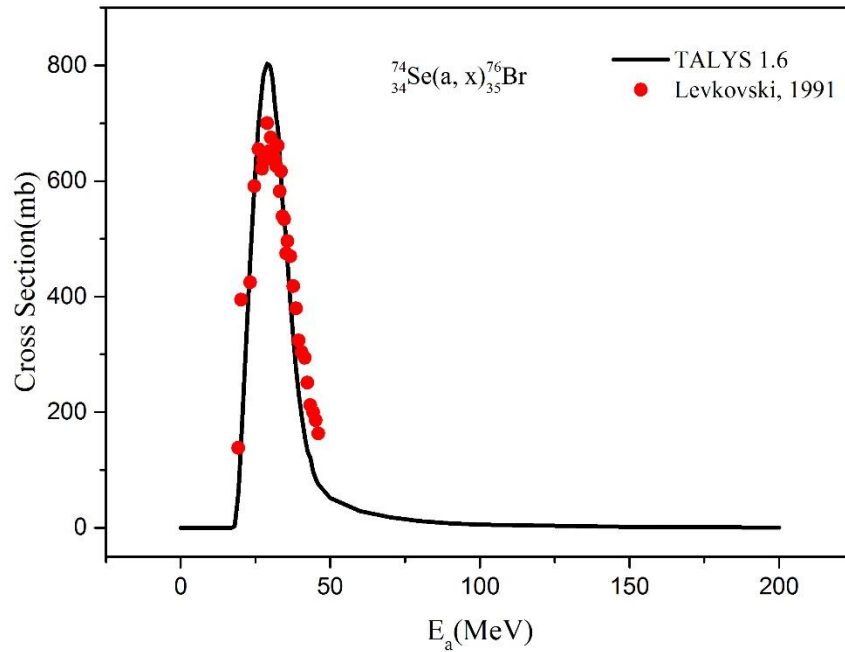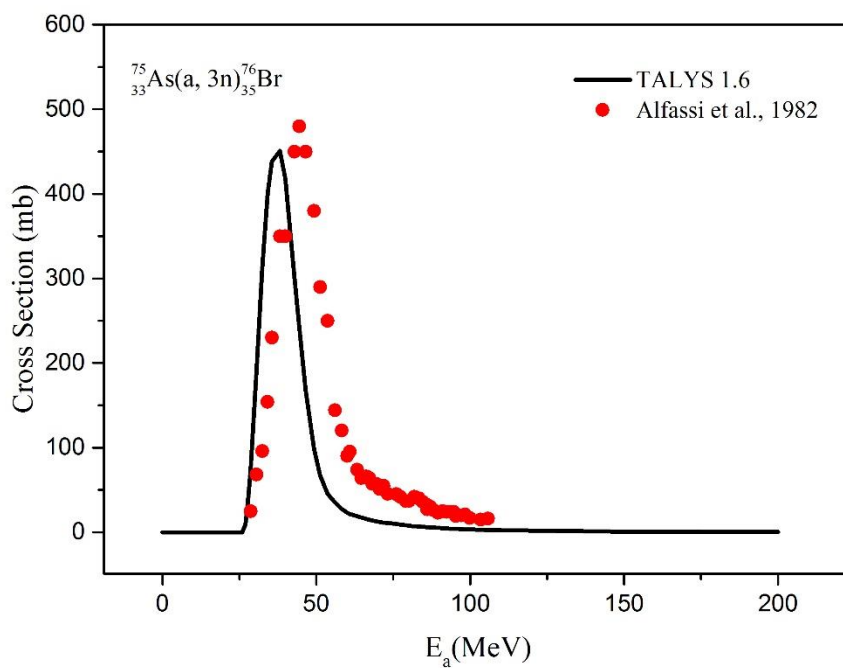
Figure 4.32. Total cross section for ^{94}Mo(p, n)^{94}Tc reaction and comparison with the experimental data
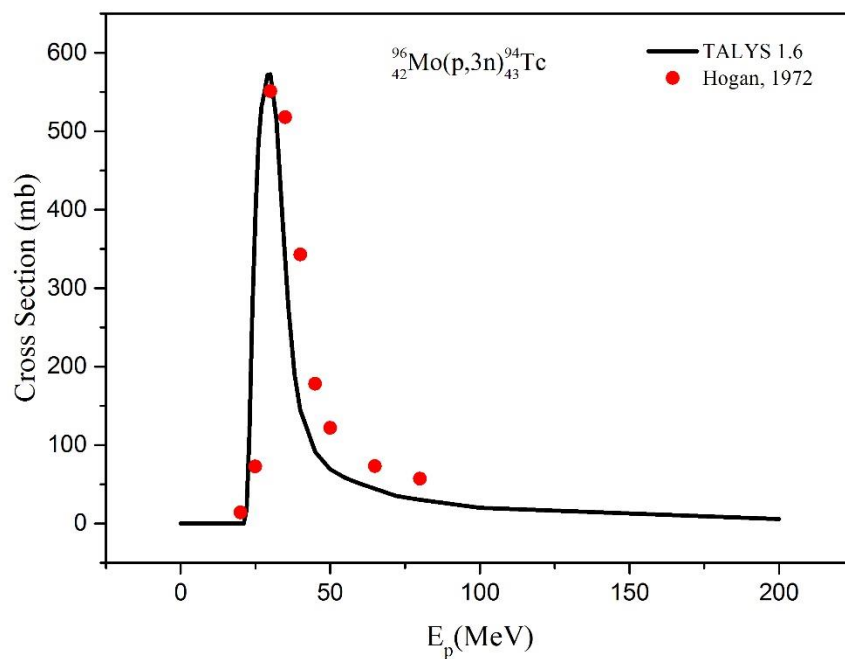
Figure 4.33. Total cross section for ^{96}Mo(p, 3n)^{94}Tc reaction and comparison with the experimental data

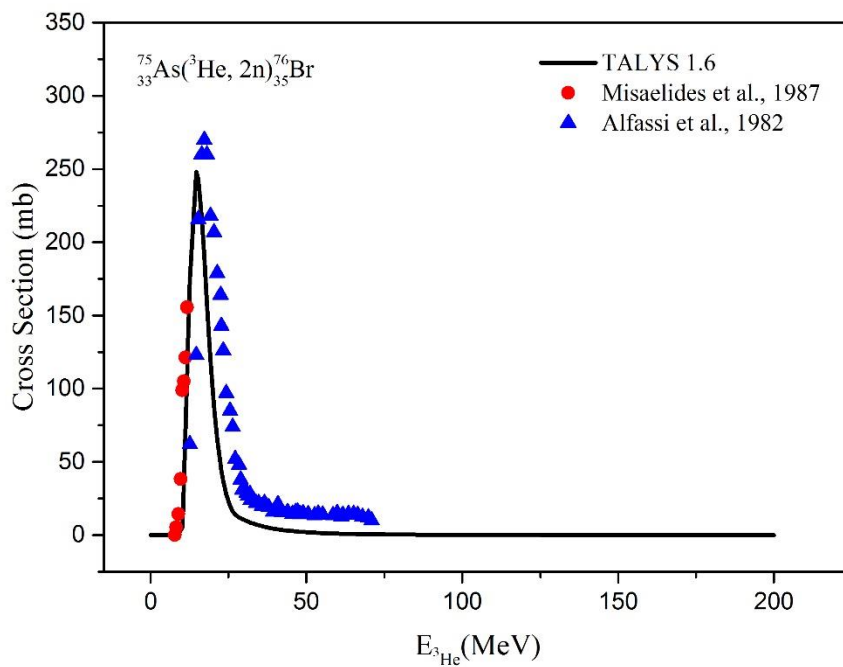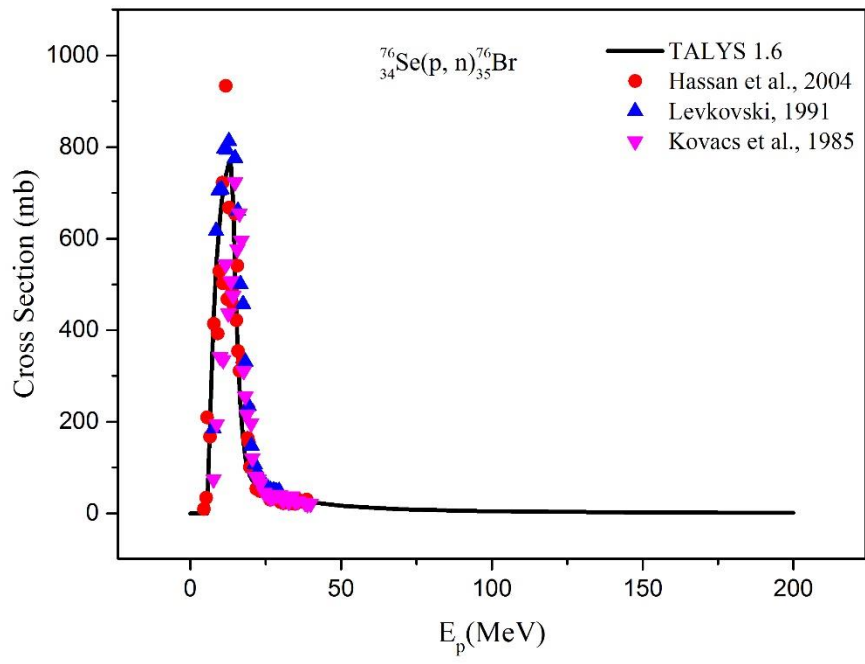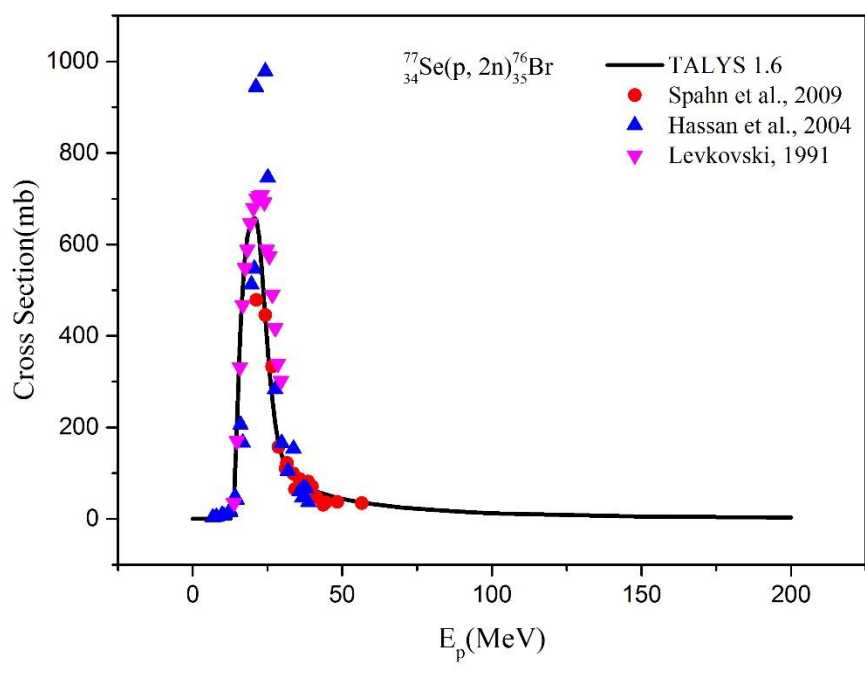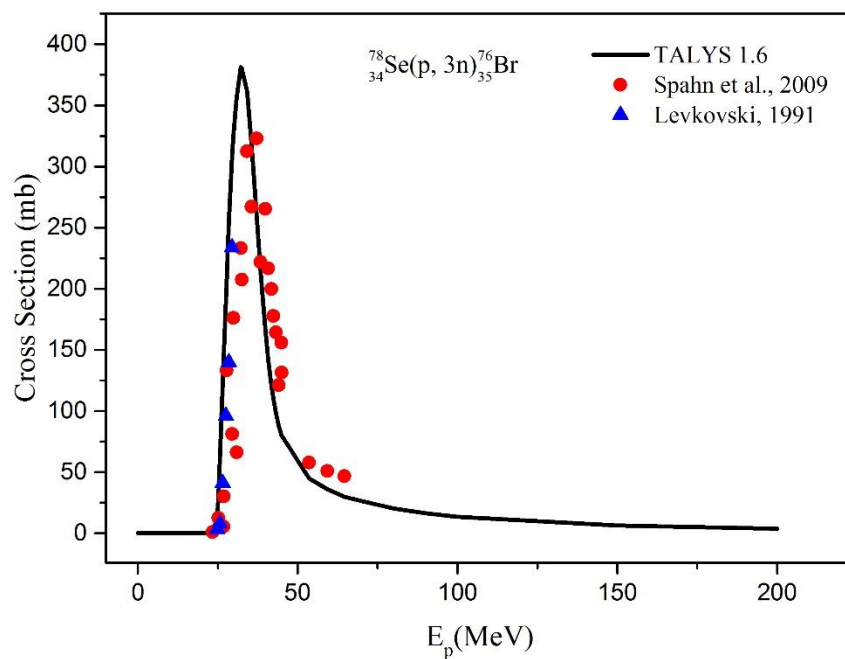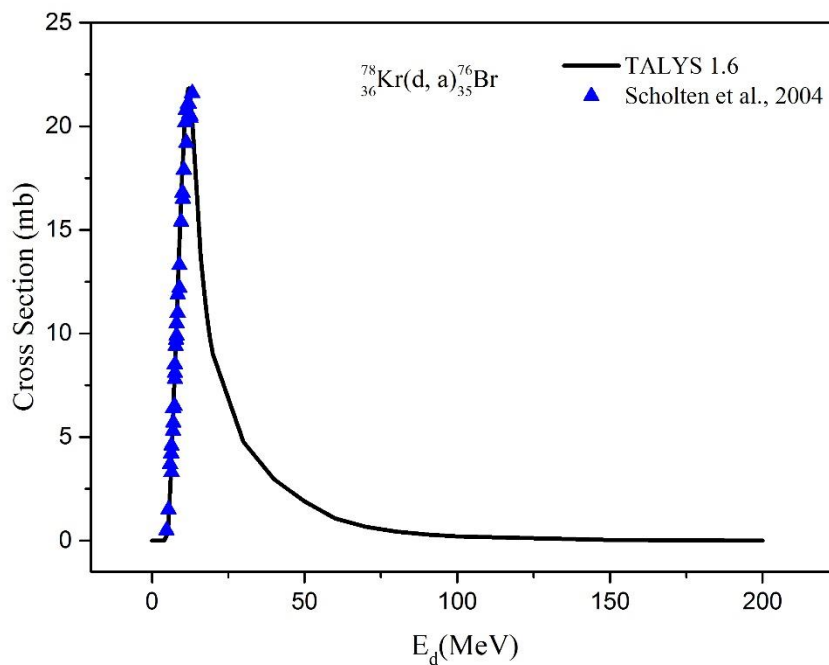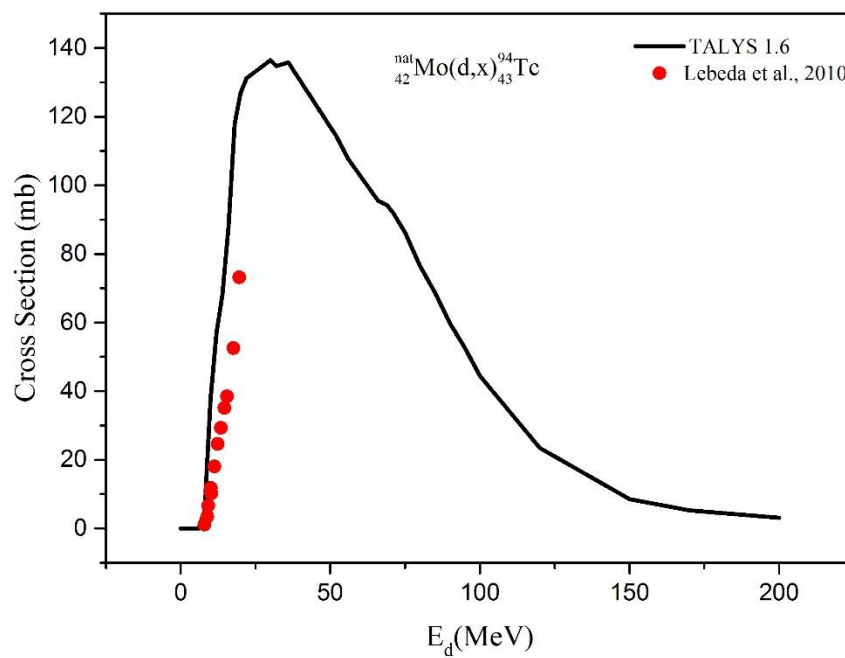Figure 4.34. Total cross section for ^{nat}Mo(d, x)^{94}Tc reaction and comparison with the experimental data
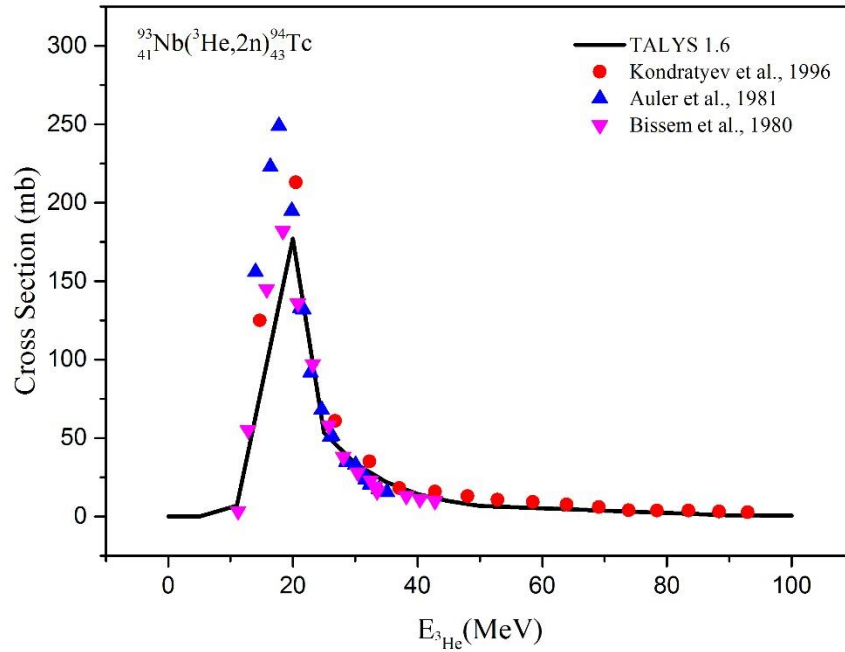
Figure 4.35. Total cross section for ^{93}Nb(^{3}He, 2n)^{94}Tc reaction and comparison with the experimental data
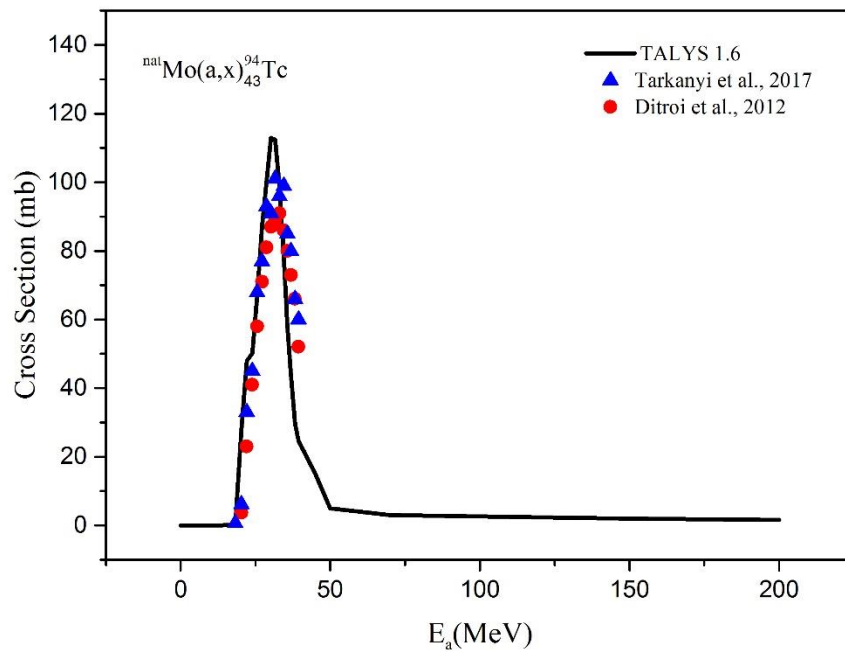
Figure 4.36. Total cross section for ^{nat}Mo(a, x)^{94}Tc reaction and comparison with the experimental data
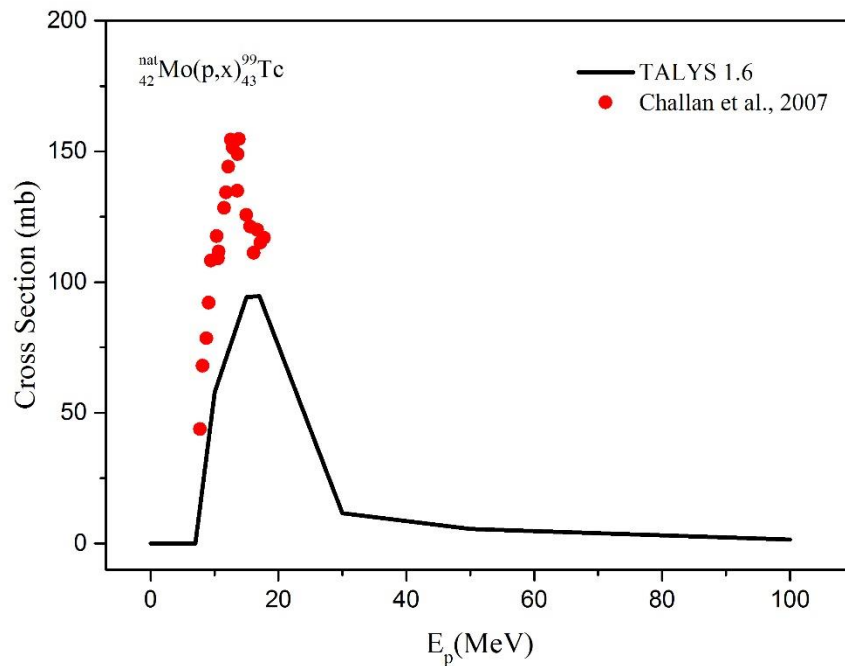
Figure 4.37. Total cross section for ^{nat}Mo(p, x)^{99}Tc reaction and comparison with the experimental data

In Figure 4.31 a good agreement was shown by the comparison between the cross section calculated with TALYS 1.6 for incident proton and experimental value reported by Uddin et al. (2004). ^{94}Mo(p, n)^{94}Tc reaction which shown in Figure 4.32. Present calculated cross section for incident proton, have been completely identical with the experimental works made by Skakum et al. (1987) in the range of energy from 5.5 to 9 MeV, Flynn et al. (1979) in the range of energy from 5.1 to 6.6 MeV, and Zhuravlev et al. (1994) in the range of energy from 5.43 to 7.2 MeV. Unfortunately, there are no empirical data after 9 MeV energy value.

In Figure 4.33, when the experimental data reported by Hogan (1972) and theoretical cross section calculations are compared, it is observed general good agreement for ^{96}Mo(p, 3n)^{94}Tc reaction. ^{nat}Mo(d, x)^{94}Tc reaction in Figure 4.34 where it was shown the comparison of calculated cross section with available only one literature data made by Lebeda et al. (2010) in 8-19.5 MeV energy range, there is no practical data after 19.5 MeV, so the theoretical calculations of ^{94}Tc production in this study helps to do other experiments for this reactions.

64

The calculated cross section results and experimental data obtained for the ^{93}Nb(^{3}He, 2n)^{94}Tc reaction are shown in Figure 4.35. By comparison, of present calculation results with literature data made by Kondaratyev et al. (1996), Auler et al. (1981) and Bissem et al. (1980). A good agreement was observed between current calculated results with literature data. As noted, present study is more in line after 27 MeV with the data reported by Kondaratyev et al. (1996), and from 11 to 42 MeV with data reported by Bissem et al. (1980).

In Figure 4.36 experimental and theoretical cross section calculations are compared for ^{nat}Mo(a, x)^{94}Tc reaction a good agreement noted between present calculation results were carried by TALYS 1.6 and experimental data made by Ditroi et al. (2012) and Tarkanyi et al. (2017). To produce Technetium-99, ^{nat}Mo(p, x)^{99}Tc reaction as shown in Figure 4.37 it is seen that there is agreement between the results obtained in the calculations and the experimental data made by Challan et al. (2007). From the calculation of cross sections of ^{94}Tc radioisotope production the optimum energy range, threshold energy (E-threshold) and Q-values of each reaction are shown in table 4.5.

Table 4.5. Optimum energy range, the average cross section of these energies, E-threshold and Q-values for ^{94,99}Tc production

Reactions	Optimum energy range (MeV)	Average cross Section (mb)	E-threshold (MeV)	Q-values (MeV)
^{nat}Mo(p, x)^{94}Tc	$E_p = 30 \rightarrow 50$	$60 \rightarrow 70$		
^{94}Mo(p, n)^{94}Tc	$E_p = 8 \rightarrow 13$	$450 \rightarrow 500$	5.1689	-5.0381
^{96}Mo(p, 3n)^{94}Tc	$E_p = 28 \rightarrow 35$	$425 \rightarrow 475$	21.788	-21.6515
^{nat}Mo(d, x)^{94}Tc	$E_d = 20 \rightarrow 50$	$105 \rightarrow 120$		
^{93}Nb(^{3}He,2n)^{94}Tc	$E_h = 17 \rightarrow 23$	$125 \rightarrow 150$	4.4058	-4.26733
^{nat}Mo(a, x)^{94}Tc	$E_a = 29 \rightarrow 35$	$80 \rightarrow 90$		
^{nat}Mo(p, x)^{99}Tc	$E_p = 14 \rightarrow 20$	$60 \rightarrow 75$		

4.2. Differential Cross Sections

4.2.1. Cobalt-57 production

In the present study the differential cross section for Cobalt-57 were calculated for the $^{56}Fe(d,n)^{57}Co$ reaction at incident deuteron energy 2.7 MeV and 3.8 MeV. The calculation were made with nuclear reaction simulation program TALYS 1.6 code that based on Monte Carlo. The obtained results are compared with the experimental data available in EXFOR library separately in Figures 4.38 and 4.39.

The energies of 2.7 MeV and 3.8 MeV were used as the experimental data available by Zhuravlev et al. (2014). A very good agreement of deuteron induced reactions with ^{56}F target in $^{56}Fe(d, n)^{57}Co$ reaction is observed between the calculated differential cross sections and expeirnental data reported by Zhuravlev et al. (2014) and these are shown in Figure 4.38 for 2.7 MeV deuteron incident energy and Figure 4.39 for 3.8 MeV deuteron incident energy.

Figure 4.38. Calculated differential cross sections of neutron spectrum compared with experimental data at incident deuteron energy 2.7 MeV for $^{56}Fe(d,n)^{57}Co$ reaction

Figure 4.39. Calculated differential cross sections of neutron spectrum compared with experimental data at incident deuteron energy 3.8 MeV for $^{56}Fe(d,n)^{57}Co$ reaction

4.2.2. Manganese-50 production

The differential cross section for Manganese-50 for the $^{50}Cr(p,n)^{50}Mn$ reaction at incident proton energy 25 MeV have been obtained. Calculation were made with nuclear reaction simulation program TALYS 1.6 code and obtained results are compared with the present experimental data (EXFOR) in Figure 4.40.

The energy of 25 MeV were used as the experimental available data in this energy by Scobel et al. (1984) and Blann et al. (1985). A good agreement of proton induced reactions with ^{50}Cr target nuclei in $^{50}Cr(p,n)^{50}Mn$ reaction is observed between the calculated differential cross section and expeirnental data reported by Scobel et al. (1984) in the energy range between 7 MeV to 15 MeV. While the data provided by Blann et al. (1985) is lower than present calculated results these are shown in Figure 4.40.
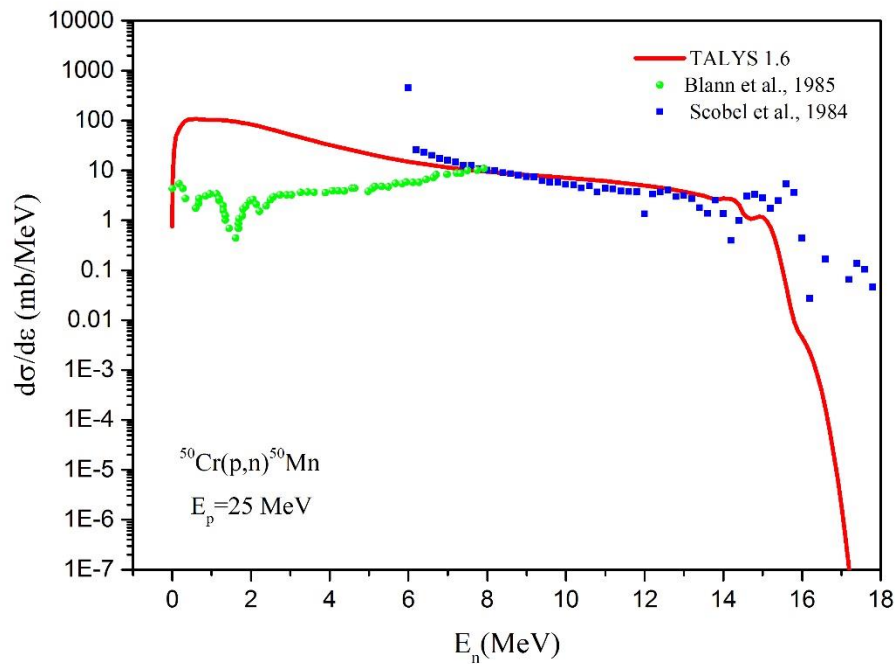
Figure 4.40. Calculated differential cross section of neutron spectrum compared with experimental data at incident proton energy 25 MeV for $^{50}Cr(p,n)^{50}Mn$ reaction

4.2.3. Proton emission spectrum

The proton emission spectrum is calculated using nuclear reaction simulation program TALYS 1.6 code for the ^{19}F (n,xp) reaction at 14.1 MeV neutron incident energy and compared with Terada et al. (2002). The comparision between the calculated results and experimental data are shown in Figure 4.41.

The 14.1 MeV incident neutron energy was bombared with ^{19}F target nuclei the emission proton spectrum was calculated. As it is noted from the Figure 4.41 that the calculated results and the experimental data provided by Terada et al. (2002) in good agreement with each other.
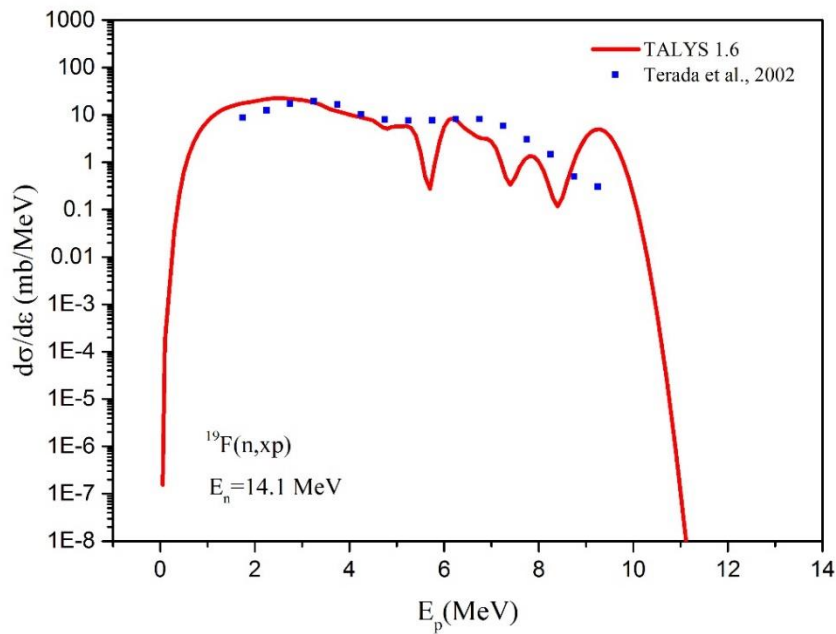
Figure 4.41. Calculated differential cross sections of proton spectrum compared with experimental data at incident neutron energy 14.1 MeV for ^{19}F (n,xp) reaction

4.2.4. Neutron emission spectrum

The neutron emission spectrum was calculated using nuclear reaction simulation program TALYS 1.6 code for the ^{19}F (n,xn) reaction at 14.1 MeV neutron incident energy and compared with results of Takahashi et al. (1987). The comparison between the calculated results and experimental data are shown in Figure 4.42. It has been observed that the theoretical and experimental calculations for the ^{19}F (n, xn) reaction generated by the neutron with 14.1 MeV of incoming energy are quite compatible with each other.
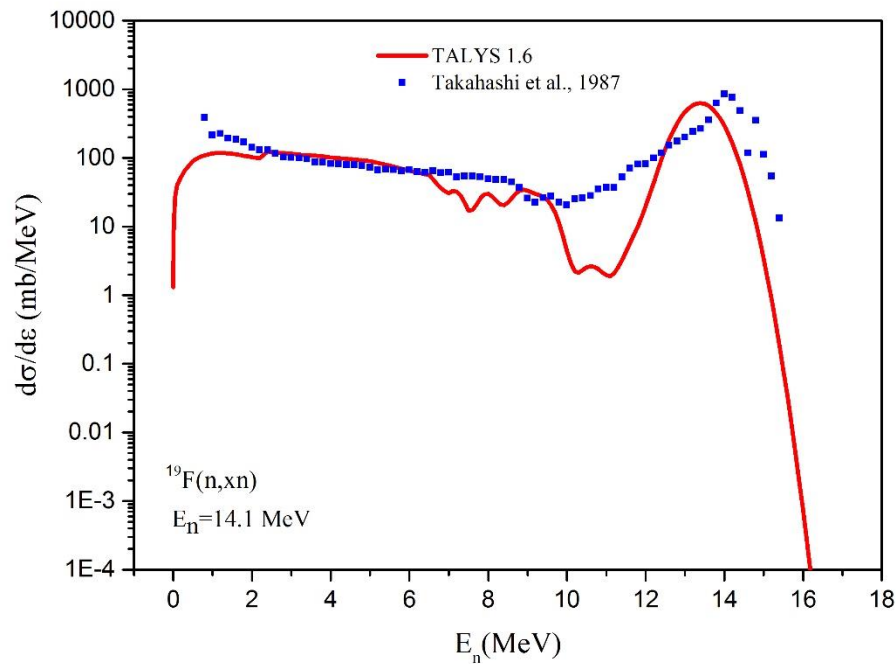
Figure 4.42. Calculated differential cross sections of neutron spectrum compared with experimental data at incident neutron energy 14.1 MeV for ^{19}F (n,xn) reaction

4.2.5. Alpha emission spectrum

The alpha emission spectrum is calculated using nuclear reaction simulation program TALYS 1.6 code for the ^{19}F (n,xa) reaction at 14.1 MeV neutron incident energy and the results were compared with experimental data of Terada et al. (2002). The comparision between the calculated results and experimental data are shown in Figure 4.43. For 10 MeV energy a minimum spectrum value was obtained in the present theoretical calculation, but this minimum value is not confirmed by the data from the experiment. It is observed that the experimental data are lower than the calculated results in general compatible with each other.
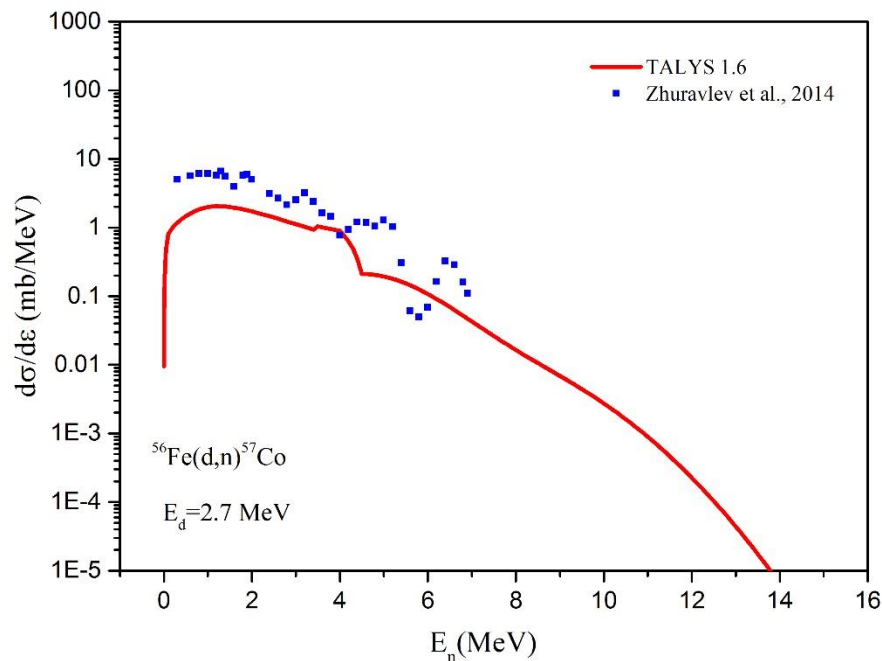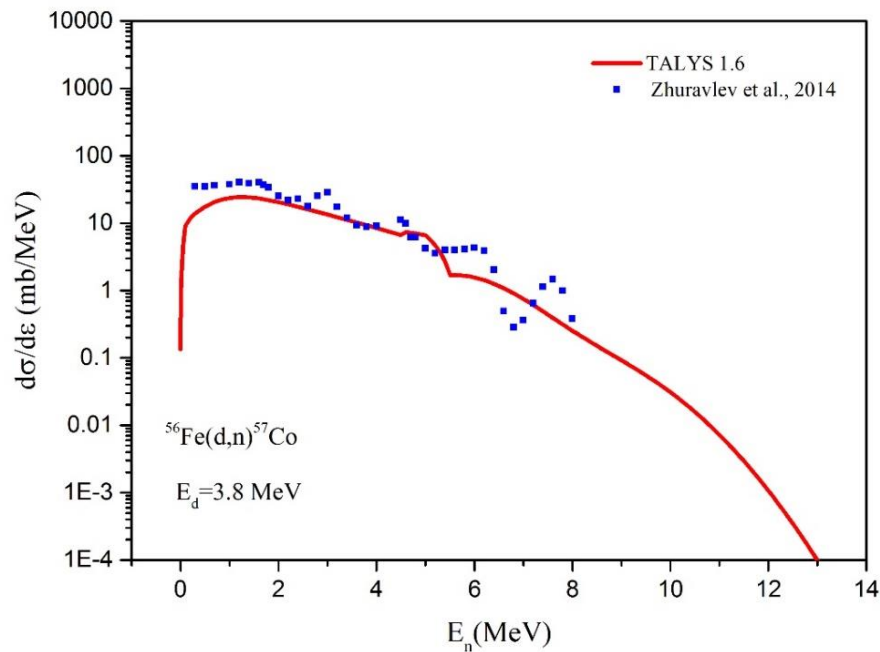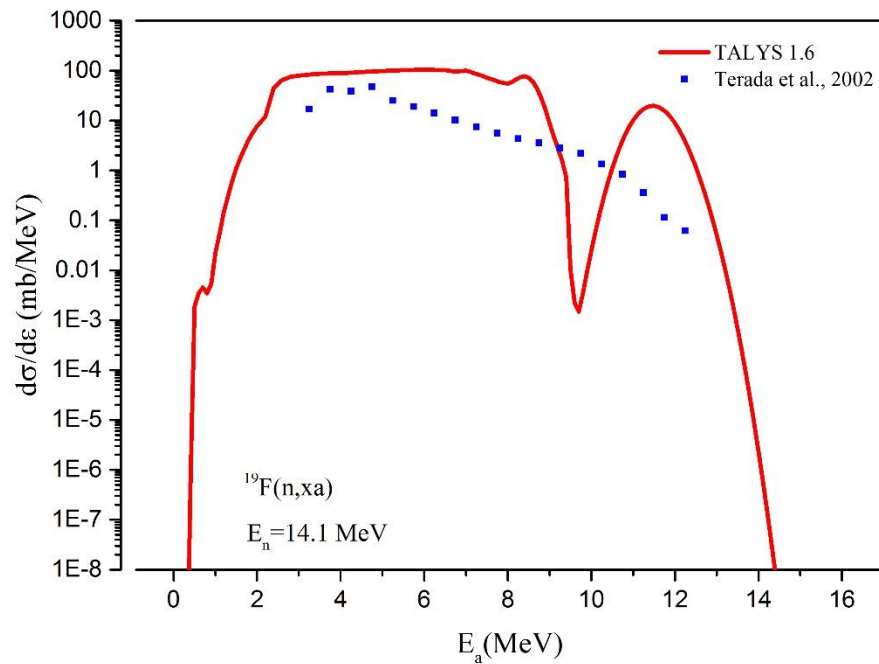
Figure 4.43. Calculated differential cross sections of alpha spectrum compared with experimental data at incident neutron energy 14.1 MeV for ^{19}F (n,xa) reaction

4.3. Double Differential Cross Sections

The double differential cross section is important quantity in nuclear reactions as it can be possible to obtain certain results for certain angle and also for certain energy. On the other hand to collect enough number of particle is hard and this required especially long long experimental time. This will cause extra time and extra financial budget to perform an experiment. Thus the theoretical calculation become important in this point of view.

4.3.1. Carbon-11 production

4.3.1.1. DDX calculations at Ep= 30, 50 MeV and different angles

The double differential cross section (DDX) were calculated using nuclear reaction simulation program TALYS 1.6 code, for the neutron emission angles 2° and 20° at incident proton energies of 30 MeV and 50 MeV respectively, to product ^{11}C

radioisotope which used in nuclear medicine in PET technique. The results of calculation of DDX for $^{11}B(p,n)$ ^{11}C reaction were carried out using TALYS 1.6 are plotted in Figures 4.44 and 4.45 and are compared with the experimental data of Clough et al. (1970) taken from the EXFOR library.

Figure 4.44. Calculated double differential cross sections of neutron emission compared with experimental data for 30 MeV incident proton energy, angle 2˚ for $^{11}B(p,n)$ ^{11}C reaction

Figure 4.45. Calculated double differential cross sections of neutron emission compared with experimental data for 50 MeV incident proton energy, angle 20˚ for $^{11}B(p,n)$ ^{11}C reaction

In Figure 4.44 the proton at 30 MeV bombarded to the target ^{11}B core and the theoretical calculations results are compared with experimental data reported by Clough et al. (1970). It can be seen from both Figures that at lower energies there is no available experimental data and thus we did not have any chance for comparison. In Figure 4.44, for the case of higher energies, the theoretical calculations decreased sharply while experimental results keep goes to be smooth line as lower energies.

4.3.1.2. DDX calculations at Ep= 186 MeV and different angles

The double differential cross sections (DDX) were calculated using nuclear reaction simulation program TALYS 1.6 code to produce Carbon-11. For the neutron emission angles at θ= 0˚, 5˚, 10˚, 15˚, 20˚, 24.4˚, 29.4˚, 34.4˚, 39.4˚, 44.4˚, 48.9˚and with incident proton energies equal to 186 MeV. The calculation achieved by using proton on ^{11}B target in the ^{11}B(p,n)^{11}C reaction to production Carpon-11 radioisotope which is used in nuclear medicine in PET technique.

The results of calculation for DDX for ^{11}B(p,n)^{11}C reaction were carried out using TALYS 1.6, are plotted in Figures 4.46-4.56 and compared with the experimental data reported by Wang et al. (1994) from the EXFOR library. It was observed from Figures that the experimental data and the theoretical DDX calculations were harmonious. With well-matched at small angle as in Figures 4.46-4.51 and with phase difference at low energies with increasing of angles as shown in Figures 4.52-4.56. The differences between experimental and calculated results at low energy could be the results of difficulties of neutron measurements at lower neutron energies.

Figure 4.46. Calculated double differential cross sections of neutron emission compared with experimental data for 186 MeV incident proton energy, angle 0° for ^{11}B(p,n)^{11}C reaction

Figure 4.47. Calculated double differential cross sections of neutron emission compared with experimental data for 186 MeV incident proton energy, angle 5° for ^{11}B(p,n)^{11}C reaction

Figure 4.48. Calculated double differential cross sections of neutron emission compared with experimental data for 186 MeV incident proton energy, angle 10° for ^{11}B(p,n)^{11}C reaction

Figure 4.49. Calculated double differential cross sections of neutron emission compared with experimental data for 186 MeV incident proton energy, angle 15° for ^{11}B(p,n)^{11}C reaction

Figure 4.50. Calculated double differential cross sections of neutron emission compared with experimental data for 186 MeV incident proton energy, angle 20° for $^{11}B(p,n)^{11}C$ reaction

Figure 4.51. Calculated double differential cross sections of neutron emission compared with experimental data for 186 MeV incident proton energy, angle 24.4° for $^{11}B(p,n)^{11}C$ reaction

Figure 4.52. Calculated double differential cross sections of neutron emission compared with experimental data for 186 MeV incident proton energy, angle 29.4˚ for ^{11}B(p,n)^{11}C reaction

Figure 4.53. Calculated double differential cross sections of neutron emission compared with experimental data for 186 MeV incident proton energy, angle 34.4˚ for ^{11}B(p,n)^{11}C reaction

Figure 4.54. Calculated double differential cross sections of neutron emission compared with experimental data for 186 MeV incident proton energy, angle 39.4° for ^{11}B(p,n)^{11}C reaction

Figure 4.55. Calculated double differential cross sections of neutron emission compared with experimental data for 186 MeV incident proton energy, angle 44.4° for ^{11}B(p,n)^{11}C reaction
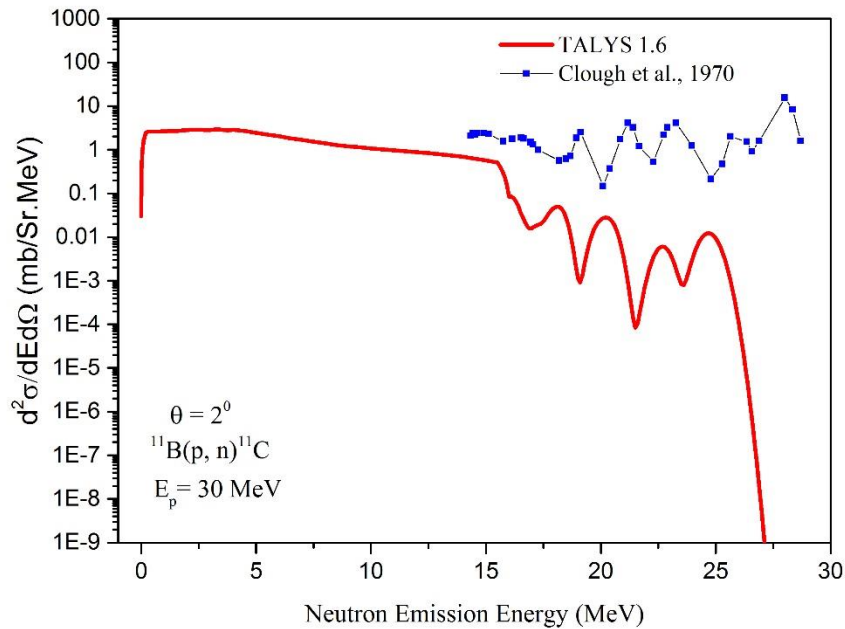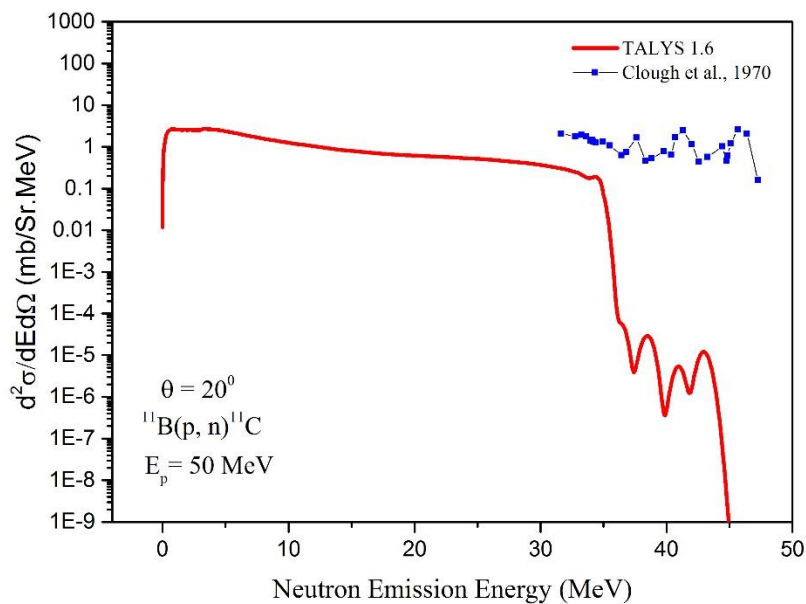
Figure 4.56. Calculated double differential cross sections of neutron emission compared with experimental data for 186 MeV incident proton energy, angle 48.9° for ^{11}B(p,n)^{11}C reaction

4.3.2. Nitrogen-13 production

4.3.2.1. DDX calculations at Ep = 186 and different angles

Double differential cross sections DDX for the (p,n) reaction have been calculated with proton incident energy 186 MeV for Nitrogen-13 production. Neutron emission with angles 0°, 5°, 10°, 15°, 20°, 24.4°, 29.4°, 34.4°, 39.4°, 44.4°, 48.9°. The results of calculation of DDX for ^{13}C(p,n)^{13}N reaction were carried out using TALYS 1.6 are displayed in Figures 4.57-4.67 and compared with the experimental data of Wang et al. (1994) taken from the EXFOR library. In Figures 4.57- 4.63, it is absorved that the experimental data reported by Wang et al. 1994 and the theoretical DDX calculations were in agreement in an acceptable manner at energy above 20 MeV, While the phase difference is clear at lower energies up to 20 MeV as shown in Figures 4.64-4.67.

Figure 4.57. Calculated double differential cross sections of neutron emission compared with experimental data for 186 MeV incident proton energy, angle 0° for $^{13}C(p,n)^{13}N$ reaction

Figure 4.58. Calculated double differential cross sections of neutron emission compared with experimental data for 186 MeV incident proton energy, angle 5° for $^{13}C(p,n)^{13}N$ reaction

Figure 4.59. Calculated double differential cross sections of neutron emission compared with experimental data for 186 MeV incident proton energy, angle 10° for ^{13}C(p,n)^{13}N reaction

Figure 4.60. Calculated double differential cross sections of neutron emission compared with experimental data for 186 MeV incident proton energy, angle 15° for ^{13}C(p,n)^{13}N reaction

Figure 4.61. Calculated double differential cross sections of neutron emission compared with experimental data for 186 MeV incident proton energy, angle 20° for $^{13}C(p,n)^{13}N$ reaction
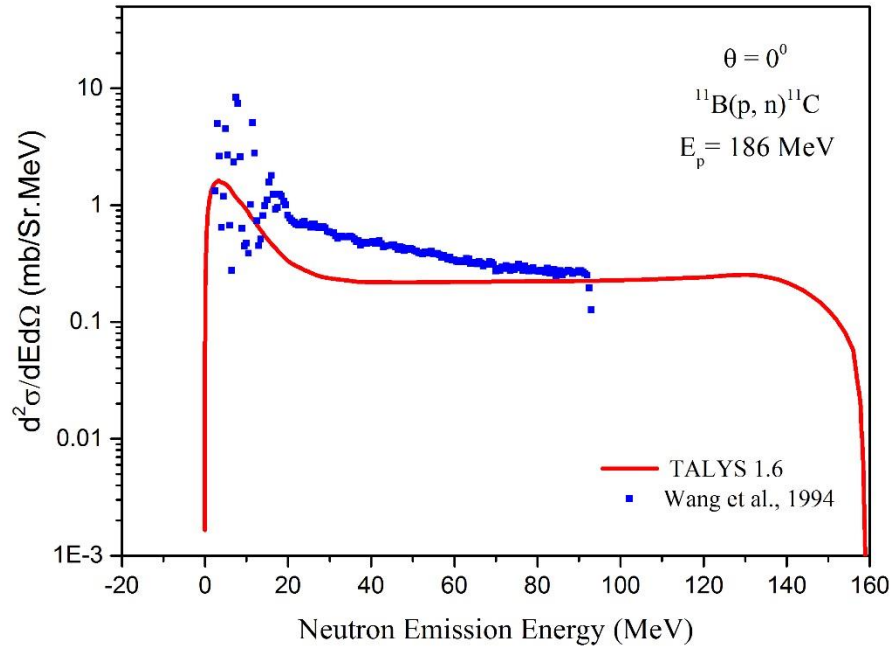

Figure 4.62. Calculated double differential cross sections of neutron emission compared with experimental data for 186 MeV incident proton energy, angle 24.4° for $^{13}C(p,n)^{13}N$ reaction

Figure 4.63. Calculated double differential cross sections of neutron emission compared with experimental data for 186 MeV incident proton energy, angle 29.4° for $^{13}C(p,n)^{13}N$ reaction
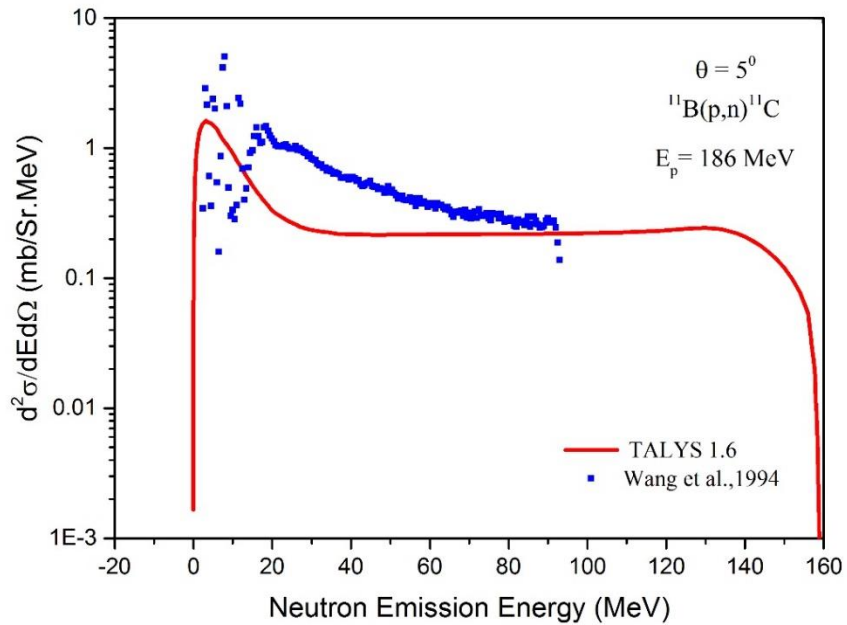

Figure 4.64. Calculated double differential cross sections of neutron emission compared with experimental data for 186 MeV incident proton energy, angle 34.4° for $^{13}C(p,n)^{13}N$ reaction
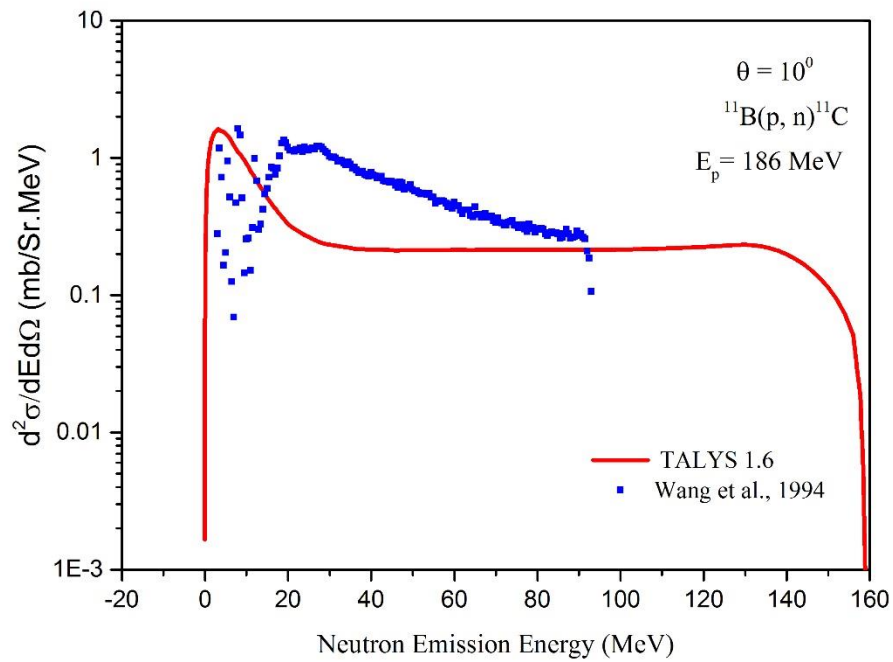
Figure 4.65. Calculated double differential cross sections of neutron emission compared with experimental data for 186 MeV incident proton energy, angle 39.4° for $^{13}C(p,n)^{13}N$ reaction

Figure 4.66. Calculated double differential cross sections of neutron emission compared with experimental data for 186 MeV incident proton energy, angle 44.4° for $^{13}C(p,n)^{13}N$ reaction
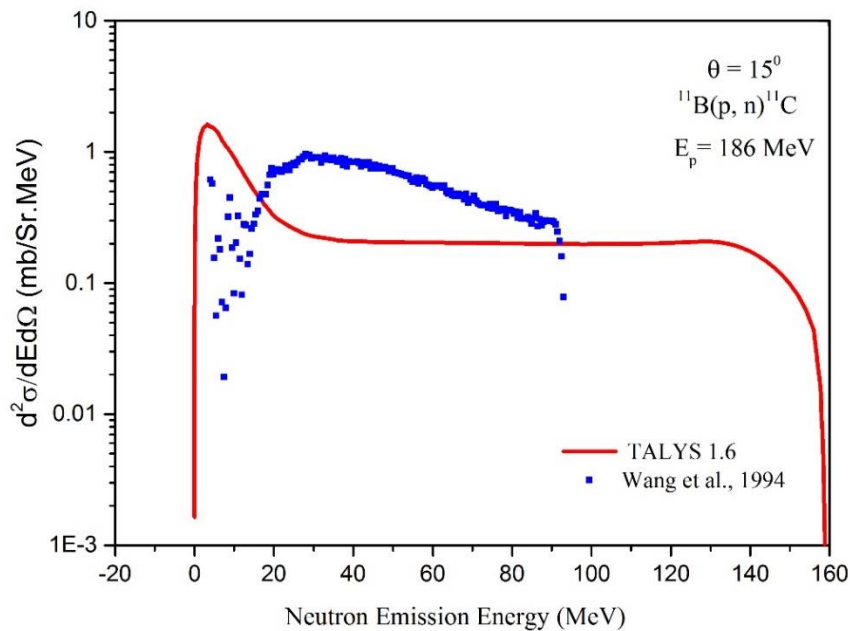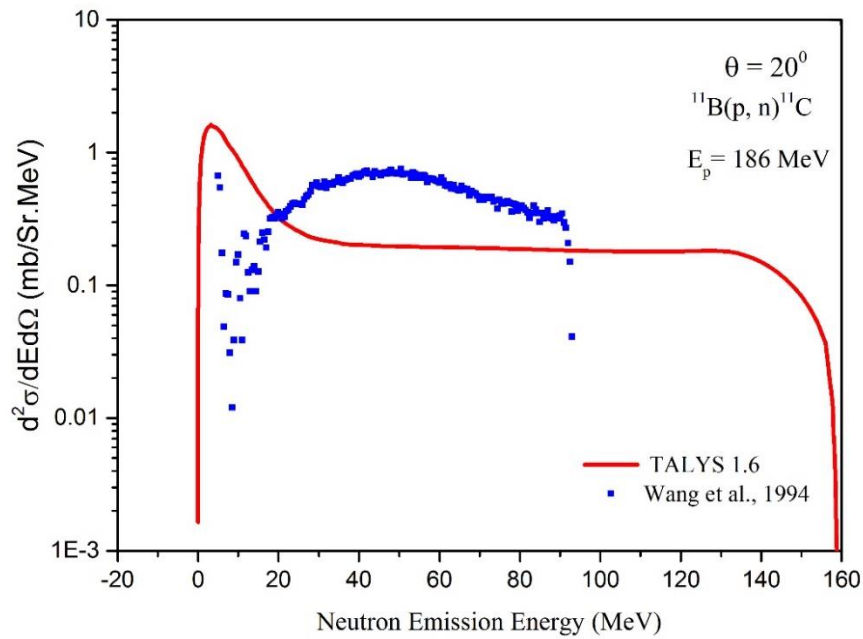
Figure 4.67. Calculated double differential cross sections of neutron emission compared with experimental data for 186 MeV incident proton energy, angle 48.9˚ for ^{13}C(p,n)^{13}N reaction

4.3.2.2. DDX calculations at Ep = 30 MeV and θ = 60˚

Double differential cross sections DDX for the ^{13}C(p,n)^{13}N reaction have been calculated with proton incident energy 30 MeV using nuclear reaction simulation program TALYS 1.6 code to produce Nitrogen-13 at the neutron emission angle of 60˚. The results of calculation of DDX for ^{13}C(p,n)^{13}N reaction were carried out using TALYS 1.6 are plotted in Figure 4.68 and compared with the experimental data of Clough et al. (1970) taken from the EXFOR library. From Figure 4.68 it can be said that the calculated results with the TALYS 1.6 code show a similarity with experimental data of Clough et al. (1970).
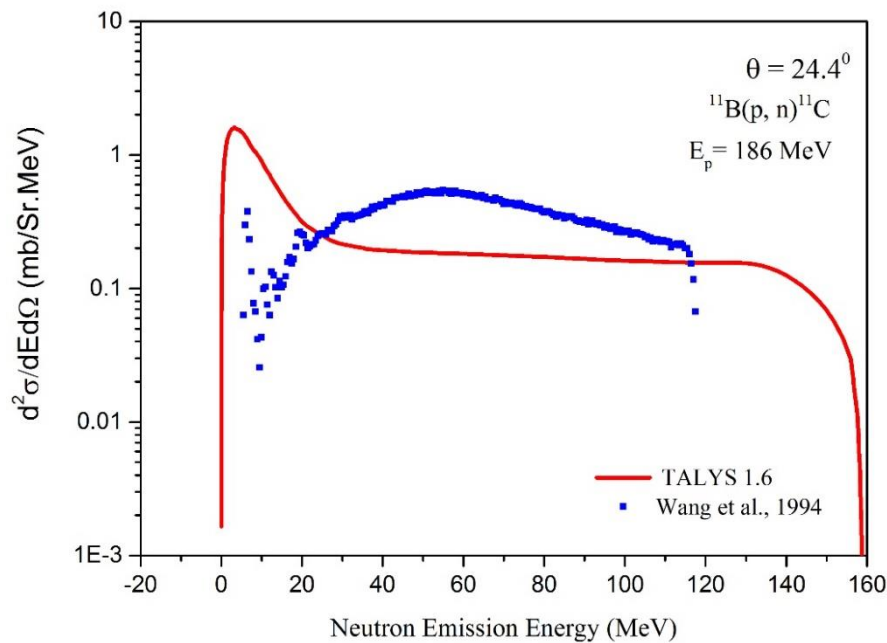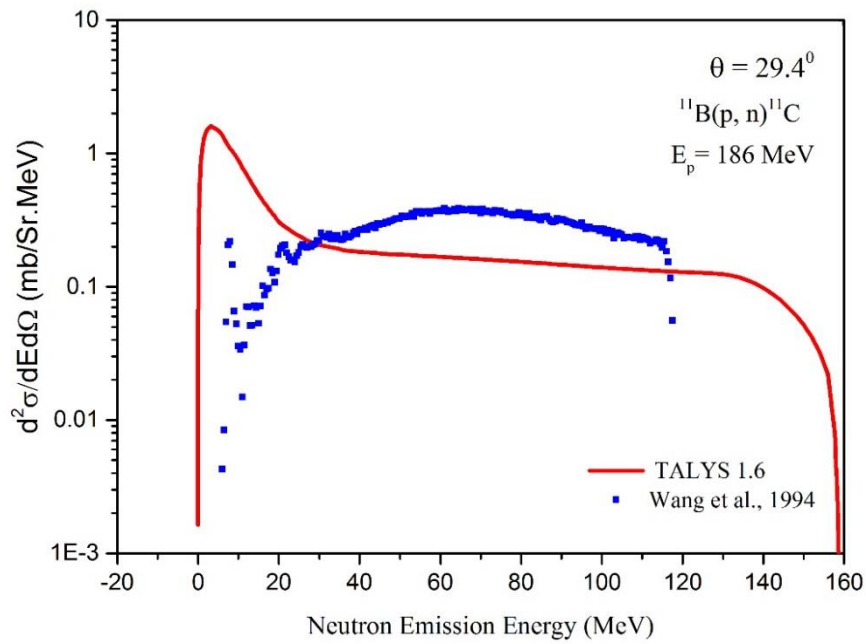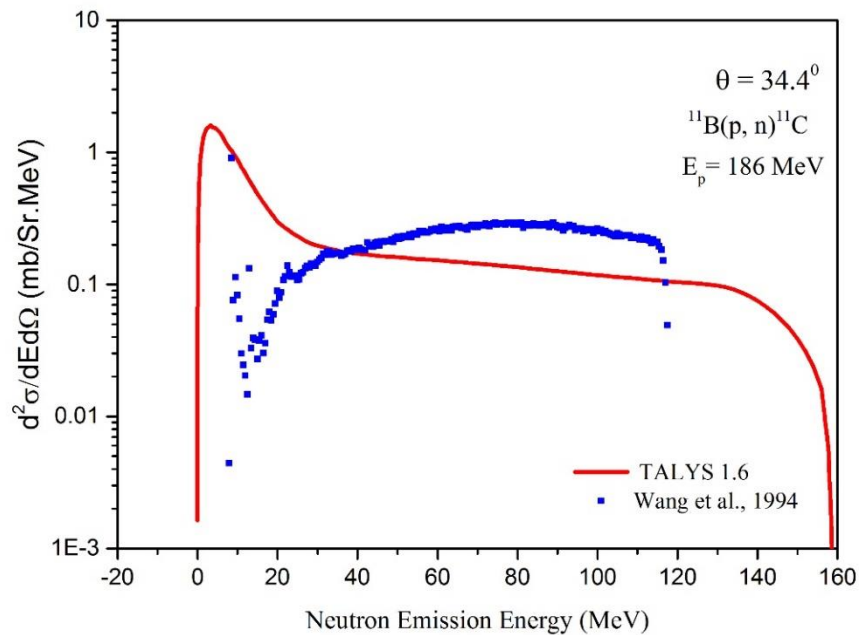
Figure 4.68. Calculated double differential cross sections of neutron emission compared with experimental data for 30 MeV incident proton energy, angle 60° for $^{13}C(p,n)^{13}N$ reaction

4.3.2.3. DDX calculations at Ep = 50 MeV and θ = 20°

The DDX ($d^2\sigma$ /dE dΩ) of ^{13}C target nuclei at neutron emission angle 20° for $^{13}C(p,n)^{13}N$ reaction has been calculated by nuclear reaction simulation TALYS 1.6 code at 50 MeV incident proton energy. The calculated results of the emitted neutron particle at given angle have been compared with the available experimental data of Clough et al. (1970) taken from the EXFOR library shown in Figure 4.69. From the comparison it is noted that the experimental data performed by Clough et al. (1970) in a good agreement with present calculated results from 30 MeV to 37 MeV. For the case of higher energies (above 37 MEV) a similar differences has been observed with the Figure 4.45.
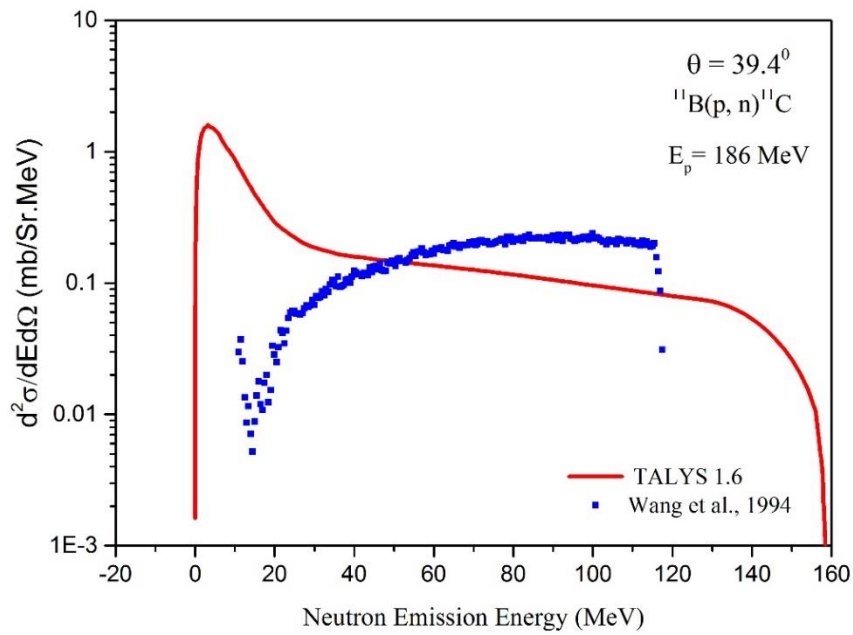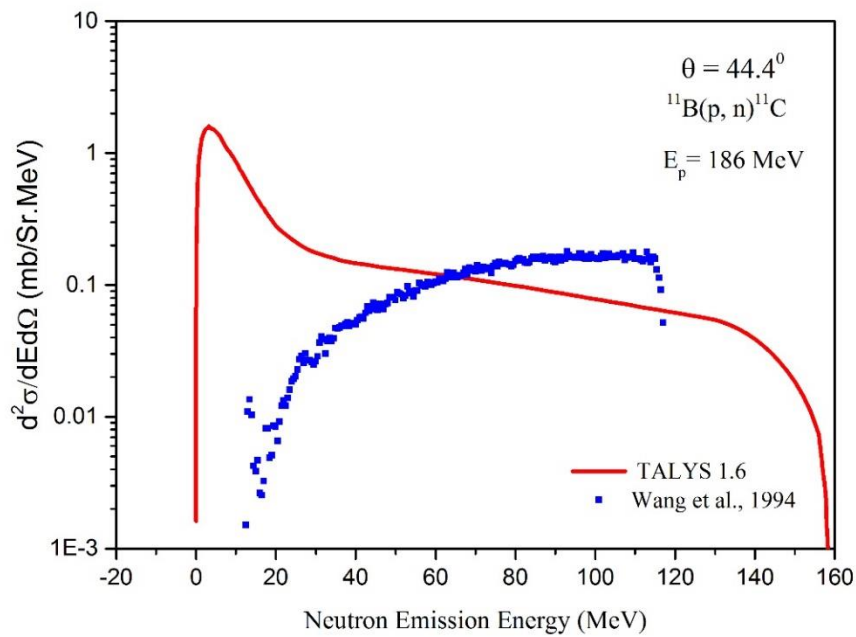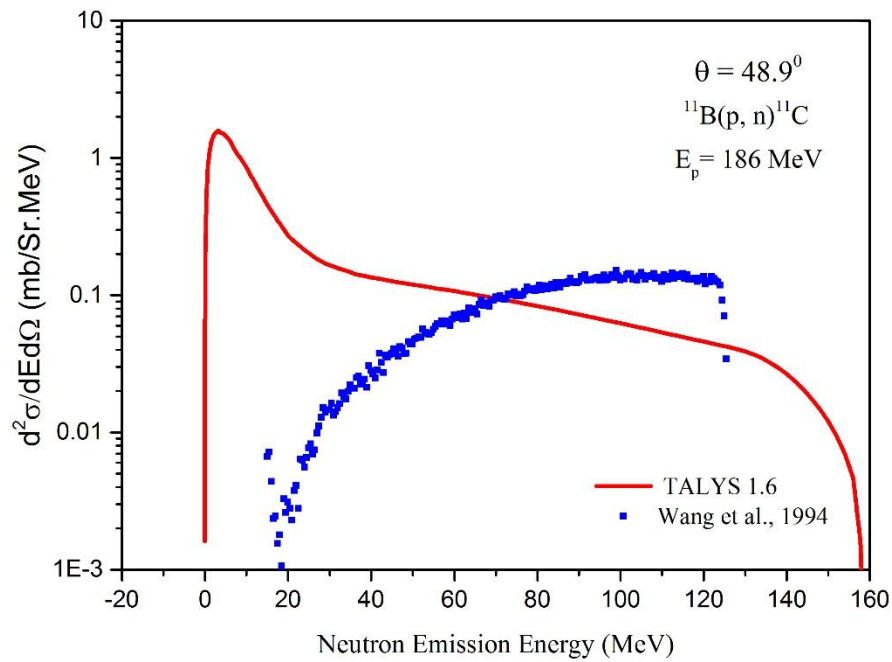
Figure 4.69. Calculated double differential cross sections of neutron emission compared with experimental data for 50 MeV incident proton energy, angle 20° for $^{13}C(p,n)^{13}N$ reaction

4.3.2.4. DDX calculations at Ep = 392 MeV and different angles

Double differential cross sections DDX for neutron emission cross sections for ^{13}C target nuclei at emission angles 12°, 20° and 28° for $^{13}C(p,n)^{13}N$ reaction have been calculated by nuclear reaction simulation TALYS 1.6 code at 392 MeV incident proton energy. The results of calculation of DDX of the emitted neutron particle at given angle for $^{13}C(p,n)^{13}N$ reaction were carried out using TALYS 1.6 are plotted in Figures 4.70-4.72 and comparison with the experimental data of Otsu, (1995) taken from the EXFOR library. In the comparison it is observed that the experimental data and the theoretical DDX calculations were in good agreement.
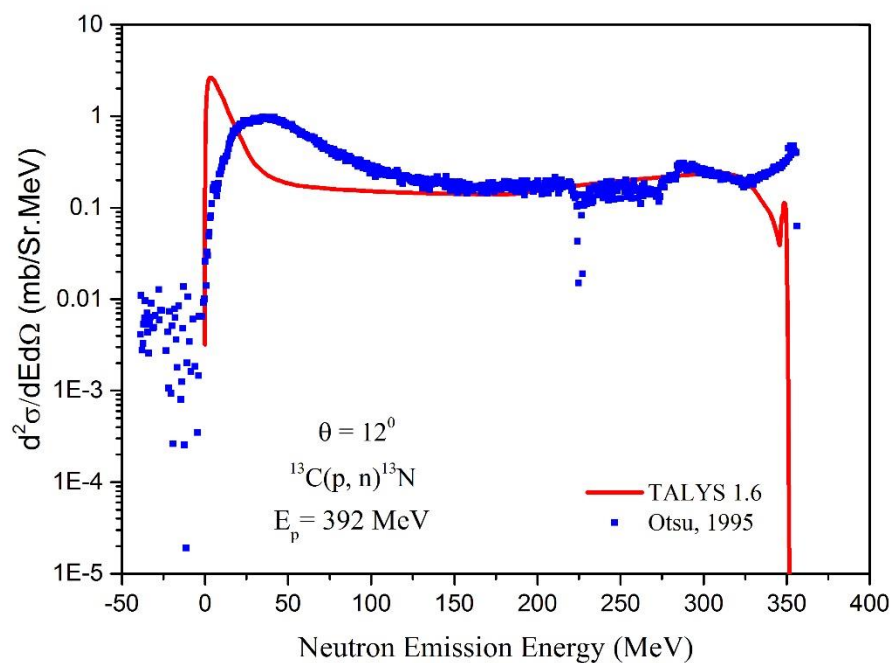
Figure 4.70. Calculated double differential cross sections of neutron emission compared with experimental data for 392 MeV incident proton energy, angle 12° for $^{13}C(p,n)^{13}N$ reaction
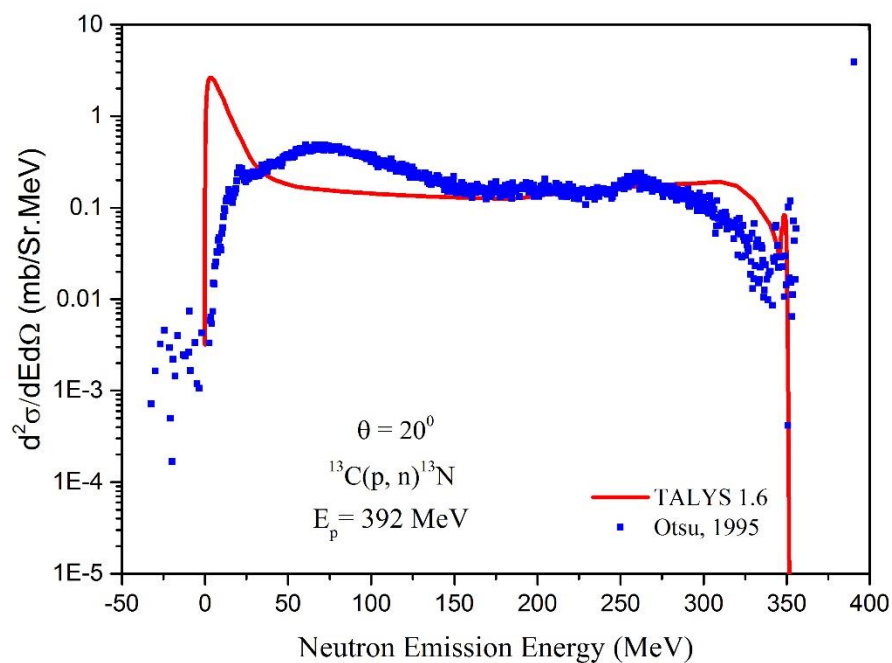
Figure 4.71. Calculated double differential cross sections of neutron emission compared with experimental data for 392 MeV incident proton energy, angle 20° for $^{13}C(p,n)^{13}N$ reaction
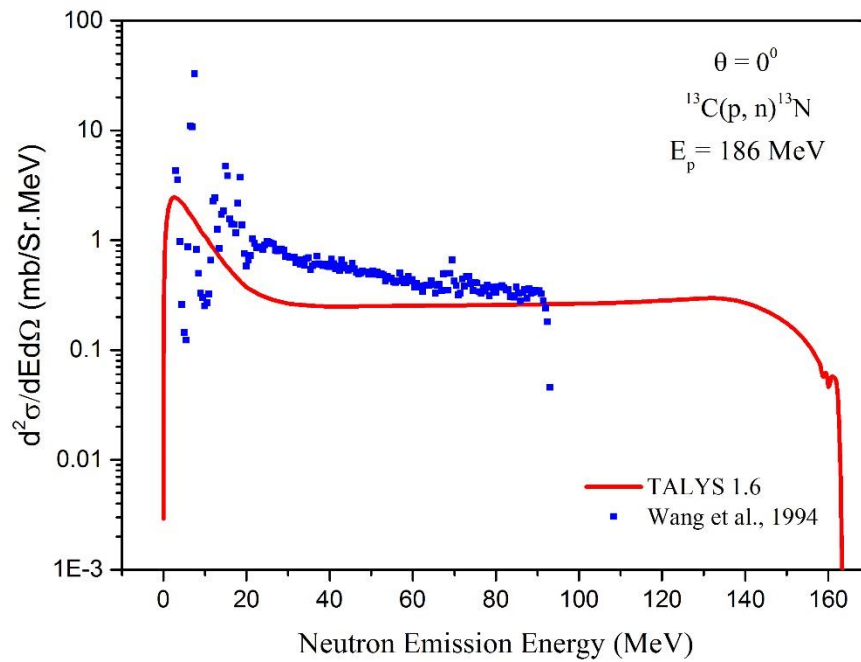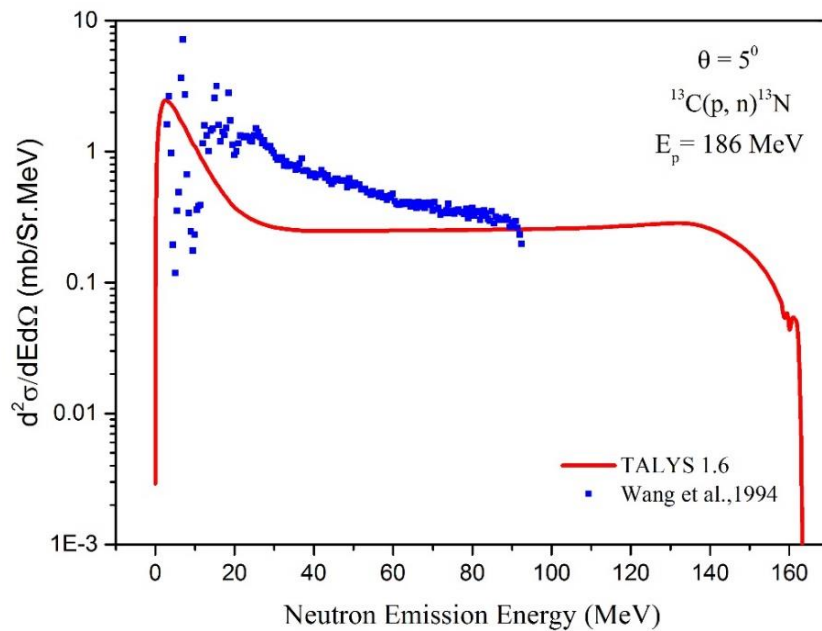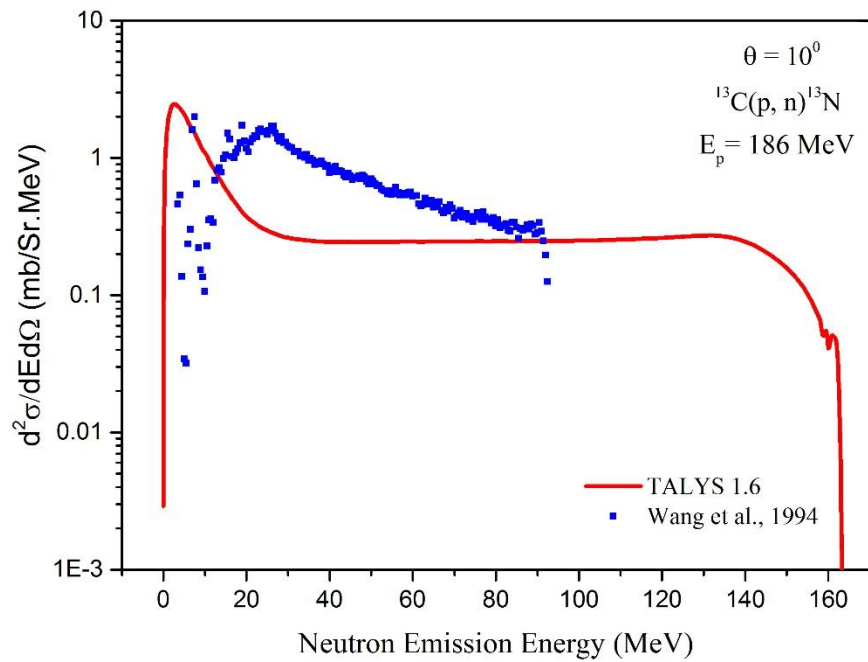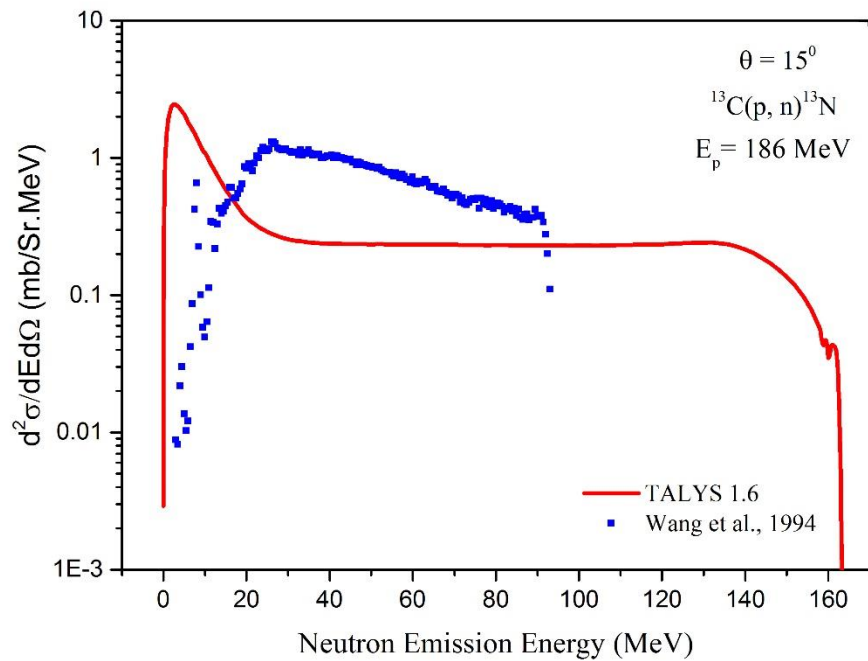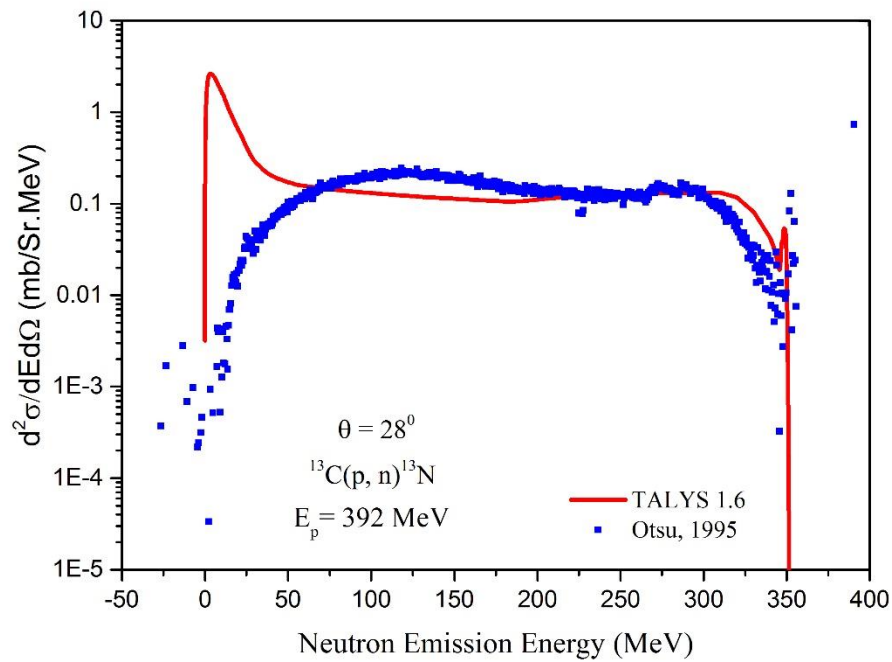
Figure 4.72. Calculated double differential cross sections of neutron emission compared with experimental data for 392 MeV incident proton energy, angle 28° for $^{13}C(p,n)^{13}N$ reaction

4.3.3. Copper-64 production

4.3.3.1. DDX calculations at En=9 MeV and different angles

The DDX ($d^2\sigma$ /dE dΩ) for proton emission cross sections for ^{63}Cu target nuclei at emission angles 30°, 60° and 120 ° have been calculated by nuclear reaction simulation TALYS 1.6 code at 9 MeV incident neutron energy. The calculation achieved by sending neutron on ^{63}Cu target in the $^{63}Cu(n,p)^{64}Cu$ reaction to produce Copper-64 radioisotope which used in nuclear medicine in PET technique. The calculated results of the emitted proton particles at given angles have been compared with the available experimental data of Ahmad et al. (1987) taken from the EXFOR library are shown in Figures 4.73- 4.75. In the comparison of present calculated results with experimental data reported by Ahmad et al. (1987) a general good agreement were obtained for all angles.
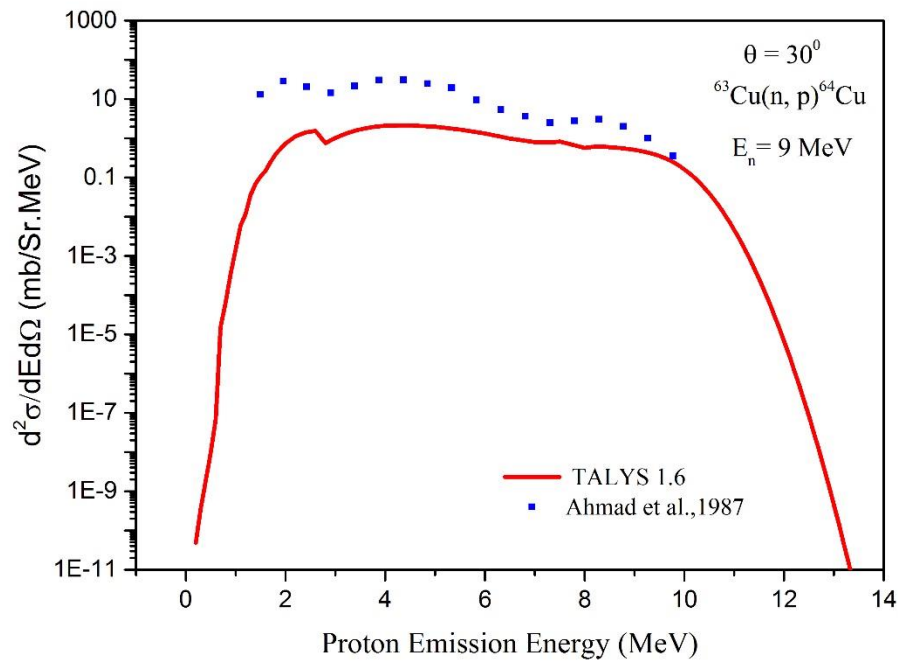
Figure 4.73. Calculated double differential cross sections of proton emission compared with experimental data for 9 MeV incident neutron energy, angle 30° for $^{63}Cu(n,p)^{64}Cu$ reaction
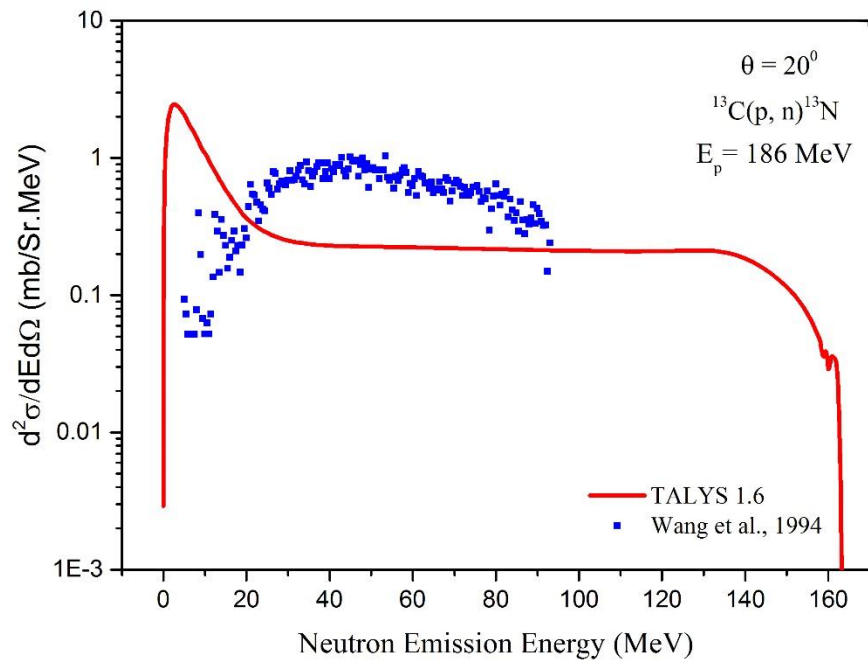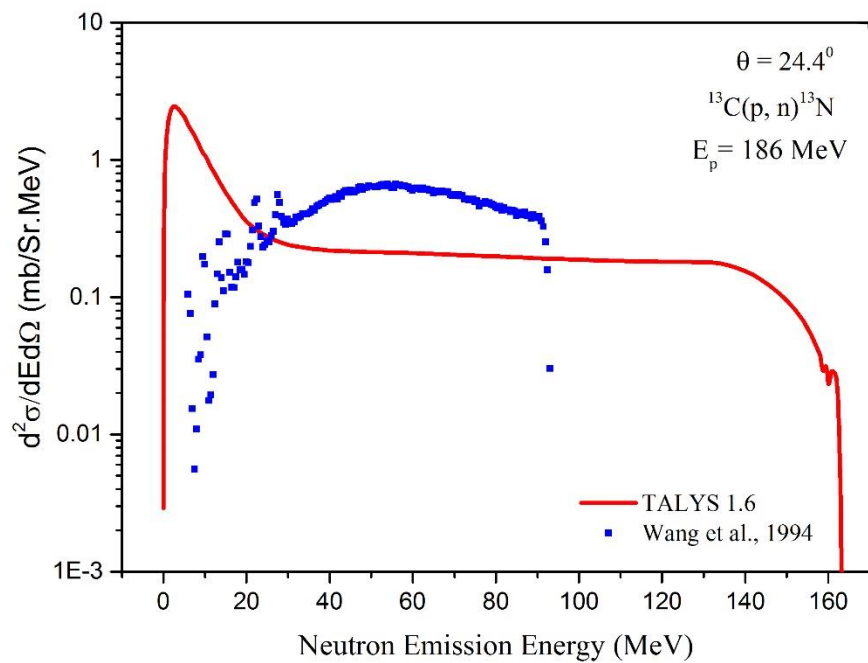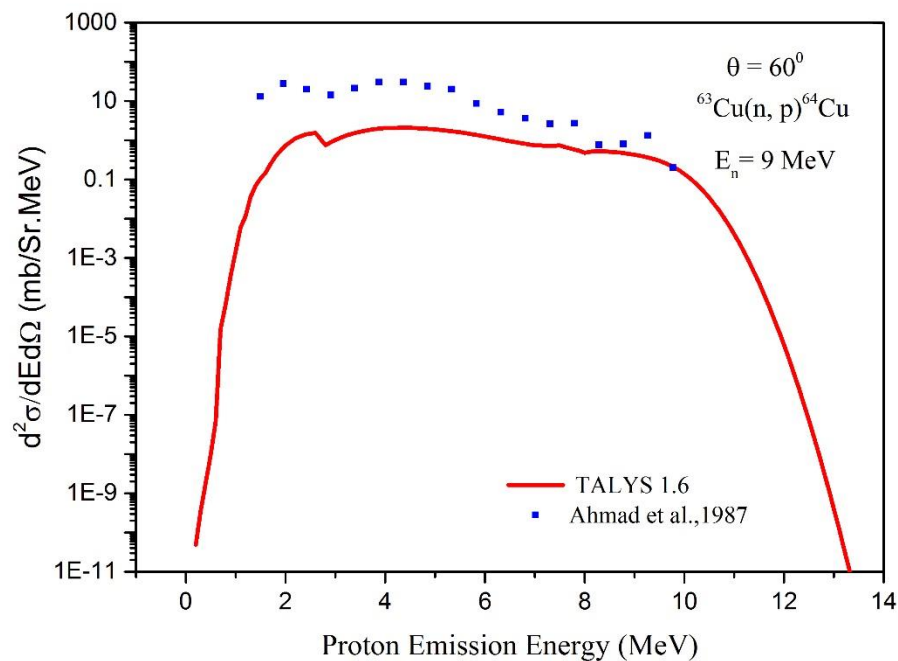

Figure 4.74. Calculated double differential cross sections of proton emission compared with experimental data for 9 MeV incident neutron energy, angle 60° for $^{63}Cu(n,p)^{64}Cu$ reaction
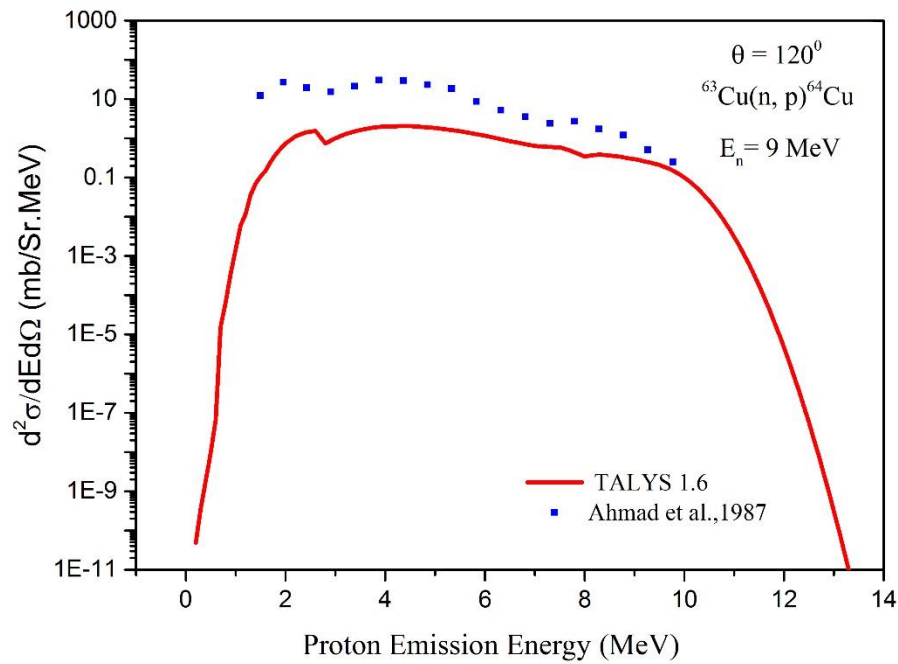
Figure 4.75. Calculated double differential cross sections of proton emission compared with experimental data for 9 MeV incident neutron energy, angle 120° for ^{63}Cu(n,p)^{64}Cu reaction

4.3.3.2. DDX calculation at En = 11 MeV and different angles

Double differential cross sections DDX for proton emission cross sections for ^{63}Cu target nuclei at emission angles 30°, 60°, 105° and 130° for ^{63}Cu(n,p)^{64}Cu reaction have been calculated by nuclear reaction simulation TALYS 1.6 code at 11 MeV incident neutron energy. The results of the calculations are plotted in Figures 4.76-4.79 and compared with the experimental data of Ahmad et al. (1987) taken from the EXFOR library. The results of the comparison shown a good agreement between the results calculated in present study and the previous data displayed by Ahmad et al. (1987) for all angles.
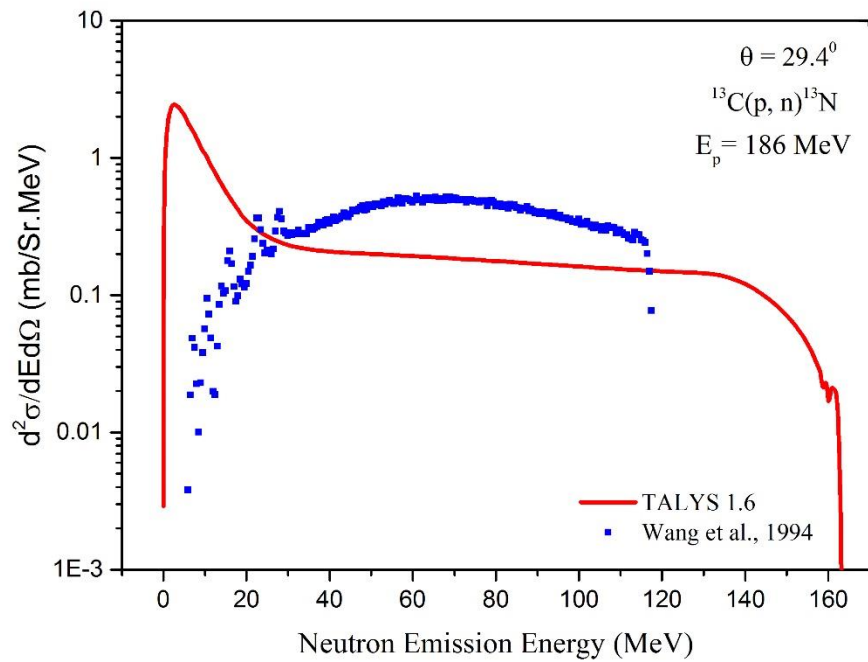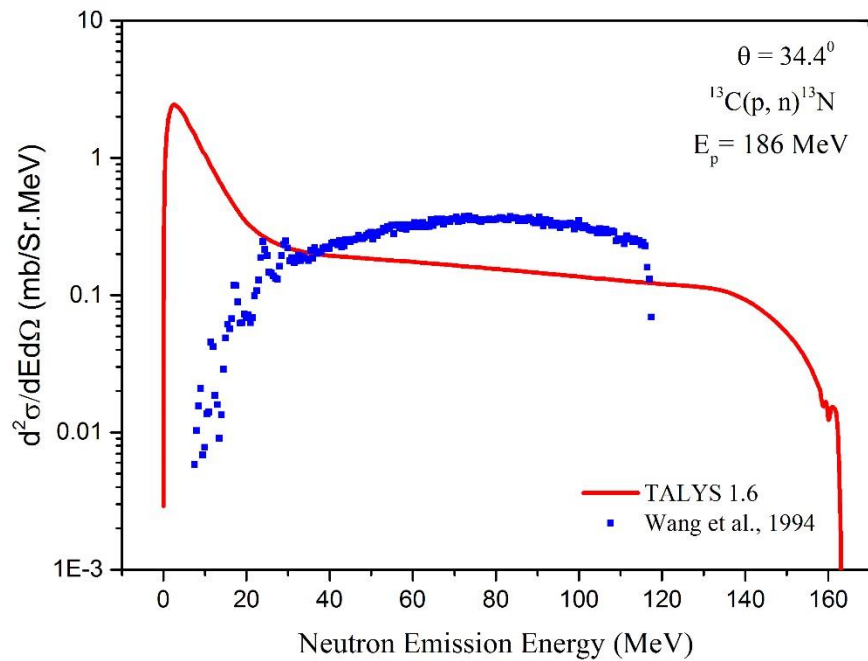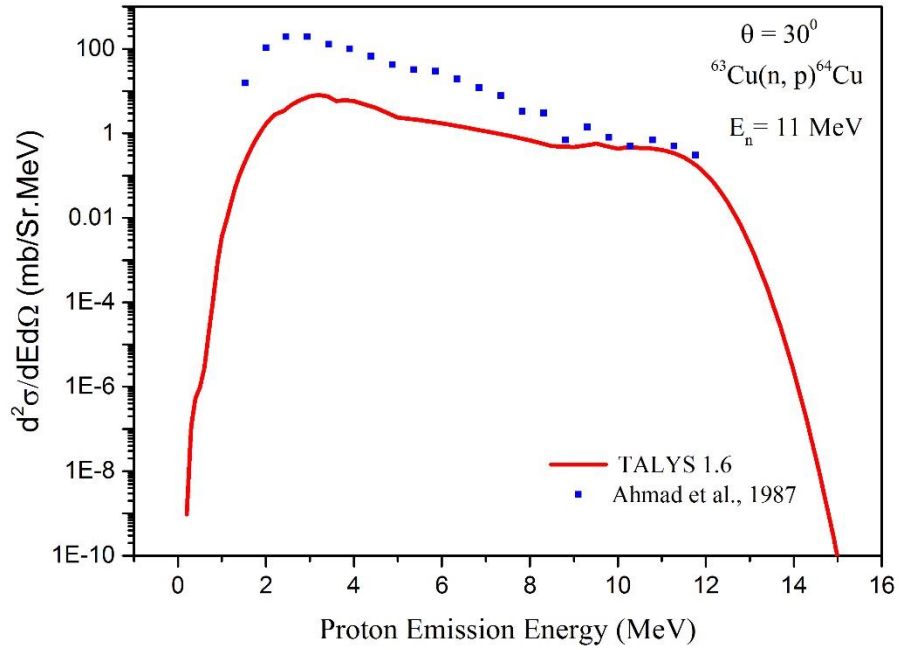
Figure 4.76. Calculated double differential cross sections of proton emission compared with experimental data for 11 MeV incident neutron energy, angle 30° for ^{63}Cu(n,p)^{64}Cu reaction
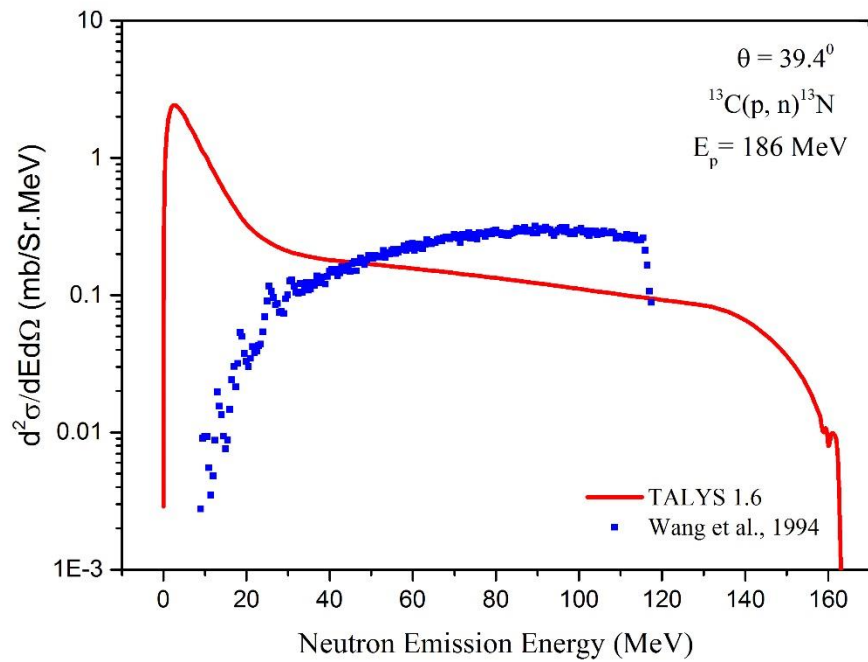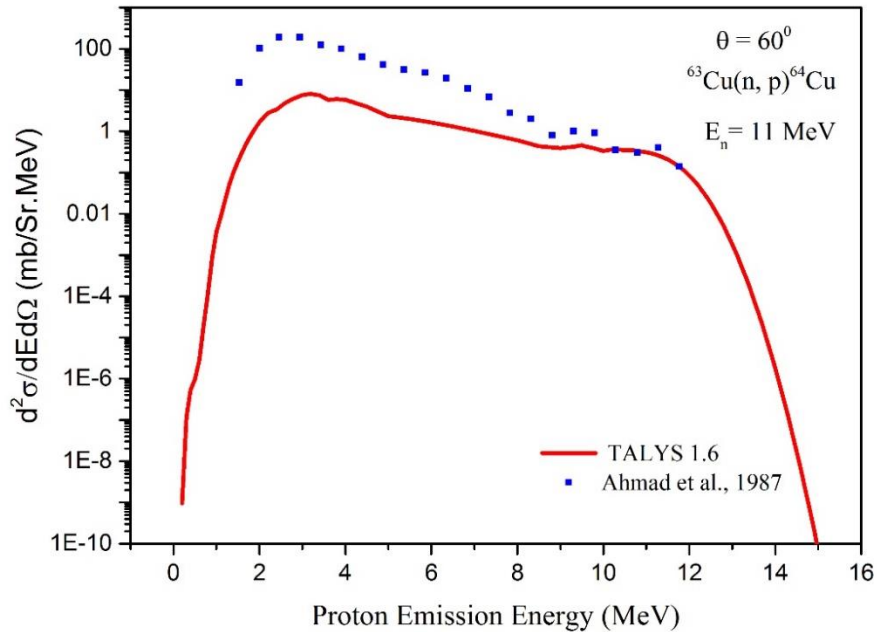

Figure 4.77. Calculated double differential cross sections of proton emission compared with experimental data for 11 MeV incident neutron energy, angle 60° for ^{63}Cu(n,p)^{64}Cu reaction
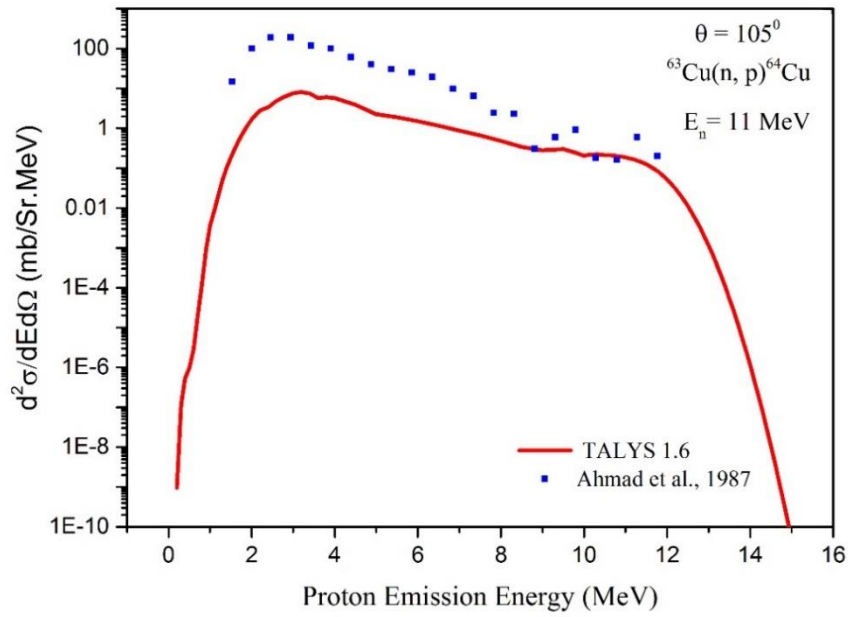
Figure 4.78. Calculated double differential cross sections of proton emission compared with experimental data for 11 MeV incident neutron energy, angle 105° for $^{63}Cu(n,p)^{64}Cu$ reaction
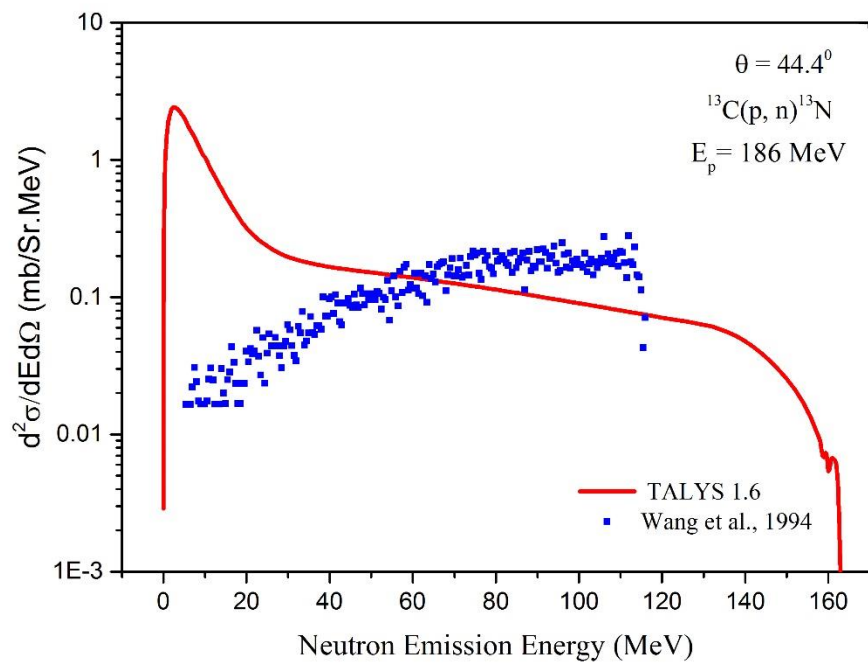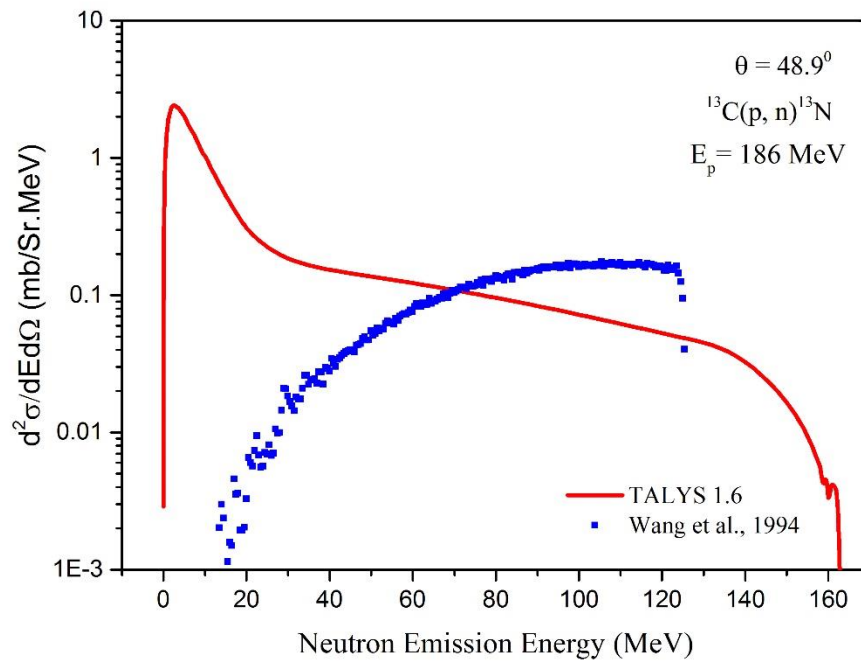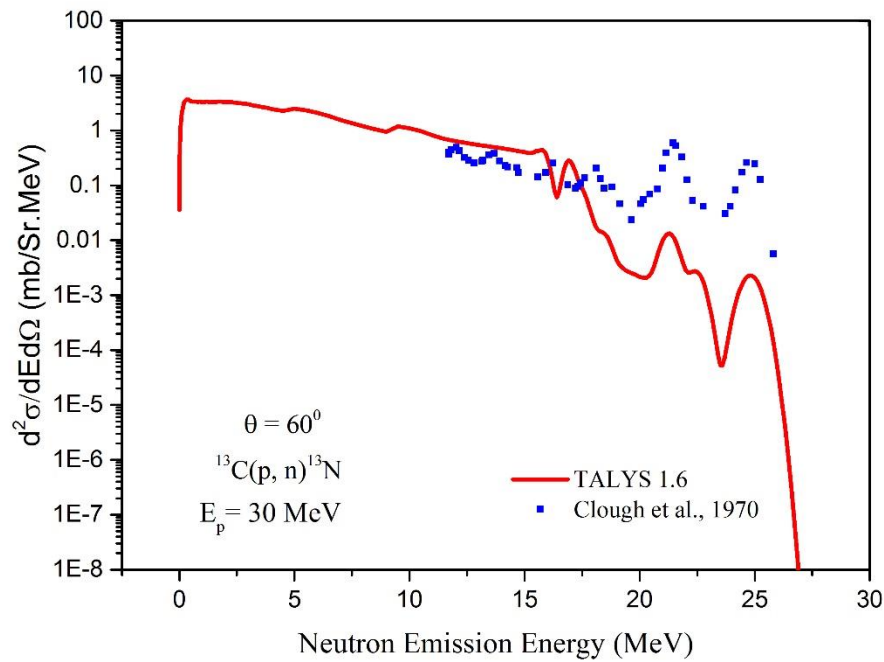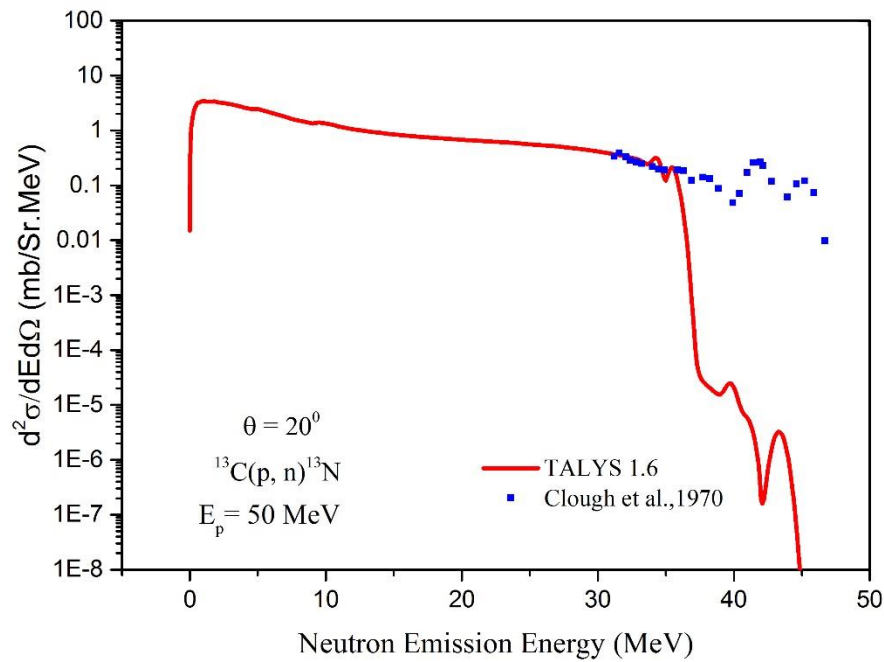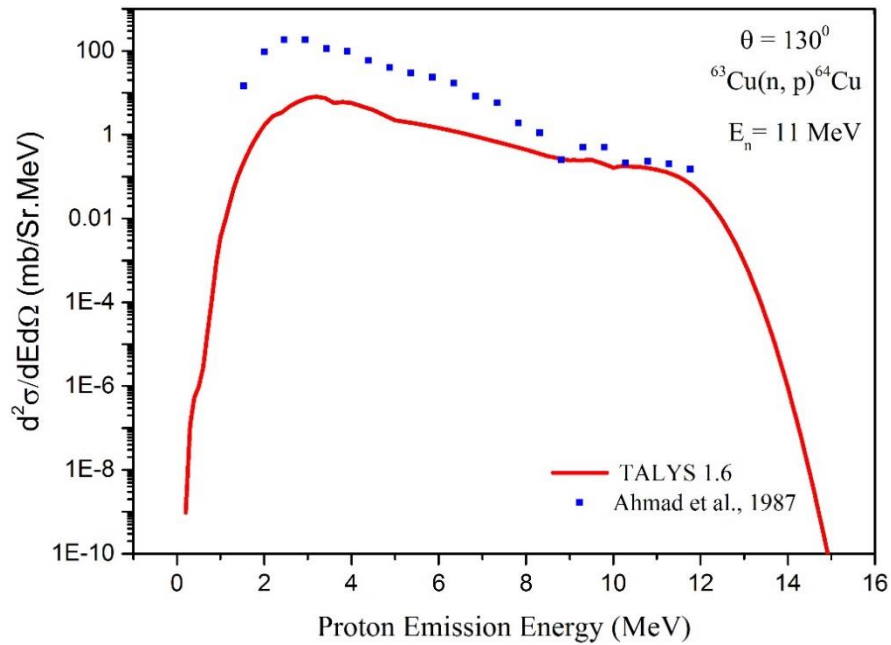

Figure 4.79. Calculated double differential cross sections of proton emission compared with experimental data for 11 MeV incident neutron energy, angle 130° for $^{63}Cu(n,p)^{64}Cu$ reaction

5. CONCLUSIONS

In nuclear medicine, the radionuclides are used for useful applications, where the nuclear properties of radioactive substances concerning human health in diagnosis, therapy, prevention of many serious ailments and research to evaluate metabolic, physiologic and pathologic conditions of the human body. This provided success in production and usage of these radionuclides in oncology, cardiology and even psychiatry by imaging procedures where it gives virtually information about the function of every major organ/ tissue of the human body.

A large number of radionuclides used in nuclear medicine are produced in cyclotrons, accelerators or in nuclear reactors, and their production is an important and constantly evolving issue. The cross section data are generally well-known and can be satisfactorily reproduced by nuclear model calculations. In particular, if the experimental measurements are unobtainable or are improbable to be produced because of the experimental difficulties, then theoretical models of nuclear reactions are needed to obtain the prediction of the reaction cross-sections. For reactions where no experimental data are available, the application of nuclear reaction theory seems to be a feasible method to get more information on the data required. A number of nuclear model codes were developed first to gain theoretical understanding of the nuclear reaction processes involved. Later, they have been also used to calculate excitation functions for charged particle induced reactions of medical interest and compared their results with experimental ones. Calculations based on nuclear reaction models play an important role in the development of reaction cross sections.

Nuclear reaction simulation TALYS 1.6 code has been successfully applied to calculate a cross section of nuclear reactions with neutrons, protons, photons deuterons, helium-3 and alpha particles both in entrance and exit channel. We have to point out, however, that the theoretical calculations cannot replace experiments at all as the model parameters like optical model parameters, level density parameters and preequilibrium model parameters need adjustment to experimental data to supply results with sufficient accuracy. To obtain accurate results each calculations of unknown cross sections should be based on parameters, which simultaneously reproduce available experimental data in the mass region of interest. The degree of

the agreement may then give an estimate for the accuracy of the unknown cross sections.

The resulting radioisotopes in this study ^{11}C, ^{13}N, ^{18}F, ^{50}Mn, ^{57}Co, ^{75}Br, ^{76}Br, ^{94}Tc, ^{99}Tc, ^{64}Cu and ^{124}I are important and widely used in diagnostic and therapeutic applications.

Some of the radionuclides for PET, such as ^{11}C and ^{13}N are isotopes of natural elements that constitute most biochemical substances and drugs. In such cases, the radiopharmaceuticals developed are ideal probes for molecular imaging because they are biochemically indistinguishable from their natural counterparts. However, for practical application, the half-lives ($T_{1/2}$) of these three radionuclides are too short (^{11}C: $T_{1/2}$ = 20 min; ^{13}N: $T_{1/2}$ = 10 min), which may limit both the chemical synthesis processes as well as the length of PET studies.

The calculated results with the TALYS 1.6 code program agree in an acceptable manner with the experimental data obtained from the International Atomic Energy Agency EXFOR (Experimental Nuclear Reaction Data Library), with some exceptions, it was observed some of which are higher or lower than the calculated results, this could be due to the older experimental technique in the measurement. On the other hand this work contributes to the development of radioisotope and neutron production technology, investigation of nuclear structure, the strengthening of the nuclear database and can be a guide to the work to be done in order to develop accelerator and reactor technology.

As a results; in the total cross section calculations for the production of radioisotopes from the reactions used in this study, in the ^{18}F radioisotope production it can be said that for (^{3}He,p) reaction have maximun cross section with compared other reactions at energy range 5-10 MeV. For the production of ^{124}I and ^{75}Br radionuclides at energy range between 15-25 MeV in (p,2n) reaction it is considered the best production way. For ^{76}Br and ^{94}Tc production in (p,n) reaction at 10-15 MeV and 8-13 MeV energy range respectively, the cross section higher than others. In the production of ^{57}Co radioisotope at incident deuteron energy of 2.7 MeV and 3.8 MeV it the energy value of largest neutron emission spectrum is at 0.5-2.5 MeV. In Manganese-50 productions for ^{50}Cr(p,n)^{50}Mn reaction at incident proton energy 25

MeV the largest neutron emission spectrum has been obtained at 0.2-2 MeV. For ^{11}C radioisotope production (p,n) reaction at 186 MeV proton incident energy and for different angles highest neutron emission spectrum obtained at 2-5 MeV. As for the production of ^{13}N (p,n) reaction at different proton incident energy and different angles, the energy range between 2-5 MeV approves the largest neutron emission spectrum.

In produc of ^{64}Cu radioisotope the proton emission double differential cross section calculations in different neutron incident energies 9 MeV and 11 MeV at different angles the dependence of energies and angles is apparent. As the excitation energy increases the maximum value of the neutron-proton (n, p) reaction double differential cross section decreased.

It can be concluded that in the field of nuclear physics even in high energies, theoretical work is important in carrying out a guideline for experimental work which is difficult or impossible.

REFERENCES

Acerbi, E., Birattari, C., Castiglioni, M., Resmini, F., Villa, M., 1975. Production of ^{123}I for Medical Purposes at the Milan AVF Cyclotron, The International Journal of Applied Radiation and Isotopes, 26(12), 741-747.

Ahmad, M., Brient, C. E., Egun, P. M., Grimes, S. M., Saraf, S., Satyanarayana, H., 1987. Charged-Particle Emission in Reactions of 9- and 11-MeV Neutrons with ^{63,65}Cu, Nuclear Science and Engineering, 95(4), 296-303.

Ahrens, J., 1985. Nuclear Physics, A446, 229c.

Akkoyun, S., Bayram, T., Kara, SO., 2015. Photonuclear Reaction Cross Sections for Gallium Isotopes, NUBA Conference, Nuclear Physics and Astrophysics, Journal of Physics, Conference Series 590, 012047.

Akkurt, İ., 1998. The Study of (γ,n) Reactions in Light Nuclei at Intermediate Photon Energy. Glasgow University, Department of Physics and Astronomy, Ph.D. Thesis, 140p, İskoçya.

Al-Abyad, M., 2011. Evaluation of Excitation Functions of Reactions Used in Cyclotron Production of Some Medical Radioisotopes, Journal of Nuclear and Radiation Physics, 6(1,2), 43-53.

Alfassi, Z. B., Weinreich, 1982. The Production of Positron Emitters ^{75}Br and ^{76}Br: Excitation Functions and Yields for ^{3}He and α-particle Induced Nuclear Reactions on arsenic, Radiochimica Acta, 30(2), 67-72.

Artun, O., Haytekin, H., 2017. Investigation of Excitation Functions of Proton Induced Reactions on $^{94,\ 96,\ 98,\ 100}$Mo Targets for Production of Radioisotopes $^{94m,\ 94g,\ 96m,\ 96g,\ 96,\ 99m}$Tc, Turkish Journal of Physics, 41, 295-302.

Auler, L. T., Da Silva, A. G., Newton, G. W. A., 1981. Excitation Functions and Isomer Ratios in ^{93}Nb(^{3}He,xn) Reactions with X = 2 and 3, Journal of Inorganic and Nuclear Chemistry, 43(11), 2611-2615.

Aydin, A., Tel, E., Kaplan, A., Büyükuslu, H., 2010. Pre-equilibrium Cross Section Calculations in Alpha Induced Reactions on ^{65}Cu and ^{209}Bi, Annals of Nuclear Energy, 37, 1316–1320.

Azzam, A. Said, S.A. Al-abyad, M., D., 2014. Evaluation of Different Production Routes for the Radio Medical Isotope ^{203}Pb Using TALYS 1.4 and EMPIRE 3.1 Code Calculations, Applied Radiation and Isotopes, 91, 109–113.

Backhausen, H., Stocklin, G., Weinreich, R., 1981. Formation of ^{18}F via Its ^{18}Ne Precursor: Excitation Functions of the Reactions ^{20}Ne(d,x)^{18}Ne and ^{20}Ne(^{3}He,αn)^{18}Ne, Radiochimica Acta, 29(1), 1-4.

Bair, J. K., 1973. Total Neutron Yields from the Proton Bombardment of ^{17,18}O, Physical Review, Part C, Nuclear Physics, 8(1), 120-123.

Bergere, R., Beil, H., Carlos, P., Veyssiere, A., 1969. Sections Efficaces Photoneutroniques de I, Ce, Sm, Er et Lu, Nuclear Physics A, 133(2), 417-437.

Bielajew, A.F. 2001. Fundamentals of the Monte Carlo Method for Neutral and Charged Particle Transport, Ann Arbor, Michigan, The University of Michigan.

Bissem, H. H., Georgi, R., Scobel, W., Ernst, J., Kaba, M., Rama Rao, J., Strohe, H., 1980. Entrance and Exit Channel Phenomena in d- and ^{3}He-induced Preequilibrium decay, Physical Review C, Nuclear Physics, 22(4), 1468-1484.

Blair, J. M., Leigh, J .J., 1960. Total Cross Sections of the O^{18}(p,α)N^{15} and O^{18}(p,n)F^{18} Reactions, Physical Review, 118(2), 495-498.

Blann, M. Grimes, S. M., Hansen, L. F., Komoto, T. T., Pohl, B. A., Scobel, W., Trabandt, M., Wong, C., 1985. Single-Particle Effects in Precompound Reactions: Influence of the f7/2 Shell Closure, Physical Review C, Nuclear Physics, 32(2), 411-417.

Blaser, J. P., Boehm, F., Marmier, P., Scherrer, P., 1951. Excitation Functions of the (p,n) Reaction for Light Elements, Helvetica Physica Acta, 24, 465.

Boffi, S., Passatore, G., 1976. Nuclear Optical Model Potential, by Springer-Verlag Berlin Heidelberg, Germany.

Bormann, M., Fretwurst, E., Schehka, P., Wrege, G., Buttner, H., Lindner, A., Meldner, H., 1965. Some Excitation Functions of Neutron Induced Reactions in the Energy Range 12.6-19.6 MeV, Nuclear Physics, 63(3), 438-448

Braghirolli, A. M. S., Waissmann, W., Silva, J. B., Santos, G. R., 2014. Production of Iodine-124 and Its Applications in Nuclear Medicine, Applied Radiation and Isotopes, 90, 138-148.

Brill, O. D., Vlasov, N. A., Kalinin, S. P., Sokolov, L. S., 1961. Cross Section of the (n,2n) Reaction in C^{12},N^{14},O^{16} and F^{19} in the Energy Interval 10-37MeV, Doklady Akademii Nauk, 136(1), 55.

Brown, D., Gronberg, J., Verbeke, J., Wright, D., 2010. Photonuclear Physics and Data Evaluations, Lawrence Livermore National Laboratory, LLNL-TR-455702.

Calboreanu, A., Pencea, C., Salagean, O., 1982. The Effect of Gamma de-excitation Competition on the (α,n) and (α,2n) Reactions on Gold and Antimony, Nuclear Physics A, 383(2), 251-263.

Chadwick, J., Goldhaber, M., 1935. The Nuclear Photoelectric Effect, The Royal Society, 151(873), 479-493.

Challan, M. B., Cosman, M. N. H., Abou-Zeid, M. A., 2007. Thin Target Yields and EMPIRE-II Predictions on the Accelerator Production of Technetium-99m, Journal of Nuclear and Radiation Physics, 2(1), 1-12.

Chatterjee, A., Nath, A., Ghose, A. M., 1969. Absolute (n,2n) Cross Sections of Nuclei Near 14 MeV, Nuclear Physics and Solid State Physics Symposium, 2, 117-121.

Clough, A. S., Batty, C. J., Bonner, B. E., Williams, L. E., 1970. A Microscopic Analysis of the (p,n) Reaction on 1p-Shell Nuclei, Nuclear Physics A, 143(2), 385-403.

Cole, E. L., Stewart, M. N., Littich, R., Hoareau,R., Scott, P. J. H., 2014. Radiosyntheses Using Fluorine-18: the Art and Science of Late Stage Fluorination, Current Topics in Medicinal Chemistry, 14(7), 875–900.

Joliot, F., Curie, I., 1934. Artificial Production of a New Kind of Radio-Element, Nature, 133, 201-202.

Das, T., 2015. Application of Radioisotope in Medicine, Science and Culture, 81(9-10), 230-236.

Del Bianco, W. E., Stephens, W. E., 1962. Photonuclear Activation by 20.5-MeV Gamma Rays, Physical Review, 126(2), 709-717.

Ditroi, F., Hermanne, A., Tarkanyi, F., Takacs, S., Ignatyuk, A. V., 2012. Investigation of the α-particle Induced Nuclear Reactions on Natural Molybdenum, Nuclear Instruments and Methods in Physics Research Section B: Beam Interactions with Materials and Atoms, 285, 125-141.

Duchemin, C., Guertin, A., Haddad, F., Michel, N., Métivier, V., 2015. Production of Medical Isotopes from a Thorium Target Irradiated by Light Charged Particles up to 70 MeV, Physics in Medicine & Biology, 60, 931-946.

Eslami, M., Kakavand, T., 2014. Simulation of the Direct Production of ^{99m}Tc at a Small Cyclotron, Nuclear Instruments and Methods in Physics Research B, 329, 18-21.

Evans, R. D., 1955. The Atomic Nucleus, McGraw-Hill Book Inc., India, New Delhi.

Fitschen, J., Beckmann, R., Holm, U., Neuert, H., 1977. Yield and Production of ^{18}F by ^{3}He Irradiation of Water, Applied Radiation and Isotopes, 28(9), 781-784.

EXFOR/CSISRS, Experimental Nuclear Reaction Data File, 2017. Brookhaven National Laboratory, National Nuclear Data Center.

Flynn, D. S., Hershberger, R. L., Gabbard, F., 1979. Sub-Coulomb Proton Absorption for Isotopes of Zirconium and Molybdenum, Physical Review C, Nuclear Physics, 20(5), 1700-1705.

Gass, J., Muller, H. H., 1976. ^{3}He Induced Activation Cross sections on ^{10}B, ^{16}O and ^{19}F, Nuclear Instruments and Methods, 136(3), 559-561.

Glaser, M., Luthra, S. K., Brady, F., 2003. Applications of Positron-Emitting Halogens in PET Oncology (Review), International Journal of Oncology, 22, 253-267.

Grassi, I., Nanni, C., Allegri, V., Morigi, J. J., Montini, G. C., Castellucci, P., Fanti, S., 2012. The Clinical Use of PET with ^{11}C-acetate, American Journal of Nuclear Medicine and Molecular Imaging, 2(1), 33-47.

Guertin, A., Duchemin, C., Fardin, A., Guigot, C., Nigron, E., Remy, C., Haddad, F´., Michel, N., M´etivier, V., 2017. How Nuclear Data Collected For Medical Radionuclides Production Could Constrain Nuclear Codes, EPJ Web of Conferences 146, 08008.

Hahn, R. L., Ricci, E., 1966. Interactions of ^{3}He Particles with ^{9}Be, ^{12}C, ^{16}O, and ^{19}F, Physical Review, 146(3), 650-659.

Hartmann, C. L., DeLuca, Jr., P. M., 1991. Measurement of the ^{19}F(n,2n)^{18}F Cross Section from 18 to 27 MeV, Nuclear Science and Engineering, 109(3), 319-323.

Hassan, H. E., Qaim, S. M., Shubin, Yu., Azzam, A., Morsy, M., Coenen, H. H., 2004. Experimental Studies and Nuclear Model Calculations on Proton-Induced reactions on ^{nat}Se, ^{76}Se and ^{77}Se with Particular Reference to the Production of the Medically Interesting Radionuclides ^{76}Br and ^{77}Br, Applied Radiation and Isotopes, 60(6), 899-909.

Hassan, K. F., Qaim, S. M., Saleh, Z. A., Coenen, H. H., 2006. Alpha Particle Induced Reactions on ^{nat}Sb and ^{121}Sb with Particular Reference to the Production of the Medically Interesting Radionuclide ^{124}I, Applied Radiation and Isotopes, 64(1), 101-109.

Hayward, E., 1970. Photonuclear Reactions, Center for Radiation Research, Nat. Bur. of Stand. Washington, U.S. Monogr. 118.

Hess, E., Takacs, S., Scholten, B., Tarkanyi, F., Coenen, H. H., Qaim, S. M., 2001. Excitation Function of the ^{18}O(p,n)^{18}F Nuclear Reaction from Threshold up to 30 MeV, Radiochimica Acta, 89(6), 357-362.

Hevesy, V. G., 1923. The Absorption and Translocation of Lead by Plants, Biochemical Journal, 17(4-5), 439-445.

Hogan, J. J., 1973. Isomer Ratios of Tc Isotopes Produced in 10-65 MeV Bombardments of ^{96}Mo, Journal of Inorganic and Nuclear Chemistry, 35(3), 705-712.

Hohn, A., Nortier, F. M., Scholten, B., Van der Walt T. N., Coenen, H. H., Qaim, S. M., 2001. Excitation Functions of ^{125}Te(p,xn)-Reactions from Their Respective Thresholds up to 100 MeV with Special Reference to the Production of ^{124}I, Applied Radiation and Isotopes, 55(2), 149-156.

Holly, T. A., Abbott,B. G., Al-Mallah, M., Calnon, D.A., Cohen, M. C., DiFilippo, F.P., Ficaro, E. P., Freeman, M. R., Hendel, R. C., Jain, D., Leonard, S. M., Nichols, K. J., Polk, D. M., Soman, p., 2010. Single Photon-Emission Computed Tomography, Journal of Nuclear Cardiology, 1071-3581.

IAEA (International Atomic Energy Agency), 2000. Handbook on Photonuclear Data for Applications Cross sections and Spectra. Final Report of a CRP 1996-1999, IAEA-TECDOC-1178.

IAEA, 2001. Charged Particle Cross-Section Database for Medical Radioisotope Production: Diagnostic Radioisotopes and Monitor Reactions, TECDOC-1211: IAEA Vienna.

Ikeda, Y., Konno, C., Oishi, K., Nakamura, T., Miyade, H., Kawade, K., Yamamoto, H., Katoh, T., 1988. Activation Cross Section Measurements for Fusion Reactor Structural Materials at Neutron Energy from 13.3 to 15.0 MeV Using FNS facility, AERI Reports, No.1312

Ismail, M., 1989. Hybrid Model Analysis of the Excitation Function for Alpha Induced Reaction on ^{121}Sb and ^{123}Sb, Pramana - J. Physics, 32(5), 605-618.

Ismail, M., 1990. Measurement and Analysis of the Excitation Function for Alpha-Induced Reactions on Ga and Sb Isotopes, Physical Review C, Nuclear Physics, 41(1), 87-108.

Issa, S. A. A. M., 2009. Cross Section for Residual Nuclide Production by Proton–Induced Reaction with Heavy Target Elements at Medium Energies, Ph.D. Thesis in Experimental Nuclear Physics, Al-Azhar University Faculty of Science Assiut, Egypt.

Jacobson, O., Kiesewetter, D. O. Chen, X., 2015. Fluorine-18 Radiochemistry, Labeling Strategies and Synthetic Routes, Bioconjugate Chemistry, 26, 1-18.

Joos, G., 1958. Theoretical Physics, third edition, Blackie & son limited, London.

Kakavand, T., 2017. Cyclotron Production of ^{94m}Tc via Proton-Induced Reaction on ^{94}Mo Target, Proceedings of the DAE Symposiun on Nuclear Physics, 62, 576-577.

Kara, A., Korkut, T., Yiğit, M., Tel, E., 2015. Modelling Study on Production Cross Sections of ^{111}In Radioisotopes Used in Nuclear Medicine, Kerntechnik, 80(3), 270-274.

Karpuz, N., 2014. Theoretical Investigation of Some Nuclei Photonuclear Reaction Cross-Sections, Süleyman Demirel University, Ph.D. Thesis, 132p, Turkey.

Karpuz, N., Mavi, B., 2016. Theoretical Production of Radiopharmaceuticals Used in Mycardial Perfusion Scintigraphy, Acta Physica Polonica A, 130(1), 304-305.

Kilinç, F., Karpuz, N., Çetin, B., 2016. Calculation of the (p,n) Reaction Cross Section of Radionuclides Used for PET Applications, Acta physica polonica A, 130(1), 318- 139.

Kılınç, F., Karpuz, N., Çetin, B., 2016. Investigation of the Excitation Functions for Some Medical Radioisotope Production, EPJ Web of Conferences, TESNAT, 128, 01003.

Kılınç, F., Karpuz, N., Çetin, B., 2016. Theoretical Cross-Section Calculation of In-111, Tc-99m, Co-57 Radioisotopes Used for Kidney Imaging, Acta Physica Polonica A, 130(1), 311-312.

Kitson, S. L., Cuccurullo, V., Ciarmiello, A., Salvo, D. and Luigi Mansi, L., 2009. Clinical Applications of Positron Emission Tomography (PET) Imaging in Medicine: Oncology, Brain Diseases and Cardiology, Current Radiopharmaceuticals, 2, 224-253.

Kitwanga, S. W., Leleux, P., Lipnik, P., Vanhorenbeeck, J., 1990. Production of ^{14,15}O,^{18}F, and ^{19}Ne Radioactive Nuclei from (p,n) Reactions up to 30 MeV, Physical Review, Part C, Nuclear Physics, 42(2), 748-752.

Knoll, E. G. 2000. Radiation Detection and Measurement, John Wiley & Sons, New York.

Kobychev, V. V., Popov, S. B., 2005. Constraints on the Photon Charge from Observations of Extragalactic Sources, Astronomy Letters, 31(3), 147–151.

Koehler, L., Gagnon, K., McQuarrie, S., Wuest, F., 2010. Iodine-124: A Promising Positron Emitter for Organic PET Chemistry, Molecules, 15, 2686-2718.

Kondo, K., Lambrecht, R. M., Wolf, A. P., 1977. Iodine-123 Production for Radiopharmaceuticals – XX, The International Journal of Applied Radiation and Isotopes, 28(4), 395-401.

Kondratyev, S. N., Lobach, Yu. N., Sklyarenko, V. D., Tokarevsky, V. V., 1996. Cross Sections of He3 Interaction with Nb-93 Nuclei: Experimental Data and Possibilities of Their Prediction, Yadernaya Fizika, 59, 2121.

Koning, A. J., Hilaire, S., Goriely, S., 2013. TALYS 1.6 a Nuclear Reaction Program Nuclear Research and Consultancy Group (NRG), Netherlands.

Koning, A.J., Rochman, D., 2012. Modern Nuclear Data Evaluation with the TALYS Code System Nuclear Data Sheets, 113, 2841–2934.

Koning, A.J., Duijvestijn, M.C., 2004. A Global Pre-equilibrium Analysis from 7 to 200 MeV Based on the Optical Model Potential, Nuclear Physics A, 744, 15–76.

Kovacs, Z., Blessing, G., Qaim, S. M., Stocklin, G., 1985. Production of ^{75}Br via the ^{76}Se(p,2n)^{75}Br Reaction at a Compact Cyclotron, Applied Radiation and Isotopes, 36(8), 635-642.

Kragh, H., 2014. Photon: New Light on an Old Name, Cornell University Library, arXiv: 1401, 0293.

Krane, K. S., 2006. Introductory Nuclear Physics. Translate Şarer, B. Palme Publishing, Volume I, II. Printing, Ankara.

Lapenas, A. A., Bondars, Kh. Ja., Vejnbergs, Ja. K., 1975. Evaluated Data for Neutron Dosimetry Reactions, Point Data, Lapenas,Neutron Spect. Meas.by Activ., Riga

Lebeda, O., Fikrle, M., 2010. New Measurement of Excitation Functions for (d,x) Reactions on ^{nat}Mo with Special Regard to the Formation of ^{95m}Tc, $^{96m+g}$Tc, ^{99m}Tc and ^{99}Mo, Applied Radiation and Isotopes, 68(12), 2425-2432.

Lee, H. -Y.,.Beard, M, Becker, H. -W., Couder, M., Couture, A., Gorres, J., Lamm L.,, LeBlanc, P., `Brien, S., O Palumbo, A., Stech, E., Strandberg, E., Tan, W., Ugalde, C., Wiescher, M., 2005. ^{18}F(α,p)^{21}Ne Reaction: Neutron Source For r-Process in Supernovae, 12th International Symposium. AIP Conference proceedings, 819, 581-582.

Levkovski, V. N., 1991. Cross Sections of Medium Mass Nuclide Activation (A=40-100) by Medium Energy Protons and Alpha Particles (E=10-50 MeV), (Experiment and Systematics), Inter-Vesti, Moscow.

Lilley J.S., 2001, Nuclear Physics - Principles and Applications, John Wiley & Sons Ltd.

Mastren, T., Marquez, B. V., Sultan, D. E., Bollinger, E., Eisenbeis, P., Voller, T., Lapi, S. E., 2015. Cyclotron Production of High Specific Activity ^{55}Co and in vivo Evaluation of the Stability of ^{55}Co Metal-Chelate-Peptide Complexes, HHS Public Access, Author manuscript, 14, 526–533.

McCrary, J. H., Morgan, I. L., 1960. (n,2n) Cross Sections of N^{14}, F^{19}, Cu^{63}, Cu^{65} and Sb^{121} in the Energy Region of 13.3 MeV to 15.2 MeV, Bulletin of the American Physical Society, 5, 246(HA5).

Menlove, H. O., Coop, K . L., Grench, H. A., Sher, R., 1967. Activation Cross Sections for the F^{19}(n, 2n)F^{18}, Na^{23}(n, 2n)Na^{22}, Mn^{55}(n,2n)Mn^{54}, In^{115}(n, n)In^{114m}, Ho^{165}(n, 2n)Ho^{164m}, In^{115}(n,n`)In^{115m}, and Al^{27}(n,α)Na^{24} Reactions, Physical Review, 163(4), 1308-1314.

Misaelides, P., Krauskopf, J., Wolf, G., Bethge, K., 1987. Determination of Carbon and Oxygen in GaAs by Means of ^{3}He-activation, Nuclear Instruments and Methods in Physics Research Section B: Beam Interactions with Materials and Atoms, 18(1-6), 281-285.

Nasrabadi, M. N., Sepiani, M., 2015. Study of Components and Statistical Reaction Mechanism in Simulation of Nuclear Process for Optimized Production of ^{64}Cu and ^{67}Ga medical radioisotopes using TALYS, EMPIRE and LISE++ nuclear Reaction and Evaporation Codes, American Institute of Physics, AIP Conference Proceedings, 1653, 020076-1–020076-6.

Noori, S. S., Akkurt, İ., Karpuz, N., 2017. Comparison of Excitation Functions of Longer and Shorter Lived Radionuclides, Acta Physica Polonica A, 132 (3II), 1186-1188.

Nozaki, T., Iwamoto, M., Ido, T., 1974. Yield of ^{18}F for Various Reactions from Oxygen and Neon, Applied Radiation and Isotopes, 25(9), 393-399.

Obata, A., Kasamatsu, S., McCarthy, D. W., Welch, M. J., Saji, H., Yonekura, Y., Fujibayashi, Y., 2003. Production of Therapeutic Quantities of ^{64}Cu Using a 12 MeV Cyclotron, Nuclear Medicine and Biology 30, 535–539.

Otsu, H., 1995. Study of Reaction Mechanisms for (p,n) and (p,p`) Quasi Elastic Scattering, Thesis: Otsu.

P.E. Hodgson, 1963. The Optical Model of Elastic Scattering, Clarendon Press, Oxford.

Paans, A. M. J., Welleweerd, J., Vaalburg, W., Reiffers, S., Woldring, M. G., 1980. Excitation Functions for the Production of Bromine-75: A Potential Nuclide for the Labelling of Radiopharmaceuticals, The International Journal of Applied Radiation and Isotopes, 31(5), 267-273.

Pahk, K., Park, K. W., Pyun, S. B., Lee, J. S., Kim, S., Choe, J. G., 2015. The Use of Fluorine-18 Fluorodeoxyglucose Positron Emission Tomography for Imaging Human Motor Neuronal Activation in the Brain, Experimental and Therapeutic Medicine, 10, 2126-2130.

Pentlow, K. S., Graham, M. C., Lambrecht, R. M., Daghighian, F., Bacharach, S. L., Bendriem, B., Finn, R. D., Jordan, K., Kalaigian, H., Karp, J. S., Robeson, W. R., Larson, S. M., 1996. Quantitative Imaging of Iodine-124 with PET, the Journal of Nuclear Medicine, 37, 1557-1562.

Phillips, A. C., 1994. The Physics of Stars, The Manchester Physics Series, John Wiley & Sons Ltd, 159-203, ISBN 0-471-94057-7.

Picard, J., Williamson, C. F., 1965. The (n,p),(n,α) And (n,2n) Cross Sections for F^{19} and Na^{29} Between 13 and 21 MeV, Nuclear Physics, 63, 673.

Qaim, S. M., 2001. Nuclear Data Relevant to the Production and Application of Diagnostic Radionuclides, Radiochim. Acta 89, 223–232.

Qaim, S.M., 2004. Use of Cyclotrons in Medicine, Radiation Physics and Chemistry, 71, 917–926.

Rayburn, L. A., 1962. (n,2n) Reactions in f-19 and Cu-65, Reaction Mechanisms Conference, Padua, 322.

Ribeiro, M. J., Almeida, P., Strul, D., Ferreira, N., Loc'h, C., Brulon, V., Trebossen, R., Maziere, B., Bendriem, B., 1999. Comparison of Fluorine-18 and Bromine-76 Imaging in Positron Emission Tomography, European Journal of Nuclear Medicine and Molecular Imaging, 26, 758–766.

Ruth, T. J., Wolf, A. P., 1979. Absolute Cross Sections for the Production of ^{18}F via the ^{18}O(p,n)^{18}F Reaction, Radiochimica Acta, 26(1), 21-24.

Ryves, T. B., Kolkowski, P., Zieba, K. J., 1978. Cross Section Measurements of ^{14}N(n,2n)^{13}N, ^{19}F(n,2n)^{18}F,^{54}Fe(n,2n)^{53}Fe, ^{27}Al(n,p)^{27}Mg and ^{27}Al(n,α)^{24}Na Between 14.7 and 19.0 MeV, Journal of Physics G Nuclear Physics, 4(11), 1783.

Sadeghi, M., Enferadi, M., Ensaf, (2012). ^{124}I Production for PET Imaging at a Cyclotron, Kerntechnik, 77(1), 45-49.

Sahan, M., Tel, E., Sahan, H., Sarpün, İ. H., 2018. Theoretical Calculations of Double Differential Neutron Emission Cross Sections of ^{209}Bi at 14.2 MeV İncident Neutron Energy, AIP Conference Proceedings 1935(1), 100001

Salman, H., Oruncak, B., Ünal, R., 2015. Calculation of Reaction Cross sections for Producing Br-75 in the Energy Range of 5–40 MeV, Acta Physica Polonica A, 128(2B), 225-227.

Sarpün, İ. H., Böyükata, M. Aydin, A., 2018. The Effect of the Deformation Parameter on the Cross Sections for Reactions: ^{110}Pd(d,n)^{111}Ag and ^{110}Pd(d,2n)^{110m}Ag, Physics of Atomic Nuclei, 81,1.

Scholten, B., Hassan, K. F., Saleh, Z. A., Coenen, H. H., Qaim, S. M., 2007. Comparative Studies on the Production of the Medically Important Radionuclide ^{124}I via p-, d-, ^{3}He- and α-particle Induced Reactions, International Conference on Nuclear Data for Science and Technology 2007, 2, 1359-1361.

Scholten, B., Kovacs, Z., Tarkanyi, F., Qaim, S. M., 1995. Excitation Functions of ^{124}Te(p,xn)^{124,123}I Reactions from 6 to 31 MeV with Special Reference to the

Production of ^{124}I at a Small Cyclotron, Applied Radiation and Isotopes, 46(4), 255-159.

Scholten, B., Takacs, S., Kovacs Z., Tarkanyi, F., Qaim, S. M., 1997. Excitation Functions of Deuteron Induced Reactions on ^{123}Te: Relevance to the Production of ^{123}I and ^{124}I at Low and Medium Sized Cyclotrons, Applied Radiation and Isotopes, 48(2), 267-271.

Scholten, B., Takacs, S., Tarkanyi, F., Coenen, H. H., Qaim, S. M., 2004. Excitation Functions of Deuteron Induced Nuclear Reactions on Enriched ^{78}Kr with Particular Relevance to the Production of ^{76}Br, Radiochimica Acta, 92(4-6), 203-207.

Scobel, W., Blann, M., Komoto, T. T., Trabandt, M., Grimes, S. M., Hansen, L. F., Wong, C., Pohl, B. A., 1984. Single Particle Effects in Precompound Reactions, Physical Review C, Nuclear Physics, 30(5), 1480-1492.

Shiokawa, T., Yagi, M., Kaji, H., Sasaki, T., 1968. The ^{19}F(n,2n)^{18}F Reaction as a 14-MeV Neutron Flux Monitor, Journal of Inorganic and Nuclear Chemistry, 30(1), 1-4.

Singh, B. P., Bhardwaj, H. D., Prasad, R., 1991. A Study of Pre-equilibrium Emission in α-induced Reactions on ^{121,123}Sb, Canadian Journal of Physics, 69(11), 1376-1382.

Singh, B. P., Sharma, M. K., Musthafa, M. M., Bhardwaj, H. D., Prasad, R., 2006. A Study of Pre-equilibrium Emission in Some Proton- and Alpha-Induced Reactions, Nuclear Instruments and Methods in Physics Research Section A: Accelerators, Spectrometers, Detectors and Associated Equipment, 562(2), 717-720.

Skakun, E. A., Batij, V. G., Rakivnenko, Yu. N., Rastrepin, O. A., 1987. Excitation Functions and Isomer Ratios for up-to-9-MeV Proton Interactions with Zr and Mo isotope nuclei, Yadernaya Fizika, 46(1), 28-39.

Spahn, I., Steyn, G. F., Vermeulen, C., Kovacs, Z., Szelecsenyi, F., Coenen, H. H., Qaim, S. M., 2009. New Cross Section Measurements for Production of the Positron Emitters ^{75}Br and ^{76}Br via Intermediate Energy Proton Induced Reactions, Radiochimica Acta, 97(10), 535-541.

Spellerberg, S., Reimer, P., Blessing, G., Coenen, H. H., Qaim, S. M., 1998. Production of ^{55}Co and ^{57}Co via Proton Induced Reactions on Highly Enriched ^{58}Ni, Applied Radiation and Isotopes, 49(12), 1519-1522.

Takacs, S., Tarkanyi, F., Hermanne, A., Paviotti de Corcuera, R., 2003. Validation and Upgrading of the Recommended Cross Section Data of Charged Particle Reactions Used for Production of PET Radioisotopes, Nuclear Instruments and Methods in Physics Research Section B Beam Interactions with Materials and Atoms, 211(2), 169-189.

Takahashi, A., Ichimura, E., Sasaki, Y., Sugimoto, H., 1987. Measurement of Double Differential Neutron Emission Cross Sections for Incident Neutrons of 14 MeV, Osaka Univ., Journal of Nuclear Science and Technology, 25(3), 215-232.

Tarkanyi, F., Hermanne, A., Ditroi, F., Takacs, S., Ignatyuk, A., 2017. Investigation of Activation Cross Section Data of Alpha Particle Induced Nuclear Reaction on Molybdenum up to 40 MeV: Review of Production Routes of Medically Relevant ^{97,103}Ru, Nuclear Instruments and Methods in Physics Research Section B: Beam Interactions with Materials and Atoms, 399, 83-100.

Tarkanyi, F., Takacs, S., Kiraly, B., Szelecsenyi, F., Ando, L., Bergman, J., Heselius, S-J., Solin, O., Hermanne, A., Shubin, Yu. N., Ignatyuk, A. V., 2009. Excitation Functions of ^{3}He- and a- particle Induced Nuclear Reactions on ^{nat}Sb for Production of Medically Relevant ^{123}I and ^{124}I Radioisotopes, Applied Radiation and Isotopes, 67(6), 1001-1006.

Tatischeff, V., Duprat, J., Kiener, J., Assunção, M., Coc, A., Engrand, C., Gounelle, M., Lefebvre, A., Porquet, M.-G., de Séréville, N., Thibaud, J.-P., Bourgeois, C., Chabot, M., Hammache, F., Scarpaci, J.-A., 2003. Cross Sections Relevant to γ-ray Line Emission on Solar Flares: ^{3}He-induced Reactions on ^{16}O Nuclei, Physical Review C, Nuclear Physics, 68(2), 025804.

Tel E., Sahan, M., Aydin, A., Sahan,H., Ugur E.A. and Kaplan, A., 2011. The Newly Calculations of Production Cross Sections for Some Positron Emitting and Single Photon Emitting Radioisotopes in Proton Cyclotrons, Radioisotopes - Applications in Physical Sciences, ISBN: 978-953-307-510-5.

Terada, Y., Takagi, H., Kokooo, Murata, I., Takahashi, A., 2002. Measurements of Double Differential Cross Sections for Charged Particle Emission Reactions by 14.1 MeV Incident Neutrons, Journal of Nuclear Science and Technology, 39(2), 413-416.

Tolmachev, V., 2011. Radiobromine-labelled Tracers for Positron Emission Tomography: Possibilities and Pitfalls, Current Radiopharmaceuticals, 4(2),76-89.

Uddin, M. S., Hagiwara, M., Tarkanyi, F., Ditroi, F., Baba, M., 2004. Experimental Studies on the Proton-induced Activation Reactions of Molybdenum in the Energy Range 22-67 MeV, Applied Radiation and Isotopes, 60(6), 911-920.

Uddin, M. S., Hermanne, A., Sudar, S., Aslam, M. N., Scholten, B., Coenen, H. H., Qaim, S. M., 2011. Excitation Functions of α-particle Induced Reactions on Enriched ^{123}Sb and ^{nat}Sb for Production of ^{124}I, Applied Radiation and Isotopes, 69(4), 699-704.

Ulu, M.O., 2008. Medical Applications of Particle Detectors, Çukurova University, Institute of Science, Master Thesis, P. 63, Adana.

Varlamov, V. V., Ishkhanov, B. S., Makarenko, I. V., Orlin, V. N., Peskov, N. N., 2006. Evaluation of ^{127}I Photoneutron Reaction Cross Sections, Moscow State University / Institute of Nuclear Physics Reports, No.2006, 9/808.

Wang, L., Yang, X., Rapaport, J., Goodman, C. D., Foster, C. C., Wang, Y., Piekarewicz, J., Sugarbaker, E., Marchlenski, D., de Lucia, S., Luther, B., Rybarcyk, L., Taddeucci, T. N., Park, B. K., 1994. (p,n) Quasifree Excitations in p-shell Nuclei at 186 MeV, Physical Review C, Nuclear Physics, 50(5), 2438-2448.

Webster, WD., Parks, GT., Titov, D., Beasley, P., 2014. The Production of Radionuclides for Nuclear Medicine from a Compact, Low-energy Accelerator System, Nuclear medicine and biology, 41, 7-15.

Wong, S. S. M., 1998. Introductory Nuclear Physics, John Wiley & Sons, Inc., 2nd edition, Weinheim, Germany.

Yalım, H., A., Balçın, N., Serpün, İ., H., 2017. Investigation of Excitation Functions of Copper Radioisotopes Used in Nuclear Medicine with TALYS Code, Süleyman Demirel University Faculty of Arts and Sciences Journal of Science, 12(2), 12-18.

Yule, H. P., Turkevich, A., 1960. Radiochemical Studies of the (p,pn) Reaction in Complex Nuclei in the 80-450 MeV Range, Physical Review, 118(6), 1591-1598.

Zhuravlev, B. V., Lychagin, A. A., Titarenko, N. N., 2014. Neutron Spectra of Fe-57(p,n)Co-57, Fe-56(d,n)Co-57 Reactions and the Density of Co-57 levels, Izv. Rossiiskoi Akademii Nauk, Ser.Fiz., 78(11), 1358-1362.

Zhuravlev, Yu. Yu., Zarubin, P. P., Kolozhvari, A. A., 1994. Excitation Functions of (p,n) Reaction on the Mo Isotope Nuclei in the Energy Interval from Thresholds to 7.2 MeV, Izvestiya rossiiskoi akademii nauk, seriya fizicheskaya, 58(5), 106.

Ziegler S. I., 2005. Positron Emission Tomography: Principles, Technology, and Recent Developments, Nuclear Physics A, 752, 679c–687c

INTERNET REFERENCES

1. http://www.world-nuclear.org/info/inf55.html Updated December 2017

2. https://www.radiochemistry.org/nuclearmedicine/radioisotopes/01_isotopes.shtml

CURRICULUM VITAE

Name Surname	: SUSAN SHUKUR NOORI NOORI
Place and Date of Birth	: Kirkuk- Iraq, 1981
Foreign Language	: English, Turkish
Marital Status	: Married
Nationality	: Iraqi
Email	: suzan_nuclear@yahoo.com

Education:

Undergraduate Education	: Mosul University/ College of Education.
Master	: Mosul University/ College of Education.

Professional Experience :

Kirkuk University/ College of Science   2006- ….. (till now)

Publications

Noori, S. S., Theoretical calculations of exitation functions of natural Fe, Ni, and Cu target to produced ^{57}Co radioisotope for medical applications, The 5th International Conference on Computational and Experimental Science and Engineering (ICCESEN-2018) Antalya – Turkey.

Noori, S. S., Akkurt, İ., Karpuz Demir, N., Calculations of cross sections of copper and zinc nuclei induced by proton, helium-3 and alpha particle to produced Gallium-66, The 5th International Conference on Computational and Experimental Science and Engineering (ICCESEN-2018) Antalya – Turkey.

Karpuz Demir, N., Akkurt, İ., Noori, S. S., Theoretical cross section calculation of alpha induced reactions for production some medical radioisotopes, The 5th International Conference on Computational and Experimental Science and Engineering (ICCESEN-2018) Antalya – Turkey.

Noori, S. S., Akkurt, İ., Karpuz Demir, N., 2018. Excitation functions of proton induced reactions of some radioisotopes used in medicine, Open Chemistry,16, 810–816

Noori, S. S., Akkurt, İ., Karpuz Demir, N., 2017. Comparison of excitation functions of longer and shorter lived radionuclides, Acta Physica Polonica A, 132 (3-II), 1186-1188

Karpuz Demir, N., Çetin, B., Akkurt, İ., Noori, S.S., 2017. Calculations of double differential cross sections on ^{56}Fe, ^{63}Cu and ^{90}Zr neutron emission in proton induced reactions, Acta Physica Polonica A, 132(3-II), 1181-1185.

Noori, S. S., Karpuz, N., Akkurt, İ., 2016. Excitation functions of (d,n) reactions on some light nuclei, Acta Physica Polonica A, 129(1), 484-486

Ibrahim, A. A., Noori, S.S., Monef, R. A., 2011. The response of the nuclear track detectors to some of etching and external parameters, Tikrit Journal of Pure Science 16(4), 205-215

ÖZGEÇMİŞ

Adı Soyadı	: SUSAN SHUKUR NOORI NOORI
Doğum Yeri ve Yılı	: Kerkük- Irak, 1981
Medeni Hali	: Evli
Uyruğu	: Iraklı
Yabancı Dili	: İngilizce, Türkçe
E-posta	: suzan_nuclear@yahoo.com

Eğitim Durumu

Lisans : Musul Üniversitesi / Eğitim Fakültesi

Yüksek Lisans : Musul Üniversitesi / Eğitim Fakültesi

Mesleki Deneyim

Kerkük Üniversitesi Fen Fakültesi   2006-…..(halen)

Yayınlar

Noori, S. S., Theoretical calculations of exitation functions of natural Fe, Ni, and Cu target to produced ^{57}Co radioisotope for medical applications, The 5th International Conference on Computational and Experimental Science and Engineering (ICCESEN-2018) Antalya – Turkey.

Noori, S. S., Akkurt, İ., Karpuz Demir, N., Calculations of cross sections of copper and zinc nuclei induced by proton, helium-3 and alpha particle to produced Gallium-66, The 5th International Conference on Computational and Experimental Science and Engineering (ICCESEN-2018) Antalya – Turkey.

Karpuz Demir, N., Akkurt, İ., Noori, S. S., Theoretical cross section calculation of alpha induced reactions for production some medical radioisotopes, The 5th International Conference on Computational and Experimental Science and Engineering (ICCESEN-2018) Antalya – Turkey.

Noori, S. S., Akkurt, İ., Karpuz Demir, N., 2018. Excitation functions of proton induced reactions of some radioisotopes used in medicine, Open Chemistry,16, 810–816

Noori, S. S., Akkurt, İ., Karpuz Demir, N., 2017. Comparison of excitation functions of longer and shorter lived radionuclides, Acta Physica Polonica A, 132 (3-II), 1186-1188

Karpuz Demir, N., Çetin, B., Akkurt, İ., Noori, S.S., 2017. Calculations of double differential cross sections on ^{56}Fe, ^{63}Cu and ^{90}Zr neutron emission in proton induced reactions, Acta Physica Polonica A, 132(3-II), 1181-1185.

Noori, S. S., Karpuz, N., Akkurt, İ., 2016. Excitation functions of (d,n) reactions on some light nuclei, Acta Physica Polonica A, 129(1), 484-486

Ibrahim, A. A., Noori, S.S., Monef, R. A., 2011. The response of the nuclear track detectors to some of etching and external parameters, Tikrit Journal of Pure Science 16(4), 205-215